UNDERSTANDING THE VIBRATIONAL FEATURES

OF HYDROGEN-BONDED DIMERS

A Dissertation

Presented to the Faculty of the Graduate School

of Cornell University

In Partial Fulfillment of the Requirements for the Degree of

Doctor of Philosophy

By Brian Lynn Van Hoozen, Jr.

August 2017

UNDERSTANDING THE VIBRATIONAL FEATURES OF HYDROGEN-BONDED DIMERS

Brian Lynn Van Hoozen, Jr.

Cornell University 2017

Hydrogen-bonded systems often exhibit very broad and unusually shaped features in their vibrational spectra. The origin of these features is oftentimes unclear. Consequently, computational methods are frequently used to model these features in order to better understand their origin. However, reproducing these features with computational methods is often quite challenging. Many methods have been developed each of which has its own advantages and disadvantages. The research presented in this thesis focuses on the development and application of new computational methods to reproduce the multi-hump (broad peak) vibrational features found in many hydrogen-bonded dimers. These methods utilize density functional theory to calculate the potential energy surface and a quantum variational approach to calculate vibrational spectra from these surfaces. One of the methods developed involves adiabatically separating lower frequency vibrational modes, which modulate the hydrogen bond length, from higher frequency modes that contribute to the structure. Another method that was developed uses a classical molecular dynamics simulation, in place of low-frequency modes, to more accurately sample configurations. The results of the calculations performed with these methods indicate that the broadness of these multi-hump features originate from low-frequency modes modulating the hydrogen bond length, while the multi-hump lineshape is derived from strong Fermi resonances between the OH stretch and the OH bending modes.

BIOGRAPHICAL SKETCH

Brian Van Hoozen, Jr. was born in Saginaw Michigan and raised in Seymour, Wisconsin. After graduating from Seymour Community High School, he went on to pursue undergraduate studies at Lawrence University in Appleton, Wisconsin. As an undergraduate he performed research in the fields of biophysics and computational chemistry at Lawrence University and in optics at the University of Twente in Enschede, the Netherlands. In 2012 Brian graduated from Lawrence University *cum laude* with degrees in chemistry and physics. He then pursued graduate work at Cornell University in Ithaca, New York. While at Cornell University he worked in the group of Prof. Poul Petersen developing theoretical methods to understand the vibrational features of hydrogen-bonded dimers.

ACKNOWLEDGEMENTS

I would like to thank several members of the Cornell chemistry faculty including my advisor Prof. Poul Petersen, my committee members Prof. Greg Ezra and Prof. Floyd Davis, and Prof. Nandini Ananth for her help with developing the theoretical methods.

I also wish to thank the other members of my group, especially Yuchen Sun. Yuchen along with my collaborators Ryan Frink and Okan Köksal (who were or are members of Farhan Rana's group in Cornell's Department of Electrical and Computer Engineering) worked extensively with me to obtain the cryogenic temperature FTIR measurements presented in Chapter 6. Without their help, these measurement would not have been possible.

I would like to thank my family for their support. I would especially like to thank my mother and grandmother for all of the hours they spent proofreading this manuscript and others.

Finally, I wish to thank the Arnold and Mabel Beckman Foundation for financially supporting my work.

TABLE OF CONTENTS

LIST OF FIGURES

1. INTRODUCTION

Hydrogen bonds are widely known to have important roles in many different biological and chemical systems. Because hydrogen bonding gives rise to anharmonic distortions of the potential energy surface, vibrational spectroscopy is a highly sensitive tool for studying hydrogen-bonded systems. For example, it is well known that hydrogen bonds lead to a redshift of the OH/NH stretching frequency, the magnitude of which is determined by the strength of the hydrogen bond.[1,2] It is also well established that the oscillator strength of the transition and width of the vibrational feature increase with the strength of the hydrogen bond.[1,3,4] For weak and medium strength hydrogen bonds, both the frequency shift and width of the OH stretching vibration can be several hundred wavenumbers, but strong hydrogen bonds can lead to much broader spectral features with unusual structures.[5–9]

Hydrogen-bonded dimers in nonpolar solvents form ideal model systems for studying the effect of the hydrogen bonding strength on vibrational modes. A demonstration of how hydrogen bonding in these model systems leads to unusual vibrational features can be seen in Figure 1.1. In Figure 1.1, the FTIR spectra of the individual monomers (naphthol and methylimidazole) dissolved in carbon tetrachloride are plotted in red and blue. In these spectra narrow features are observed which correspond to the OH and CH stretches of these molecules. However, when both species are present in the same solution (plotted in green), a hydrogen-bonded dimer forms and a much broader feature is observed in the FTIR spectrum. This feature spans over 800 cm^{-1} and has a much larger integrated intensity than the CH and OH stretches of the monomers combined. This feature is at least partially due to the OH stretch of naphthol since the free (not hydrogen-bonded) OH stretch peak at 3600 cm^{-1} has decreased substantially when compared to the

naphthol only spectrum. The broad feature is also lower in frequency than the free OH stretch of naphthol which indicates the potential energy surface along this vibrational mode has become more anharmonic. The appearance of this feature also implies that most of the naphthol molecules in solution have formed hydrogen–bonded dimers and that the OH stretch frequency is greatly perturbed in the dimer compared to the monomer as is expected upon formation of a hydrogen bond.

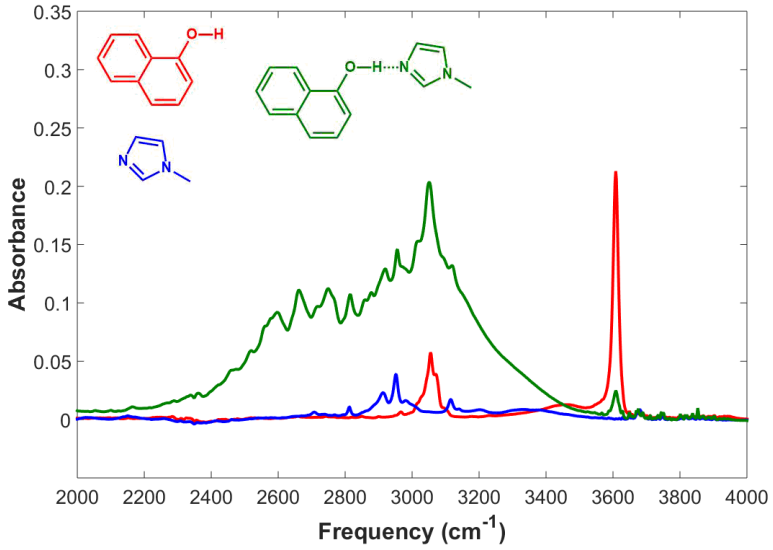

Figure 1.1: FTIR spectra of naphthol and methylimidazole. The FTIR spectra of naphthol and methylimidazole in separate carbon tetrachloride solutions are plotted in red and blue. A solution containing both species is plotted in green. The two species form a hydrogen-bonded complex which has a broad vibrational feature that is not observed in either of the monomer spectra.

Naphthol-methylimidazole is certainly not the only example of hydrogen-bonded dimers that have broad vibrational features. Another example is the 7-azaindole homodimer which exhibits a vibrational feature that has a full width half maximum of approximately 500 cm^{-1} which corresponds to the NH stretches. This feature can be seen in the top panel of Figure 1.2. This feature is similar to the vibrational feature of the naphthol-methylimidazole dimer in that it

appears to be one hump (broad peak) with some substructure. Other hydrogen-bonded dimers have vibrational features that clearly contain multiple humps. Many dimers between carboxylic acids and nitrogen containing aromatic bases have a two-hump vibrational feature spanning from 1800 to 2700 cm^{-1}.[5,8,10–12] An example of this feature can be seen in the spectrum of 7-azaindole-acetic acid which is plotted in the second panel of Figure 1.2. Yet another class of dimers exhibit what has been frequently referred to as the Hadži ABC structure which is a three-hump feature found in the homodimers of various phosphoric, phosphinic and selenic acids.[6,7,9,13–15] This feature is typically quite broad and can span from 1000 to 3500 cm^{-1}. As an example the spectrum of the dimethylphosphinic acid homodimer is shown in the third panel of Figure 1.2.

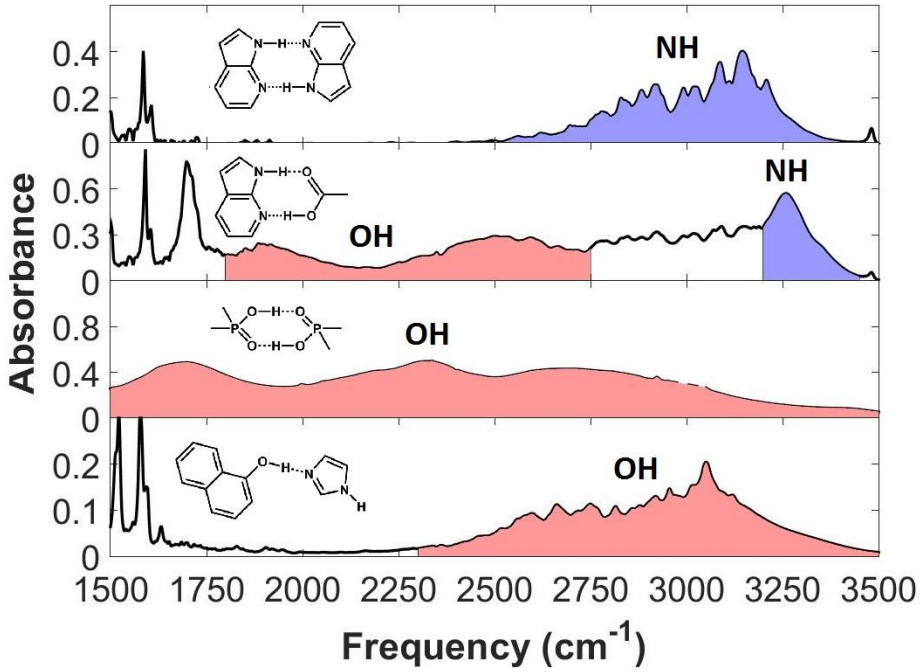

Figure 1.2: FTIR spectra of hydrogen-bonded dimers with broad vibrational features. Features assigned to the OH are colored pink while features assigned to the NH are colored blue.

It is well known that these features are associated with the hydrogen bonded OH and NH groups. However, the sources of their broadness and unusual lineshapes are much less clear. To

understand these sources better, computational methods are often used to calculate the vibrational features and thereby obtain a better understanding of their origin.

A number of computational methods have surfaced over the past several years to calculate the vibrational features of hydrogen-bonded systems. Each of these methods has strengths and limitations. However generally, these methods have shown that the broadness and unusual shape of these features originate from a couple of sources. One source is the distribution of geometries present in the system of interest. As the vibrational frequencies of oscillations involved in hydrogen bonds are very sensitive to the exact geometry of the system, the distribution of geometries often leads to very broad features. This distribution of geometries can be accounted for by including zero-point energy or lower frequency modes in the calculation or by performing molecular dynamics (MD) simulations. Fermi resonance interactions are frequently responsible for the unusual lineshapes of many of these features. These interactions arise from quantum mechanical coupling, typically between the bend and stretch modes. Typically this results in the normally forbidden overtone of the bend acquiring oscillator strength from the fundamental of the stretch which effectively creates a new transition. Many methods for calculating these unusual features have been developed which include the range of geometries inhabited and/or Fermi resonance interactions.

Most of these computational methods rely on electronic structure calculations to compute the potential energy surface. Since hydrogen bonds give rise to very anharmonic potentials, the anharmonicity of the potential must be included in the calculation to obtain meaningful frequencies. Perhaps the most common (but not necessarily the most accurate) method for calculating anharmonic frequencies is Vibrational second-order Perturbation Theory (VPT2)[16] which has been incorporated into many commercially available electronic structure packages

such as Gaussian.[17] This method relies on a finite difference procedure[18] to compute anharmonic force constants (derivatives of the potential above second order). This is accomplished by computing harmonic force constants at different geometries along a normal mode and using those constants to estimate higher order derivatives of the potential. This method computes third and fourth order derivatives from three second order derivatives along a normal mode. Consequently, the description of the potential along one dimension relies on three second order derivatives. Thus although using VPT2 is a vast improvement over a harmonic calculation, three second order derivatives does not necessarily provide the most accurate description of the potential which will ultimately determine the vibrational frequencies.

A computationally more intensive but perhaps more robust method for computing the anharmocity is to calculate the potential energy surface directly by calculating the energy at various points along the vibrational mode of interest. For one-dimension this is computationally quite trivial; however as the number of dimensions increases this task becomes more difficult. For this reason a number of computational studies of the unusual vibrational features of hydrogen-bonded dimers have relied on a combination of both potential energy surface scans and finite difference procedures to compute anharmonic force constants. For example, Dreyer computed the OH and NH features associated with the acetic acid and 7-azaindole homodimers.[19,20] He used polynomial fits to one-dimensional surface scans to obtain anharmonic force constants along one degree of freedom and a finite difference procedure to obtain anharmonic force constants that have multiple degrees of freedom. This combined approach allowed him to include many (10-14) degrees of freedom. Using the computed anharmonic force constants, he performed a high-dimensional variational calculation to obtain the eigenstates. These eigenstates were then used to construct a stick spectrum which was in semi-quantitative

agreement with the experimental spectra. He concluded that these features were arising from coupling between the OH or NH stretch mode, fingerprint modes that include OH and NH bending, and lower frequency modes that modulate the hydrogen bond length.

Alternatively one can scan the whole potential energy surface of interest. This method should give a more accurate description of the coupling between vibrational modes, but does limit the size of the system one can study and/or the number of vibrational modes that can be included. For example, Rheinecker and Bowman computed the vibrational spectrum of H_2O-Cl in full dimensionality using a full-dimensional description of the potential derived from potential energy surface scans with up to four dimensions.[21] Alternatively, one can examine larger systems by including fewer dimensions. For example Elsaesser and co-worker examined the coupling between neighboring hydrogen-bonded stretches by computing two-dimensional potential energy surfaces along the OH and/or NH stretches.[22] Thus although this method should provide a much more accurate description of the potential, it becomes very difficult to implement for larger systems or systems in which many dimensions are necessary.

For some systems calculating a potential energy surface that includes all of the dimensions is impractical. However, in many systems only a few dimensions are responsible for the transition that contributes to the vibrational structure. Oftentimes, these transitions are broadened by lower frequency modes. In these types of systems it is generally better to adiabatically separate lower frequency modes from higher frequency modes.

For calculating the features of low-temperature gas phase measurement where the distribution of molecular geometries is essentially dictated by the zero-point energy, one requires a method that can accurately calculate the ground state wavefunctions of high-dimensional systems. McCoy and co-workers have developed a method that is well designed for calculating

these types of spectra.[23,24] Their method uses Diffusion Monte Carlo[25] to obtain an accurate description of the full-dimensional ground state wavefunction. They then obtain geometries using Monte Carlo sampling based on the ground state probability distribution. The frequency of interest for each geometry is then computed using electronic structure calculations. This is a very powerful method for obtaining vibrational spectra of hydrogen-bonded systems at temperatures near absolute zero. However, this method breaks down at temperatures where excited states are populated because Diffusion Monte Carlo can only obtain ground state wavefunctions. Since hydrogen-bonded systems typically have vibration modes that are near 100 cm^{-1}, excited states can be significantly populated at temperatures as low as 40 or 50 Kelvin, limiting the utility of this approach to very low temperatures.

At higher temperatures, there has been success incorporating thermally populated geometries using classical molecular dynamics simulations.[3,26–28] These methods are often combined with electronic structure calculations. Oftentimes these dual electronic structure and molecular dynamics methods are applied to large condensed phase systems where a few vibrational modes of interest do not couple significantly with the other modes in the system. With these methods, snapshots are taken from classical molecular dynamics simulations. The vibrational frequencies of interest are then computed using electronic structure methods by performing a potential energy surface scan along the mode or modes of interest. Oftentimes the frequencies and transition dipole moments computed can be correlated with parameters that can be taken from the MD simulation alone such as electric field[3,26,27] or bond angles.[28] These so-called “spectral maps” allow for the transition properties of additional geometries, sampled by the MD simulation, to be computed without additional electronic structure calculations. This vastly increases the number of geometries that can be used in a calculation of the vibrational

spectra. With these spectra maps, the cost of calculating vibrational frequencies and transition dipole moments is small enough that the spectra can be calculated using the Fourier transform of the dipole autocorrelation function instead of just summing the transitions of the sampled geometries.

Lastly, empirical models have also been developed to better understand these unusual features. For example, Hanna and co-workers developed an empirical model for calculating the Hadži ABC structure.[15] Their model demonstrated that this feature could be reproduced by accounting for Fermi resonances of the OH stretch with the in-plane bend (IPB) and out-of-plane bend (OPB) as well as letting the OH stretch frequency be linearly dependent upon a lower frequency mode that modulates the hydrogen bond length.

Although a number of computational methods have been developed for calculating the vibrational features of hydrogen-bonded systems, the origin of the vibrational features of many hydrogen-bonded dimers are not well understood. In particular we sought to develop computational methods that could explain the multi-hump vibrational features found in a variety of hydrogen-bonded dimers. The results of this work are presented in this thesis.

The rest of this thesis is outlined as follows. Chapter 2 explains the first method that was developed for computing these feature referred to as the dimer stretch method. This method works by selecting a low-frequency mode that modulates the hydrogen bond length and computing how the higher frequency transition properties depend on this mode's coordinate. In Chapter 3 this method is applied to explaining the double-hump vibrational feature of the Py-Ac dimer. The later sections of this chapter investigate how the computed vibrational feature depends on various parameters of the calculation. Chapter 4 applies the dimer stretch method to explaining the Hadži ABC structure. This structure is among the broadest observed in the spectra

of hydrogen-bonded dimers. Chapter 5 utilizes the dimer stretch method to calculate the acid and base strength dependence of the vibrational features of dimers between pyridines and carboxylic acids. The acid and base strength dependence of these feature gives insight into how these features depend on the hydrogen bond strength. In Chapter 6, the temperature dependence of these features is examined using both theory and experiment. The experimental results are compared to those calculated using the dimer stretch method which predicts changes in the features due to different population distributions of the eigenstates of the dimer stretch mode. In Chapter 7 another method for calculating these features is introduced using an MD simulation to sample different geometries in place of the dimer stretch mode. The final chapter of this thesis summarizes the results and provides some general conclusions.

2. THE DIMER STRETCH METHOD

2.1 Motivation and Overview

In Dreyer's studies of the vibrational features of the 7-azaindole and acetic acid homodimers, it was shown that the vibrational modes responsible for these features could be divided into three categories. These categories were the OH or NH stretch modes, fingerprint modes that contain some OH or NH bending character and lower frequency modes that modulate the hydrogen bond length (dimer stretch modes). This study treated all of these vibrational modes equivalently. Hanna and co-workers conducted a study of the Hadži ABC structure and concluded that the same types of modes contributed to that structure. In their study they adiabatically separated a dimer stretch mode from the bending and stretching modes in order to reproduce the feature. The method presented in this chapter combines features of both of these methods in order to reproduce the multi-hump features found in the spectra of many hydrogen-bonded dimers. Like Dreyer's work, *ab initio* methods are used to compute the potential energy surface along the relevant vibrational modes. However, unlike Dreyer's studies, in this work the dimer stretch modes are adiabatically separated from the higher frequency bending and stretching modes, similar to Hanna's approach.

The general approach of the dimer stretch method is outlined in Figure 2.1. In this method the potential energy and dipole surface of the higher frequency modes are calculated using density functional theory. Transition frequencies and dipole moments are then computed from these surfaces. The calculation is repeated at various points along a dimer stretch mode to effectively map out how these properties depend on the dimer stretch mode. This map is then used to compute the vibrational spectrum.

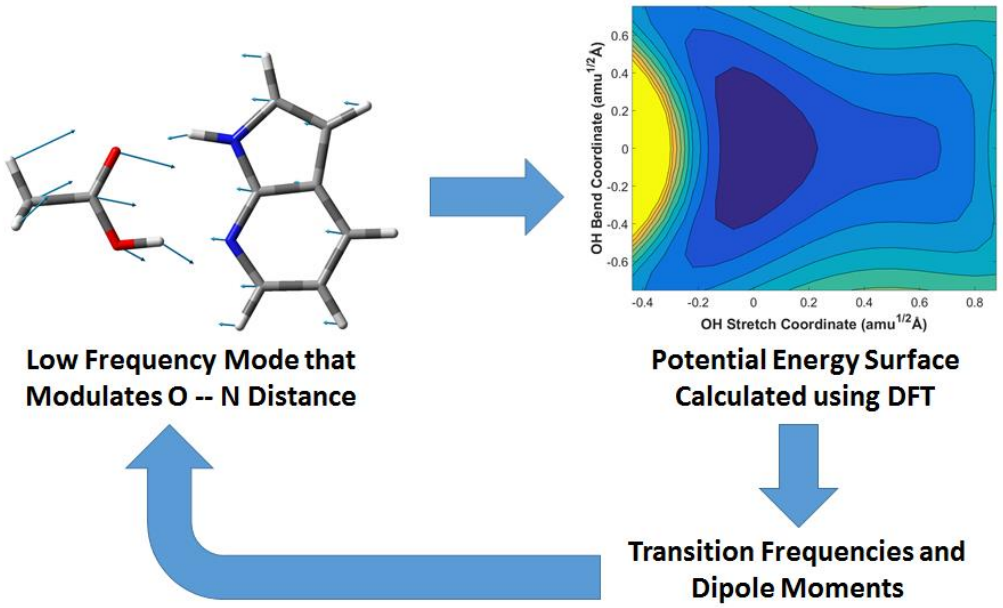

Figure 2.1: Outline of the Dimer Stretch Method.

2.2 Computational Method

All electronic structure calculations were performed at the B3LYP[29]/6-311++G(d,p) level of theory using the Gaussian 09 software package[17] unless stated otherwise. The B3LYP functional was chosen because Jens Dreyer utilized it to successfully calculate the vibrational features of the 7-azaindole and acetic acid homodimers.[19,20] The functional dependence will be examined more closely in a section 3.4. The effect of the non-polar solvent was incorporated at the dielectric continuum level using the Onsager model.

All structures were optimized and normal modes and harmonic frequencies were calculated using normal mode analysis in Gaussian 09. Normal mode analysis gives a matrix of eigenvectors $\boldsymbol{C_{ki}}$ which relate the mass-weighted Cartesian displacement atomic coordinates ($\boldsymbol{q_i}$) to the normal mode displacement coordinates ($\boldsymbol{Q_k}$) as shown in equations 2.1 and 2.2.[30] In these

equations, $\boldsymbol{m}$ is the mass of the atom, $\boldsymbol{\Delta r}$ is an individual atom's displacement along a Cartesian coordinate and $\boldsymbol{N}$ is the number of atoms in the dimer.

$$\boldsymbol{q_i = \sqrt{m_i}\,\Delta r_i} \tag{2.1}$$

$$\boldsymbol{Q_k = \sum_{i=1}^{3N} C_{ki} q_i} \tag{2.2}$$

Next, a potential energy surface was computed using OH stretch and bending normal modes as coordinates. These surfaces have 15 or 16 points along each dimension. In order to obtain transition frequencies from the potential energy surface, a variational calculation was performed using a discrete variable representation[31] of the Hamiltonian. The expression for a one-dimensional Hamiltonian is given by equations 2.3-2.5. It is then extended to two and three dimensions by equations 2.6 and 2.7. A derivation of the Hamiltonian is given in Appendix A. In equation 2.3, $\mathbf{\Delta Q}$ is the normal mode displacement coordinate spacing between the calculated points of the potential energy surface, $\hbar$ is Planck's constant and $\widehat{\boldsymbol{T}}$ is the kinetic energy operator. In equations 2.4 and 2.5, $\boldsymbol{V(Q_n)}$ are the calculated potential energies, $\widehat{\boldsymbol{V}}$ is the potential energy operator and $\widehat{\boldsymbol{H}}$ is the Hamiltonian operator.

$$\widehat{\boldsymbol{T}}_{\boldsymbol{mn}} = (-\mathbf{1})^{\boldsymbol{m-n}} \frac{\hbar^{\mathbf{2}}}{\mathbf{2\Delta Q^2}} \begin{cases} -\dfrac{\boldsymbol{\pi^2}}{\mathbf{3}}, & \boldsymbol{m = n} \\ \dfrac{\mathbf{2}}{\boldsymbol{m-n}}, & \boldsymbol{m \neq n} \end{cases} \tag{2.3}$$

$$\widehat{\boldsymbol{V}}_{\boldsymbol{mn}} = \boldsymbol{\delta_{mn} V(Q_n)} \tag{2.4}$$

$$\hat{H} = \hat{T} + \hat{V} \tag{2.5}$$

$$\hat{H}_{ijkl} = \delta_{ik}\hat{T}_{jl} + \delta_{jl}\hat{T}_{ik} + \delta_{ik}\delta_{jl}V(Q_i, Q_j) \tag{2.6}$$

$$\hat{H}_{ijklmn} = \delta_{il}\delta_{jm}\hat{T}_{kn} + \delta_{il}\delta_{kn}\hat{T}_{jm} + \delta_{kn}\delta_{jm}\hat{T}_{il} + \delta_{il}\delta_{jm}\delta_{kn}V(Q_i, Q_j, Q_k) \tag{2.7}$$

Transition frequencies were calculated from the energy differences between the computed eigenstates. The transition probabilities were also computed using a discrete variable representation as shown for one dimension in equations 2.8-2.10. Dipole operators ($\mu_{\sigma,mn}$) were constructed from the dipole surfaces ($\mu_\sigma(Q_n)$) for each Cartesian coordinate. The transition dipole moments ($\overrightarrow{\mu_{if}}$) between initial state i and final state f were calculated from the dipole operators. The transition probabilities (P_{if}) were taken as being proportional to the magnitude of the transition dipole moment squared.

$$\mu_{\sigma,mn} = \delta_{mn}\mu_\sigma(Q_n) \quad where\ \sigma = x, y\ or\ z \tag{2.8}$$

$$\overrightarrow{\mu_{if}} = (\langle\phi_f|\mu_x|\phi_i\rangle, \langle\phi_f|\mu_y|\phi_i\rangle, \langle\phi_f|\mu_z|\phi_i\rangle) \tag{2.9}$$

$$P_{if}\ \alpha\ |\overrightarrow{\mu_{if}}|^2 \tag{2.10}$$

To incorporate the effect of the dimer stretch mode, the potential energy surface calculation was repeated at several points along the dimer stretch coordinate. The points along the dimer stretch coordinate were selected to cover any region significantly inhabited at room

temperature. The transition frequencies and transition dipole moments squared at different dimer stretch coordinate values were connected by a cubic spline fit in order to obtain these values as a smooth function of the dimer stretch coordinate. This treatment results in an effective adiabatic separation of the OH stretch and bend modes from the order of magnitude lower frequency dimer stretch mode.

Since most of the dimer stretch modes examined in this work had fundamental frequencies between 80 and 170 cm^{-1}, several excited states of these modes are populated at room temperature. Therefore the distribution along the dimer stretch coordinate was calculated using a Boltzmann-weighted sum of the squares of the wavefunctions of the dimer stretch states. This sum included the ground state and up to the first five excited states which corresponds to the vast majority of the dimers at room temperature.

In order to calculate the vibrational spectrum, 101 different geometries along the dimer stretch coordinate were sampled. These geometries were equally spaced and ranged from the minimum to the maximum computed values of the dimer stretch coordinate. Each geometry was modeled as contributing a Gaussian or Lorentzian profile to the infrared spectrum (see section 3.7 for a more detailed discussion how these profiles impact the lineshape). The height of each Gaussian or Lorentzian was determined by the product of the probability of that geometry and the transition probability. The full-width-half-maximum (FWHM) of each Gaussian or Lorentzian was adjusted depending on the amount of homogenous broadening desired in the calculation. A more detailed discussion of how the FWHM impacts the computed lineshape is also presented in section 3.7. By summing all of the Gaussians or Lorentzians together, the spectral feature of a transition was calculated.

3. The Pyridine-Acetic Acid Dimer

3.1 The Out-of-Plane Bend

One of the simplest dimers between carboxylic acids and nitrogen-containing aromatic bases is the pyridine acetic acid (Py-Ac) dimer. Like many dimers in this class it exhibits a double-hump feature in its vibrational spectra that spans from 1800 to 2700 cm^{-1}. Since it is one of the simplest dimers that exhibits this unusual feature, it is an ideal system for starting an investigation into the origin of this feature. By performing the dimer stretch method calculation outlined in the previous chapter with a variety of fingerprint modes, it was found that the most important modes for explaining this feature are the OH stretch, the OH out-of-plane bend (OPB) and the dimer stretch modes. Therefore, the vibrational feature calculated with these modes will be presented first and how the feature changes when other fingerprint modes are used will be presented in section 3.2.

The dependence of the transition frequencies and dipole moments on the dimer stretch mode are shown in Figure 3.1. Negative dimer stretch coordinate values correspond to shorter O – N distances while positive values correspond to larger O – N distances. The calculation that only includes the OH stretch in the Hamiltonian is plotted with the dashed black lines. The top panel of Figure 3.1 shows the frequencies of each transition. When the components of the dimer are further apart, the OH stretch frequency approaches 2900 cm^{-1}. However, when they are closer together the frequency drops to about 2100 cm^{-1}. This is a remarkably broad range of frequencies spanning almost 800 cm^{-1}. The middle panel in Figure 3.1 displays the transition probabilities (the norm squared of the transition dipole moments). The transition probability also changes drastically as one moves along the dimer stretch coordinate, indicating that a large non-Condon effect is present. When the components of the dimer are further apart, the transition probability is

about 0.6 Debye^2. However, it more than triples to 2.0 Debye^2 as the components of the dimer come together. The bottom panel show the distribution along the OH stretch coordinate for 298 K which is derived from a Boltzmann-weighted sum of the four lowest energy harmonic dimer stretch state probabilities.

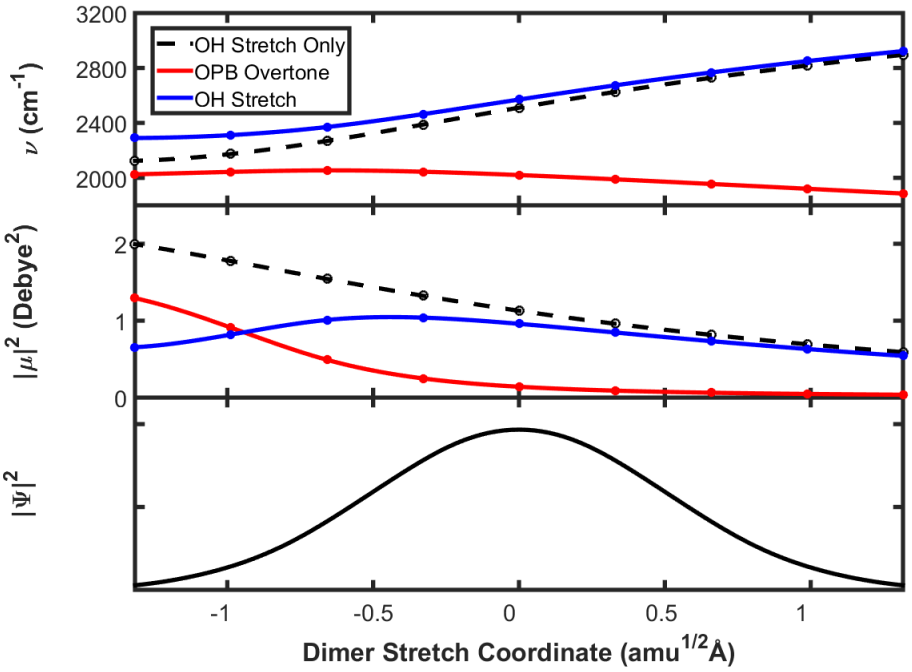

Figure 3.1: Transition frequencies and probabilities versus dimer stretch coordinate for the Py-Ac dimer. The dashed black line corresponds to a calculation that only includes the OH stretch. The solid colored lines correspond to a calculation that includes the OH stretch and OPB. The top panel shows the frequencies of each transition. The middle panel shows the transition probabilities. The bottom panel shows the distribution of geometries along the dimer stretch coordinate.

The transitions resulting from a calculation where the OPB is also included in the Hamiltonian are displayed with the solid red and blue lines in Figure 3.1. The red lines correspond to the OPB overtone while the blue lines correspond to the OH stretch fundamental. When the bending mode is included, the OH stretch also spans a very large frequency range from about 2300 to 2900 cm^{-1}. The OPB overtone also changes with the dimer stretch coordinate. This

transition's frequency changes significantly less though, spanning from a little less than 1900 cm^{-1} to a little more than 2000 cm^{-1}. However, the transition probability changes much more drastically with the dimer stretch coordinate. When the components of the dimer are closer together, the frequencies of the OPB overtone and OH stretch fundamental are similar. This results in a Fermi resonance interaction that can be seen more clearly by examining the transition probabilities. When the components of the dimer are further apart, the OPB overtone has almost no transition probability and the OH stretch has similar properties to when it is calculated without the bending mode. This implies that there is almost no Fermi resonance interaction. However in geometries where the components of the dimer are closer together, the transition probability of the OPB overtone rises and eventually overtakes that of the OH stretch. This is due to the strong Fermi resonance interaction in this region.

All of the information displayed in Figure 3.1 can be used to calculate the vibrational features associated with these two transitions. The computed spectral features are displayed in Figure 3.2. The results shown in Figure 3.2 use Lorentzians that have a FWHM of 100 cm^{-1} to account for homogenous broadening. The dependence of the computed results on these parameters will be shown in a later section. In Figure 3.2, the dashed blue line shows the results of a calculation performed without accounting for the OPB overtone. Even this calculation predicts a remarkably broad vibrational feature extending from approximately 2100 to 2800 cm^{-1}. However, this feature does not have the same double-hump line shape that is found in the experimental spectrum. This line shape is reproduced by including the OPB in the calculation. Including the OPB bend results in two overlapping features which correspond to the OPB overtone and the OH stretch. The OH stretch (which is plotted with the solid blue line) spans from roughly 2300 to 2800 cm^{-1} and reproduces the experimental higher frequency hump quite

well. The OPB overtone feature is less broad, spanning from roughly 1950 to 2100 cm^{-1}, which corresponds to the frequency range of the low-frequency hump of the experimental spectrum. The lower frequency hump is calculated to be narrower than is observed experimentally which indicates that this model is not capturing some aspect of the broadening mechanism of this feature. Nonetheless, the broadening of the higher frequency hump is captured well by this model and the overall two-hump shape and frequency range are also well reproduced

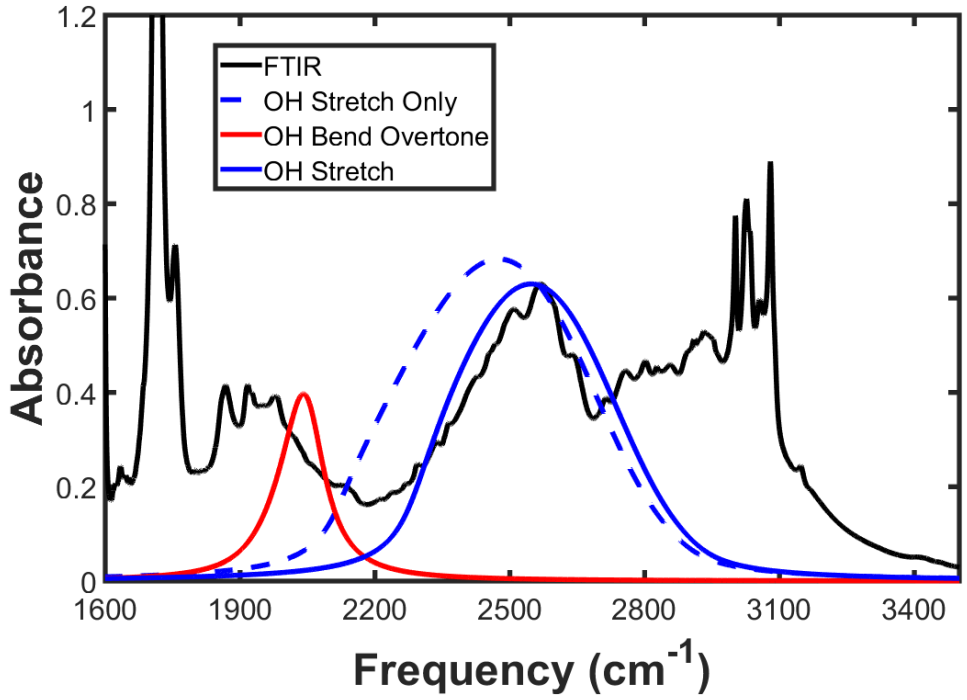

Figure 3.2: Computed spectral features of OH stretch fundamental and OPB overtone of the Py-Ac dimer. The sharp features in the 3000 to 3100 cm^{-1} region of the FTIR spectra are C-H stretches coming from the excess of pyridine used to bias the equilibrium to the heterodimer. The identity of each line is given by the legend.

3.2 Dependence on the Fingerprint Mode

In the previous section it was shown how including the OPB in the calculation resulted in a double-hump lineshape. However there are many fingerprint modes that, in principle, could give rise to Fermi resonance interactions. For example, Jen Dreyer's studies of the 7-azaindole and acetic acid heterodimers showed that many fingerprint modes were responsible for the unusual substructure found in the vibrational features of these dimers. To examine what role other fingerprint modes have in the two-hump vibrational features, the calculation described in the previous section was repeated with other fingerprint modes. The fingerprint modes examined include (a) the OPB which was discussed in the previous section and has a fundamental harmonic frequency of 1061 cm^{-1}, (b) a mode that includes OPB motion and motion of the carbonyl and methyl groups of the acetic acid at 1067 cm^{-1}, (c) a mode that includes in-plane bend (IPB) motion and motion of the carbonyl and methyl group at 1298 cm^{-1} and (d) the IPB at 1504 cm^{-1}. Although the Py-Ac acid dimer has many more fingerprint modes, these four provide examples of how different modes contribute to the structure. The results of these calculations are displayed in Figure 3.3.

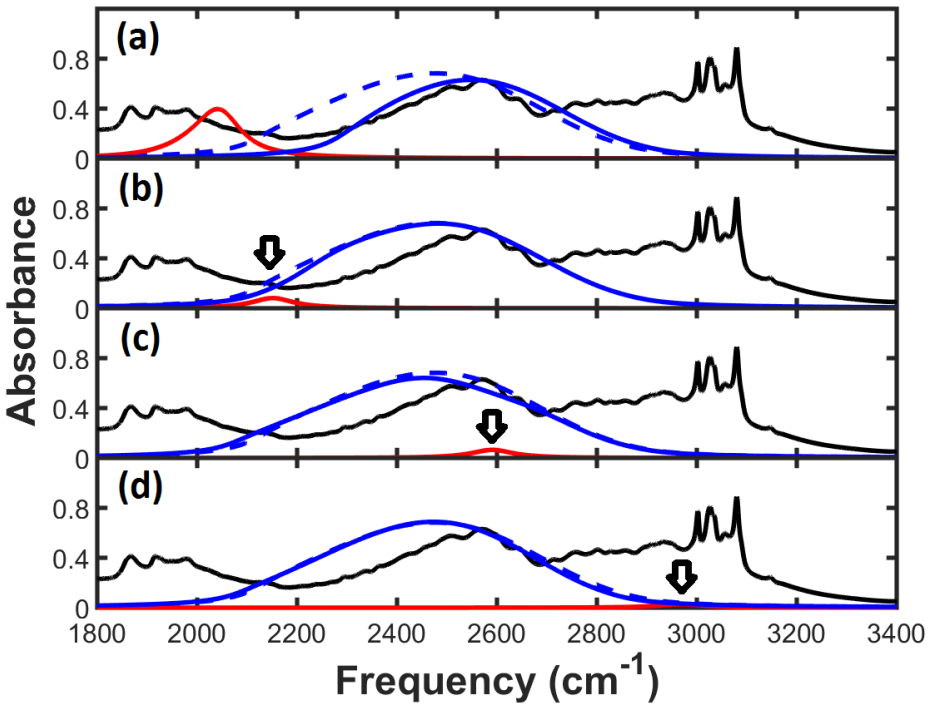

Figure 3.3: Computed spectral features of OH stretch fundamental and various overtones of the Py-Ac dimer. Each row corresponds to a different fingerprint mode included in the calculation as described in the text. The solid blue and red lines correspond to the calculated spectral features of the OH stretch and fingerprint mode overtone respectively. The dashed blue line corresponds to the calculated OH stretch feature when the fingerprint mode is not included in the calculation. The FTIR spectrum is plotted in black for comparison.

From examining Figure 3.3, it can be seen that by far the strongest Fermi resonance interaction is with the OPB. The other fingerprint modes examined in this study contribute much smaller features to the vibrational spectrum. In the case of modes b and c, this is likely due to the motion of other atoms (in the carbonyl and methyl groups) decreasing the level of coupling between the fingerprint mode and the OH stretch. These types of modes are likely responsible for the substructure of the double-hump. In the case of the IPB, the origin of the small resonance seems to be a little more complex. The frequency of the IPB overtone is about 3000 cm^{-1}. Thus the coupling between the OH stretch and this mode will be strongest when the components of the dimer are farther apart. The oscillator strength of the OH stretch is relatively small in these

geometries which limits the amount of oscillator strength that can be obtained by the IPB overtone. Additionally, the IPB calculated with normal mode analysis includes more motion of other atoms in the system than the OPB.

Overall, these results indicate that the OPB has the strongest Fermi resonance with the OH stretch which gives rise to the double-hump lineshape. Other fingerprint modes have Fermi resonances with the OH stretch but they result in much smaller vibrational features. These resonances are likely responsible for the substructure of the double-hump but do not contribute to the general shape.

3.3 Dependence on the Dimer Stretch Mode

In general, there can be multiple low-frequency modes that modulate the hydrogen bond length. In the case of the Py-Ac dimer, there are two low-frequency modes that modulate the hydrogen bond length significantly. Both modes have some twisting motion. One of the modes has a frequency of 119 cm^{-1} and involves the pyridine twisting. The other occurs at 165 cm^{-1} and involves the acetic acid twisting. The calculations shown in the previous sections have been with the 165 cm^{-1} mode, however, to examine how the calculation is impacted by changing the low-frequency mode, the calculation was repeated with the 119 cm^{-1} mode. The results of these calculations are shown in Figure 3.4. These results show that the choice of dimer stretch mode used in the calculation has a remarkably small impact on the computed lineshape. This indicates that as long as the mode selected spans a range of O -- N distances, the computed lineshapes will be very similar. The main difference in the computed spectra is the magnitude of the absorbance. Although the computed spectra are scaled by an arbitrary amount to match the experimental data, the same scaling factor can be used for multiple calculations. If the same scaling factor is used

and the dimer stretch coordinate space that is scanned corresponds to the same portion of the potential, the relative intensities of calculated spectra are meaningful. Scanning the same portion of the dimer stretch potential is accomplished by ensuring that the 101 sampled points along the dimer stretch coordinate correspond specifically to the bottom 700 cm^{-1} of the harmonic potential. Thus changing the low-frequency mode seems to have little effect on the computed lineshape, but does have some impact on the magnitude of the feature.

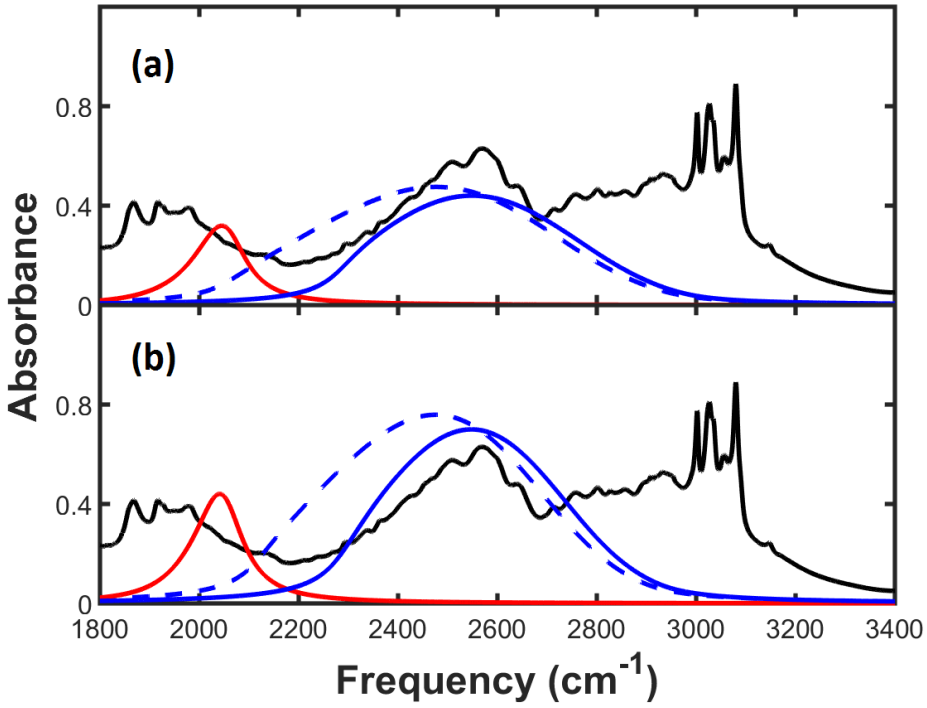

Figure 3.4: Computed spectral features of OH stretch fundamental and OPB overtone of the Py-Ac dimer for different dimer stretch modes. The top panel uses the 119 cm^{-1} dimer stretch mode while the bottom panel uses the 165 cm^{-1} dimer stretch mode.

3.4 Dependence on the Functional

In recent years, Density functional theory has become one of the most popular electronic structure methods. Many studies of the vibrational features of hydrogen-bonded systems have

relied on density functional theory to describe their potential surface. In very small system (typically 10 atoms or less), higher levels of electronic structure have been utilized such as CCSD(T). However, for systems roughly the size of Py-Ac, density functional theory is frequently utilized because it provides an excellent compromise between computational cost and accuracy for systems of this size. However, one of the largest concerns with using density functional theory is the range of results one can obtain by simply changing the functional. Sherrill and co-workers have documented how different functionals predict different hydrogen bonding strengths.[32] In order to obtain a better understanding of how the computed vibrational features depend on the functional used to calculate the potential, the calculation was repeated for several functionals. The results of these calculations are displayed in Figure 3.5.

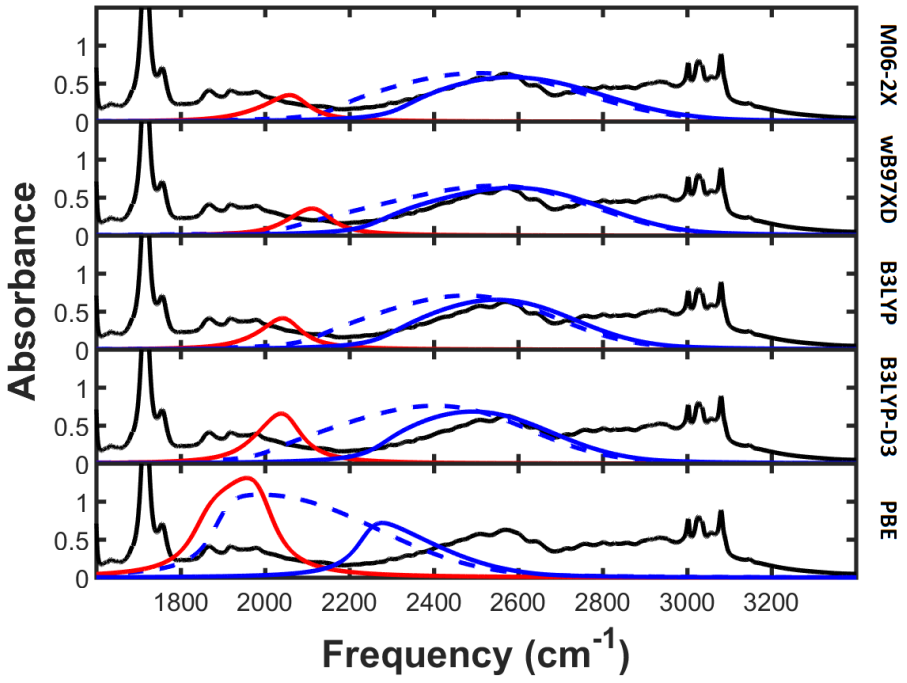

Figure 3.5: Computed spectral features of OH stretch fundamental and OPB overtone of Py-Ac dimer using different electronic structure methods. The functional used in each calculation is displayed on the right. The dashed blue line corresponds to the uncoupled OH stretch calculation. The solid blue and red lines correspond to the features calculated with the bend.

From examining Figure 3.5, the computed spectral feature can clearly depend on the functional used in the calculation. However, all of the computed spectral features have a couple of properties in common. These are all quite broad spanning from about 800 to 1000 cm^{-1} and contain a double-hump lineshape. However, the exact frequencies that the feature spans depend significantly on the functional. The three functionals towards the top of the plot (M06-2X, wb97xD and B3LYP) all have similar frequency ranges. PBE predicts the feature to be at much lower frequencies. Similar trends are observed for features of other dimer systems that have been investigated. For example, 7-azaindole-acetic acid is also calculated to have features of different center frequencies. M06-2X was found to calculate the highest center frequency followed by B3LYP and PBE. In the case of the dimethylphosphinic acid homodimer (which will be discussed in more detail in Chapter 4), M06-2X predicts the highest center frequency followed by wB97XD, B3LYP and PBE. Thus by examining a handful of different systems a pattern emerges. Each functional calculates a different hydrogen bond strength. Across a handful of systems, M06-2X tends to have the highest center frequencies, followed by wB97XD, B3LYP and PBE. Similar trends in how the features change can be observed by examining the dependence on the acid and base strength of the components of the dimer which will be examined in Chapter 5. The magnitude of the changes depends on both the system and functionals being compared. For example Py-Ac, has similar calculated features for M06-2X and B3LYP, but PBE produces very different features. In the case of 7-azaindole-acetic acid, these three functional all produce distinct results.

Van der Waals forces are not included in standard density functional theory calculations. Consequently, empirical corrections have been introduced to account for these forces. One of the

most popular is Grimme's D3 correction. To examine how these corrections may influence the computed features, the features were calculated using the B3LYP functional with D3 correction (which is plotted in the fourth panel of Figure 3.5). This corrective term resulted in lower OH stretch frequencies which in turn lead to a larger Fermi resonance with the OPB. Thus it appears that adding these corrections has a similar effect to strengthening the hydrogen bonding interaction. Since Van der Waals forces are attractive, it seems intuitive that turning them on would appear similar to strengthening a hydrogen bond.

M06-2X, wB97XD, and B3LYP all calculate similar OPB overtone features. They are all centered at roughly 2050 cm^{-1} and are of approximately the same width. However, the PBE OPB overtone feature is much broader, lower in frequency and overlaps much more with the OH stretch only calculated feature. Upon further investigation of this feature, it becomes clear that unlike all of the other calculations shown thus far, the OPB overtone frequency is not always lower than the OH stretch frequency. At points along the dimer stretch coordinate, the OH stretch fundamental is higher in frequency than the OPB overtone and at other points it is lower in frequency than the OPB overtone. One might think that this means at some dimer stretch coordinate value, the two transition frequencies must be have identical frequencies. However, due to the strong coupling between the OPB and OH stretch the transition frequencies of the eigenstates actually exhibit a very substantial avoided crossing when plotted against the dimer stretch coordinate. This behavior will be examined in depth in the next section.

3.5 The Avoided Crossing

In the previous section, it was mentioned how some functionals calculate the hydrogen bonding interaction to be stronger than others. In the case of the PBE functional, the OH stretch

frequencies are calculated to be low enough for the Py-Ac dimer that they fall below those of the OPB overtone at some points along the dimer stretch coordinate. At other points they are higher in frequency than the OPB overtone. Because of this, one might expect that the frequencies of the two transitions will cross at some point when they are plotted against the dimer stretch coordinate. However, such a crossing is never actually observed. Instead an avoided crossing is observed due to the strong coupling between the OPB and OH stretch. These avoided crossings result in the transition frequencies always being separated by at least 250 cm^{-1}.

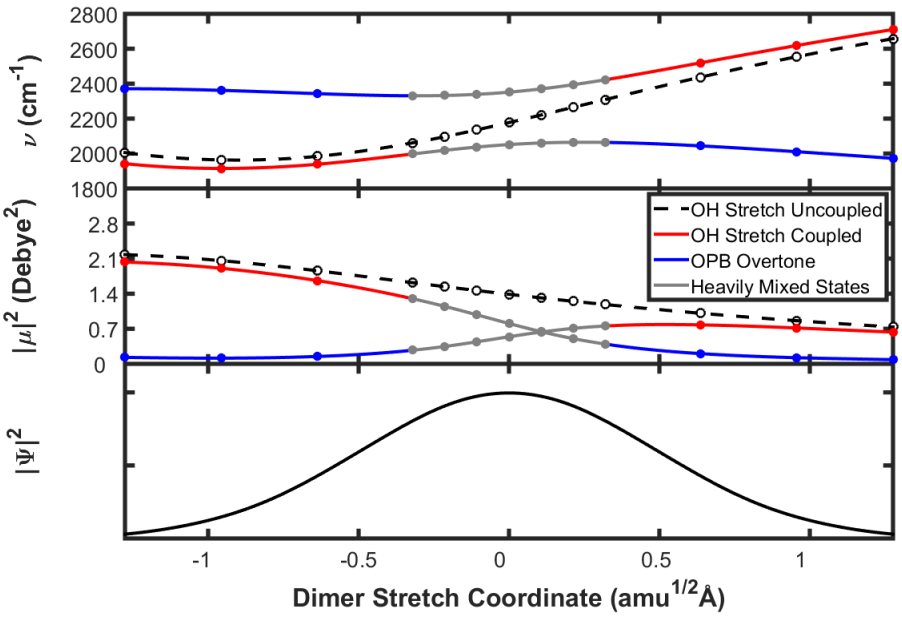

Figure 3.6: Transition frequencies and probabilities versus dimer stretch coordinate of Py-Ac dimer calculated with the PBE functional. The dashed black line corresponds to a calculation that only includes the OH stretch in the Hamiltonian. The solid lines correspond to transitions calculated using both the OH stretch and out-of-plane bend, the identity of which is given by the legend. The top panel shows the frequencies of each transition. The middle panel shows the transition probabilities. The bottom panel shows the distribution of geometries along the dimer stretch coordinate.

The avoided crossing observed when using the PBE functional to calculate the spectrum of the Py-Ac dimer is plotted in Figure 3.6. These avoided crossings result in the identity of each transition becoming more complex. In the region where the avoided crossing occurs, the wavefunction is strongly mixed between the OH stretch fundamental and OPB overtone. Due to this strong mixing, one cannot assign each transition as simply being the OPB overtone or OH stretch fundamental. When the components of the dimer are far apart (large positive dimer stretch coordinate values), the OH stretch (plotted in red) is higher in frequency than the OPB overtone (plotted in blue). When the components of the dimer are close together the OH stretch is lower in frequency than the OPB overtone. When the dimer is near its equilibrium geometry, the first excited state of the OH stretch and the second excited state of the OPB bend are heavily mixed. The transitions in this region are plotted in gray. Thus in systems where the avoided crossing region is inhabited, each of the transitions correspond to a combination of the OH stretch fundamental and the OPB bend overtone.

These avoided crossings are not as substantial for weaker Fermi resonances. To demonstrate this, the 1298 cm^{-1} fingerprint mode presented in section 3.2 will be examined. Like the OPB calculation with the PBE functional, at larger distances between the components of the dimer, the OH stretch is higher in frequency than the overtone of this mode and at smaller distances the overtone is higher in frequency. These transitions come within 26 cm^{-1} of each other (compared with >250 cm^{-1} for the OPB). Although these states do not actually cross, whether the states are modeled as crossing is of very little significance for the computed vibrational features because the avoiding crossing region corresponds to a very small range of geometries. The next few pages will demonstrate this for weak Fermi resonances and show how the approximation of having the states cross begins to break down for larger Fermi resonances.

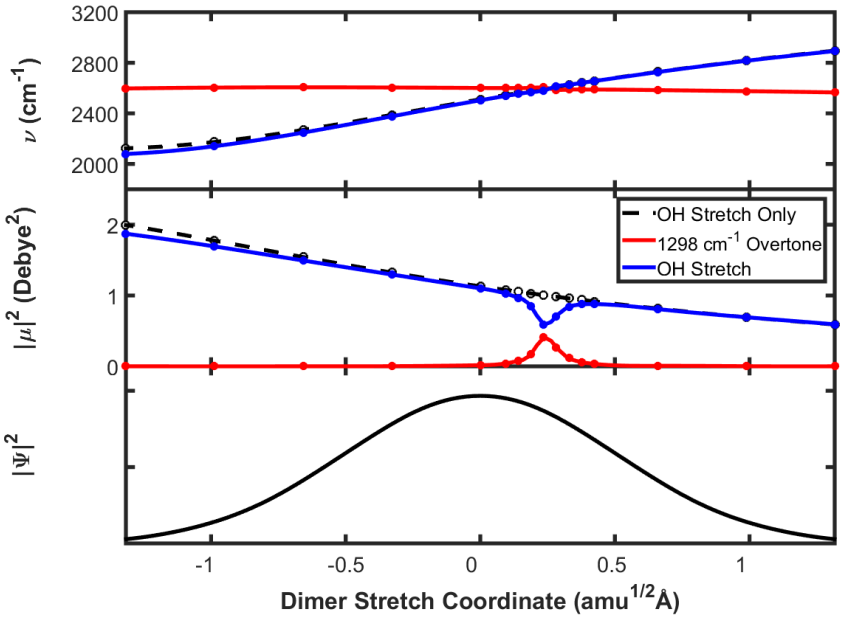

Figure 3.7: Transition frequencies and probabilities versus dimer stretch coordinate for Py-Ac using the 1298 cm^{-1} mode without the avoided crossing. The dashed black line corresponds to a calculation that only includes the OH stretch. The solid lines correspond to transitions calculated with the OH Stretch and 1298 cm^{-1} mode, the identity of which is given by the legend. The top panel shows the frequencies of each transition. The middle panel shows the transition probabilities. The bottom panel shows the distribution of geometries along the dimer stretch coordinate.

Figure 3.7 shows how the transition properties depend on the dimer stretch coordinate in the case of a weak Fermi resonance (the 1298 cm^{-1} mode) without accounting for the avoided crossing. In this calculation, the identity of the final state of each of the transitions is determined by its wavefunction. Although generally speaking these wavefunctions are mixtures of the OH stretch fundamental and the overtone of the bending mode, oftentimes the identity of the wavefunction resembles one state much more closely than the other (especially in cases where the coupling is relatively weak). This makes assigning a meaningful final state possible in most cases. This method of representing the transitions results in the frequencies crossing as can be seen in the top panel of Figure 3.7

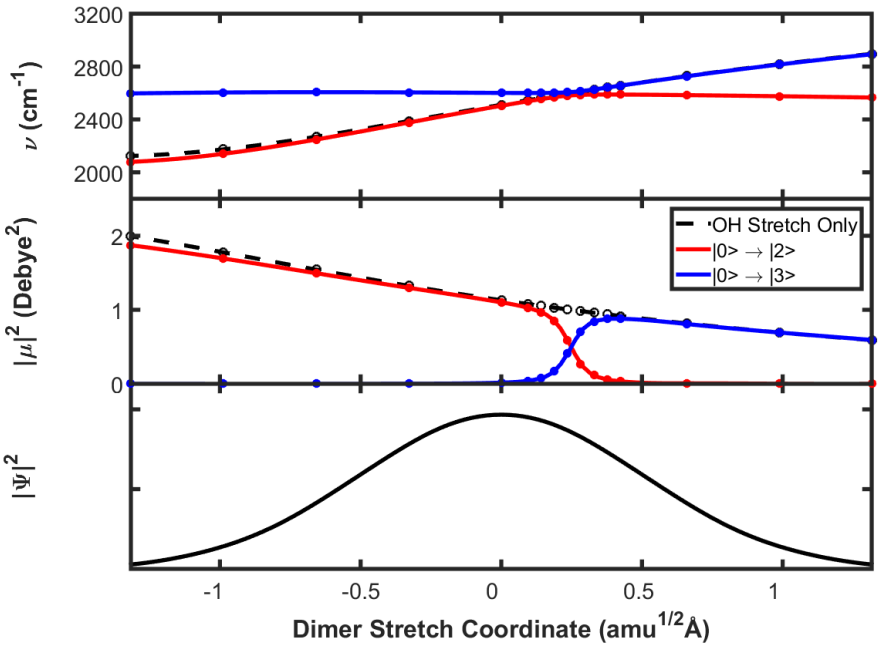

Figure 3.8: Transition frequencies and probabilities versus dimer stretch coordinate Py-Ac using the 1298 cm^{-1} mode with the avoided crossing. The dashed black line corresponds to a calculation that only includes the OH stretch. The solid lines correspond to transitions produced by a calculation that includes the OH stretch and 1298 cm^{-1} mode. The top panel shows the frequencies of each transition. The middle panel shows the transition probabilities. The bottom panel shows the distribution of geometries along the dimer stretch coordinate.

Figure 3.8 shows how the transition properties depend on the dimer stretch coordinate in the case of a weak Fermi resonance (the 1298 cm^{-1} mode) with the avoided crossing included. Accounting for the avoided crossing results in the wavefunction of the final state of each transition changing substantially with the dimer stretch coordinate. Consequently, the final states of the transitions are labeled |2> and |3> since they correspond to the second and third excited states of the Hamiltonian (|1> would be the first excited state of the 1298 cm^{-1} mode). Using this representation, the |0> to |2> transition has almost all of the oscillator strength at dimer stretch coordinate values of less than 0 $amu^{1/2}$Å while the |0> to |3> transition has almost all of the oscillator strength when the dimer stretch coordinate is above 0.5 $amu^{1/2}$Å. For dimer stretch

coordinate values between 0 and 0.5 amu$^{1/2}$Å, both transitions have some oscillator strength, facilitating a smooth transition between the two regions.

Despite Figures 3.7 and 3.8 giving very different descriptions of the two transitions, the overall calculated spectral features are nearly identical for these weak Fermi resonances. The features calculated using both representations are displayed in Figure 3.9. In the calculation without the avoided crossing most of the feature originates from the OH stretch fundamental and the 1298 cm^{-1} overtone produces a small absorbance at 2600 cm^{-1} as was seen in Figure 3.3. The sum of these features has a broad single–hump lineshape. If the avoided crossing is included, the lower frequencies originate from the |0> to |2> transition and the higher frequencies from the |0> to |3> transition. However, the sum of these features is also a broad single-hump lineshape which is nearly identical to the sum of the features calculated without the avoided crossing.

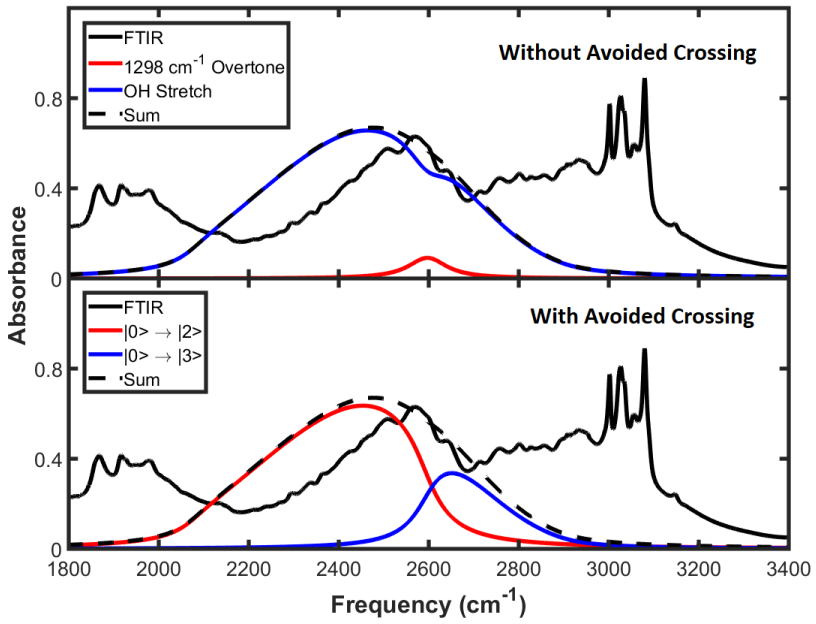

Figure 3.9: Calculated spectra of Py-Ac using 1298 cm^{-1} mode with and without the avoided crossing. Although the inclusion of the avoided crossing significantly impacts the calculated spectral features for each transition, the sums of the spectral features are nearly identical.

Although inclusion of the avoided crossing does not significantly impact the overall calculated vibrational feature for weaker Fermi resonances, performing a calculation without including the avoided crossing for stronger Fermi resonances (such as the OPB) gives rise to a couple of issues. For one, using the final state's wavefunction to determine which transition it corresponds to can be difficult and somewhat arbitrary in regions near the avoided crossing because the states are so heavily mixed. Another problem is that because the states avoid crossing by such a large frequency gap, modeling them as crossing impacts the calculated vibrational features. As an example, the calculated spectra with and without an avoided crossing of Py-Ac using the OPB and PBE functional are displayed in Figure 3.10. In this example, not including the avoided crossing results in higher absorbance between the two peaks of the overall feature and a slightly less sharp lineshape around the higher frequency peak.

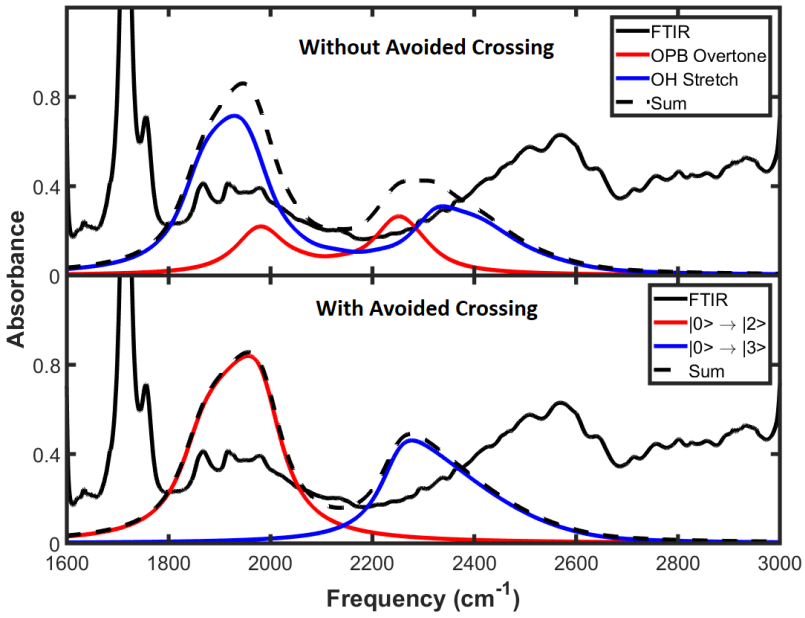

Figure 3.10: Calculated spectra of Py-Ac using OPB and PBE functional with and without the avoided crossing. The sums of the calculated features both have double-hump lineshapes spanning essentially the same frequency range. The exact lineshape of the sums of the features is different in the region between the two peaks and near the higher frequency peak.

Clearly from a standpoint of computing these vibrational features, including the avoided crossing is more important for stronger Fermi resonances than for weaker ones. The overall features calculated for weak Fermi resonances have almost no dependence on the inclusion of the avoided crossing. The features calculated for strong Fermi resonances change more noticeably; however, even these changes are small and largely quantitative. Thus, even though all of the Fermi resonances exhibit an avoided crossing, how much the overall spectral features change by approximating the states as crossing depends on the strength of the Fermi resonance.

These avoided crossings also indicate that conical intersections are present at some points in the high-dimensional space spanned by all of the low-frequency modes. The presence of these vibrational conical intersections requires that all frequencies between the two humps be present for any system with at least two low-frequency modes[33] (even without accounting for homogenous broadening which will be examined more closely in section 3.7). However, whether the geometries corresponding to the conical intersections are significantly inhabited at room temperature is likely dependent on the system.

3.6 The Solvent Dependence

None of the *ab initio* calculations presented in this thesis explicitly account for the effects of the solvent. This is done partially because the work presented here focuses on dimers dissolved in non-polar solvents (CCl_4 when possible) which are unlikely to be heavily influenced by the effects of the solvents and partially because explicitly including solvent molecules in *ab initio* calculations is computationally very expensive. Instead this work relies on implicitly modeling the solvent using the Onsager method at the dielectric continuum level. This restricts

the dimer to a confined cavity and exposes it to an electric field, the strength of which is dictated by the dielectric constant of the solvent.

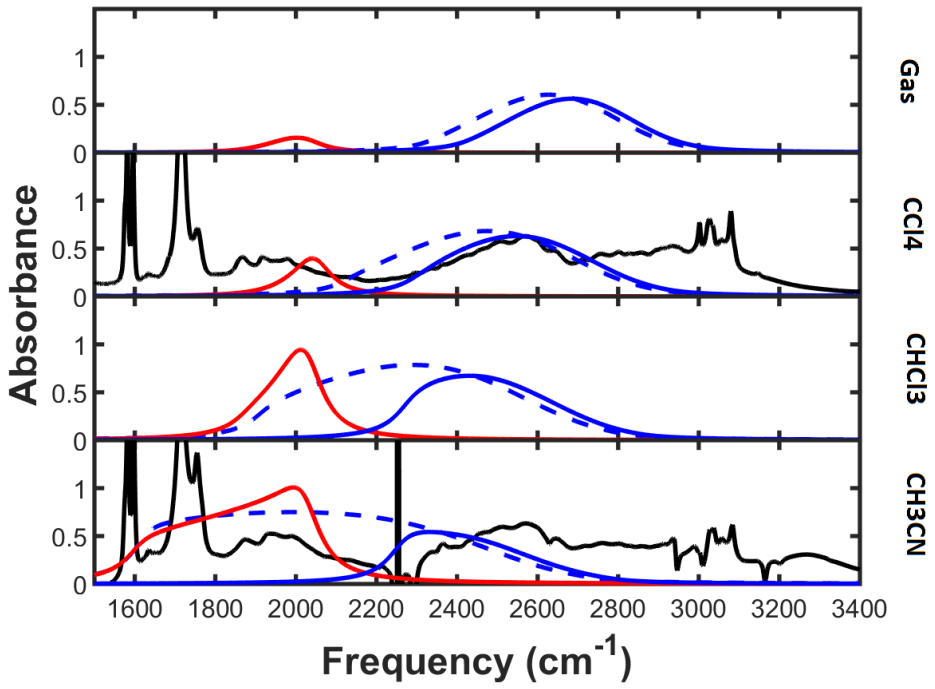

Figure 3.11: Solvent dependence of calculated double-hump feature. The solid blue line corresponds to the higher frequency transition. The solid red line corresponds to the lower frequency transition. The dashed blue line corresponds to a calculation that does not include the OPB. When available, the experimental spectra are plotted in black. The top panel is the gas phase, followed by carbon tetrachloride, chloroform and acetonitrile solvents.

To better understand the role of the solvent in computing these vibrational features, the solvent dependence of the computed features was investigated. The results are displayed in Figure 3.11. They are, in order of dielectric constant, with the gas phase at the top and increasingly polar solvents as one moves to the bottom of the figure. It can be seen that larger dielectric constants lead to lower center frequencies. In the gas phase the OH stretch frequencies are relative high (plotted in blue) and the OPB overtone (plotted in red) is relatively small. As the

dielectric constant increases, the OH stretch frequencies lower and the magnitude of the OPB overtones grow. In the case of acetonitrile the avoided crossing region is substantially inhabited leading to a continuous two-hump feature spanning from 1500 to 2700 cm^{-1}. Although using a dielectric continuum model for acetonitrile is questionable since specific interactions between these types of dimer and the lone pair on acetonitrile's nitrogen have been documented.

Overall, the spectral changes observed from changing the solvent are very similar to the changes observed when functional is changed as was presented in section 3.4. They also have a lot in common with the changes seen when the acid and/or base strength of the components of the dimer are changed which will be presented in Chapter 5.

3.7 Modeling other sources of Broadening

Although low-frequency modes are the main source of broadening in these vibrational features, homogenous broadening from the limited lifetime of the vibrational states is also important. In chapter two, it was mentioned that each of the geometries along the dimer stretch coordinate were modeled as contributing either a Gaussian or Lorentzian profile to the vibrational feature. In all of the results presented up until this point, Lorentzians with a FWHM of 100 cm^{-1} were used to generate the vibrational features. Previous studies of similar features performed by Jen Dreyer used Gaussians with a FWHM of 30 or 40 cm^{-1} to convert his computed stick spectra to a line shape. Broadening with a Gaussian line shape is often done in cases where a limited number of dimensions are included in the calculation and coupling to these other dimensions is likely to result in broadening that is not included in the calculation. However, broadening can also occur simply from the finite lifetime of the vibration state. This broadening gives rise to a Lorentzian line shape. Recent ultrafast experiments have shown that

the double-hump feature of a similar dimer (the 7-azaindole-acetic acid dimer), has a very short vibrational excited state lifetime which predicts that the lifetime associated broadening is at least 100 cm^{-1}. This is likely the second largest source of broadening in these features after the low-frequency mode. This section examines how the way in which sources of broadening other than the low-frequency are modeled impacts the computed spectral features.

Figure 3.12 shows the difference between a Gaussian and Lorentzian profile. Both of the features plotted here correspond to a single transition at 2500 cm^{-1} with a FWHM of 100 cm^{-1}. The main difference between these profiles is that the Lorentzian does not go to zero as quickly as one moves away from the center frequency. From a standpoint of modeling broad vibrational features, this means that Lorentzian profiles will result in broader features that appear more continuous even if they correspond to different transitions.

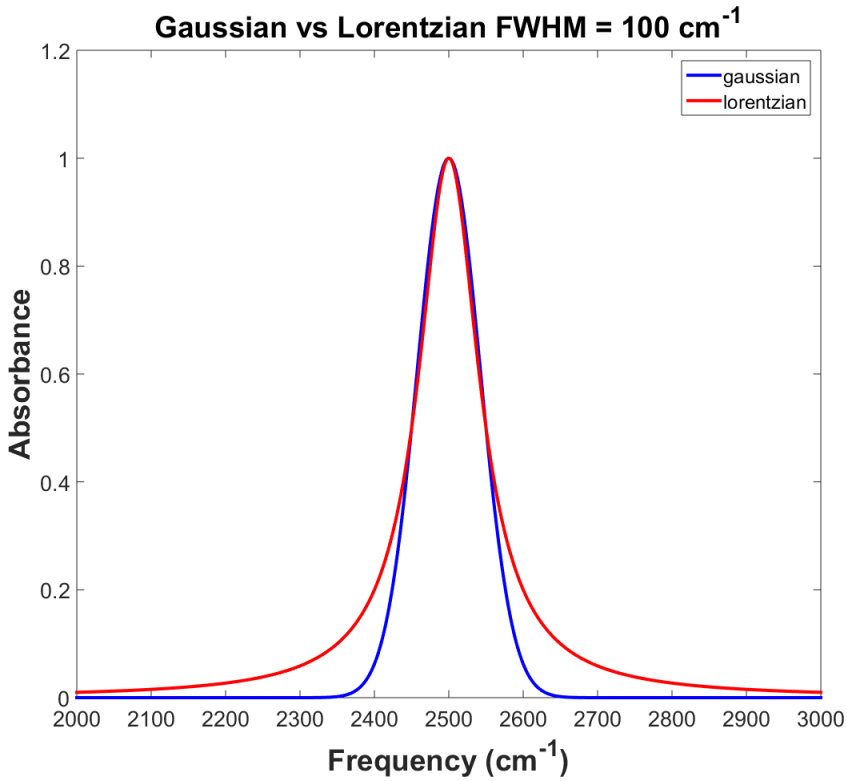

Figure 3.12: Comparison of Gaussian and Lorentzian profiles. Both are centered at 2500 cm^{-1} and have a FWHM of 100 cm^{-1}.

From a standpoint of modeling broad vibrational features, this means that Lorentzian profiles will result in broader features that appear more continuous even if they correspond to transitions separated by significantly more than the FWHM. This can be seen in the calculated features shown in Figure 3.13. When Lorentzians are used, the calculated feature appears continuous (the absorbance does not go to zero between the two humps) as is observed in the FTIR spectrum. However, if Gaussians are used, the features are not calculated to be continuous (unless a much larger FWHM is used).

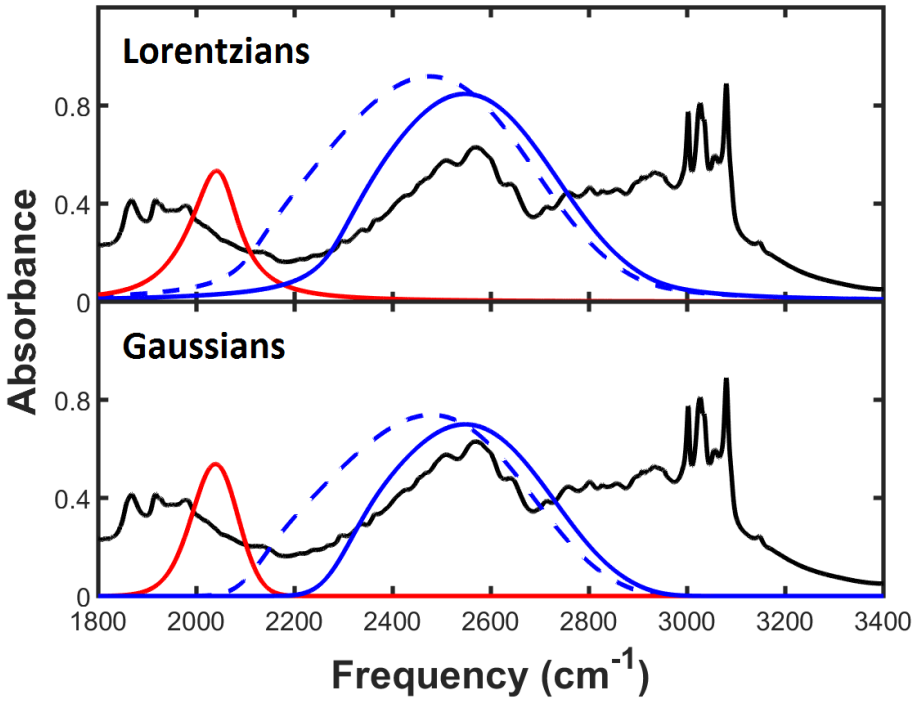

Figure 3-13: Double-hump feature of the Py-Ac dimer calculated using Lorentzians (top) and Gaussians (bottom). Both have a FWHM of 100 cm^{-1}. The features calculated using the OH stretch only is given by the dashed blue lines. The solid colored lines correspond to transitions calculated using both the OPB and OH stretch. The FTIR spectrum is plotted with solid black lines for comparison.

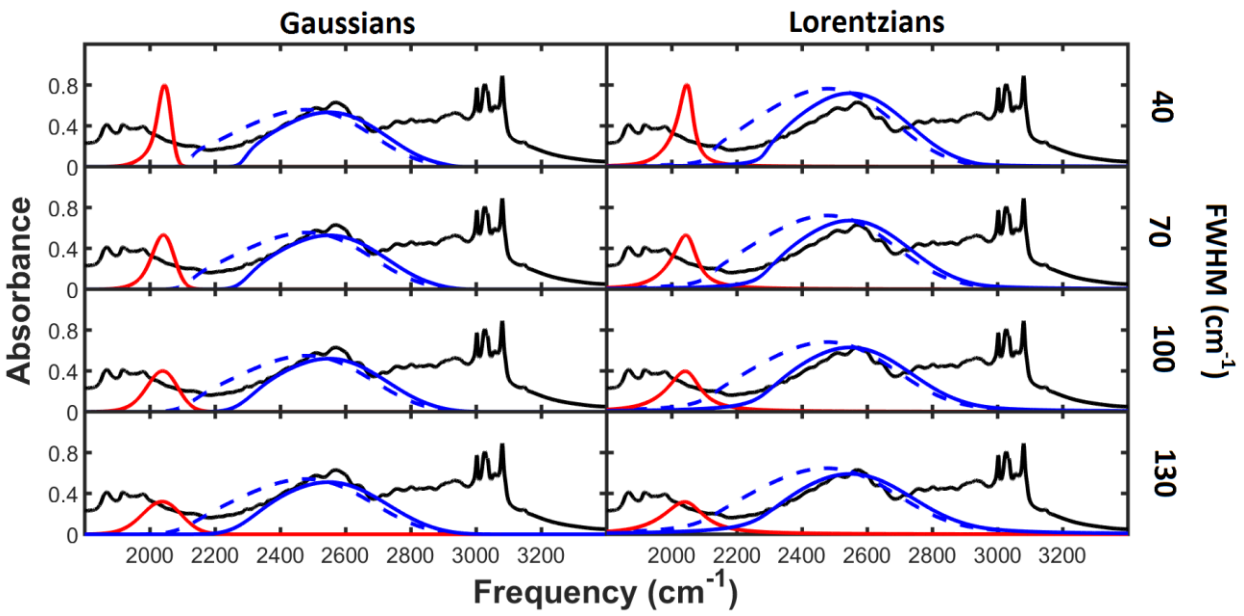

Figure 3.14: Double-hump feature of Py-Ac calculated using Gaussians (left) and Lorentzians (right) with various FWHM. The features calculated using the OH stretch only is given by the dashed blue lines. The solid colored lines correspond to transitions calculated using both the OPB and OH stretch. The FTIR spectrum is plotted with solid black lines for comparison.

The FWHM used for these profiles also has a significant impact on the computed features as is shown in Figure 3.14. Using a FWHM of 40 cm^{-1} as was used by Dreyer in his study of the acetic acid homodimer results in a very narrow OPB feature. This is because the low-frequency mode alone does not broaden this feature substantially. Thus the homogenous broadening assigned to this feature impacts its breadth significantly. Conversely, the low-frequency mode is the main broadening mechanism for the OH stretch feature which means that the homogenous broadening does not impact the overall shape as significantly. Lorentzian profiles with larger FWHM values tend to have the most agreement with experiment since they predict the feature will be continuous and that the low-frequency hump will not be exceeding narrow. Since ultrafast experiments have shown that the lifetime alone likely gives rise to a Lorentzian profile with a FWHM of at least 100 cm^{-1} and those profiles produce good agreement with the FTIR

spectrum, we have used 100 cm^{-1} broad Lorentzians to model homogenous broadening in all of the results presented in this thesis.

3.8 Similar Systems

The double-hump vibrational feature of Py-Ac is present in the spectra of numerous dimers between carboxylic acids and nitrogen-containing aromatic bases.[10,11] Some of these other dimers will be examined in Chapter 5 which presents the acid and base strength dependence of the OH vibrational feature of dimers of pyridines and carboxylic acids. The spectrum of the 7-azaindole-acetic acid (7AI-Ac) dimer also has this unusual feature. This system is particularly interesting because it contains two hydrogen bonds that collectively form a six-member ring. This makes it very similar in structure to DNA base pairs. The OH stretch and OPB feature was calculated for this dimer. The results are displayed in Figure 3.15. The calculated NH feature is also included in this figure. This feature was calculated without including coupling to any fingerprint modes or the OH modes.

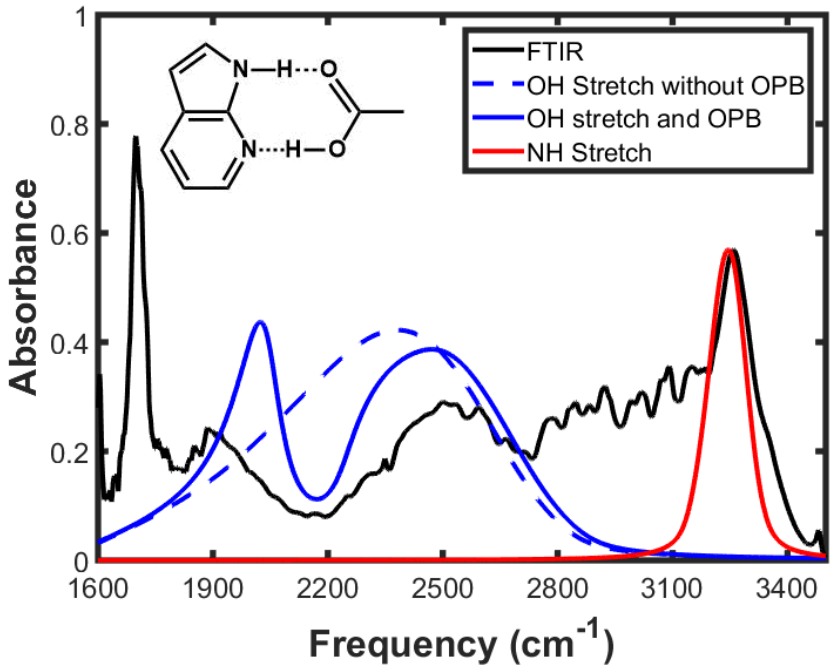

Figure 3.15: Calculated vibrational features of the 7AI-Ac dimer. The solid and dashed blue lines correspond to calculations of the OH stretch with and without the out-of-plane bend. The solid red line corresponds to a calculation of the NH stretch. The OH stretch features use 100 cm^{-1} FWHM Lorentzians to account for homogenous broadening while the NH feature uses 40 cm^{-1} FWHM Lorentzians.

Like the Py-Ac dimer, the double-hump structure of this dimer is well reproduced using the dimer stretch method. The width and location of the sharper NH feature at 3250 cm^{-1} are also well reproduced. The absorbance in the region between the two features (2700 to 3000 cm^{-1}) likely corresponds to several small Fermi resonances. This dimer has many fingerprint modes with fundamental frequencies between 1350 and 1500 cm^{-1} which contain OH and/or NH bending character. These modes are likely to have Fermi resonances with the NH and/or OH stretch giving rise to absorbance in the 2700 to 3000 cm^{-1} portion of the spectrum.

The coupling between the OH and NH has also been a topic of investigation for this system. Pump-probe and 2D-IR measurements have found that significant coupling exists

between the OH and NH stretches in this dimer.[34,35] The dimer stretch method was utilized to examine the coupling between the OH an NH stretches in this system. The results of this calculation indicate that these oscillators are coupled. This coupling gives rise to a small Fermi resonance between the NH stretch fundamental and OH stretch overtone. However, like the weak Fermi resonances presented in section 3.2, this coupling does not have a significant impact on the FTIR spectrum. However, the calculated results show that it has a larger impact on the vibrational states higher in the potential. Experimental results show this coupling impacts the vibrational dynamics as well. Consequently this coupling is more spectrally significant for higher order experiments (e.g. pump-probe and 2D-IR measurements).

3.9 Conclusion

Py-Ac is one of the simpliest dimers that exhibit the double-hump vibrational feature that is found in many dimers between carboxylic acids and nitrogen-containing aromatic bases. The calculations presented in this chapter show that the breadth of this double-hump structure is largely due to dimer stretch modes modulating the OH stretch frequency. They also indicate that the double-hump lineshape is derived from a large Fermi resonance with the out-of-plane bend. The substructure on the double-hump is likely due to less intense Fermi resonances of other bending modes. In the next chapter an even broader vibrational feature will be examined. Spanning over 1500 cm^{-1} it is one of the broadest vibrational features observed in the spectra of hydrogen-bonded dimers.

4. The Hadži ABC Structure

4.1 Introduction

Although dimers with medium and strong hydrogen bonds have vibrational features spanning several hundred wavenumbers, very strong hydrogen bonds can give rise to even broader features. Some of the strongest hydrogen-bonded dimers are homodimers of phosphinic, phosphoric and selenic acids. These dimers exhibit a characteristic three-hump vibrational feature that spans over 1500 cm^{-1} and is frequently referred to as the Hadži ABC structure. This name comes from Prof. Dusan Hadži who was among the first researchers to extensively document this feature in the 1950s and 60s.[9,13,14] The ABC refers to the original labels for each of the three peaks. Despite a large amount of experimental work being done on this feature in the middle of the 20th century, the origin of this feature was still not very well understood. In 2000, the first theoretical study of this feature was published by Gonzalez, et al.[36] In this study density functional theory was used to obtain optimized geometries and perform normal mode analysis on the phosphinic acid and dimethylphosphinic acid homodimers. This study showed that the out-of-plane bend (OPB) and in-plane bend (IPB) modes had fundamental frequencies that corresponded to roughly half the frequency of the highest and lowest frequency humps of the structure. This showed that a plausible explanation for the three-hump structure was Fermi resonances between the OH stretch and two OH bending modes. More recently, Hanna and co-workers published a study which used an empirical model to calculate the three-hump feature.[15] Their model included the OH stretch, both bending modes and a dimer stretch mode that was adiabatically separated from the other modes. Its contribution was modeled by having the OH stretch frequency depend linearly on the dimer stretch mode's coordinate. Using this model they were able to reproduce the three-hump structure as well as the deuterated isotopologue's one

hump structure. Although both of these studies provided some evidence that this feature originates from the OH stretch, the OH bends and dimer stretch modes, neither of these studies computed the coupling between these modes from first principles. This chapter presents a study that reproduces this exceedingly broad feature from first principles using the dimer stretch method.

4.2 Method

Although many dimers exhibit the Hadži ABC structure, the vibrational spectrum of the dimethylphosphinic acid homodimer was the focus of this study. This particular dimer was selected because it was commercially available for obtaining FTIR spectra and is one of the simplest dimers that exhibit the Hadži ABC structure making it computationally practical. One of the difficulties of calculating this feature is the sheer number of vibrational modes that contribute to it. Because this dimer has two hydrogen bonds, there are asymmetric and symmetric versions of each of the bends and the stretches. Combined with a dimer stretch mode, this totals seven vibrational modes which are displayed in Figure 4.1.

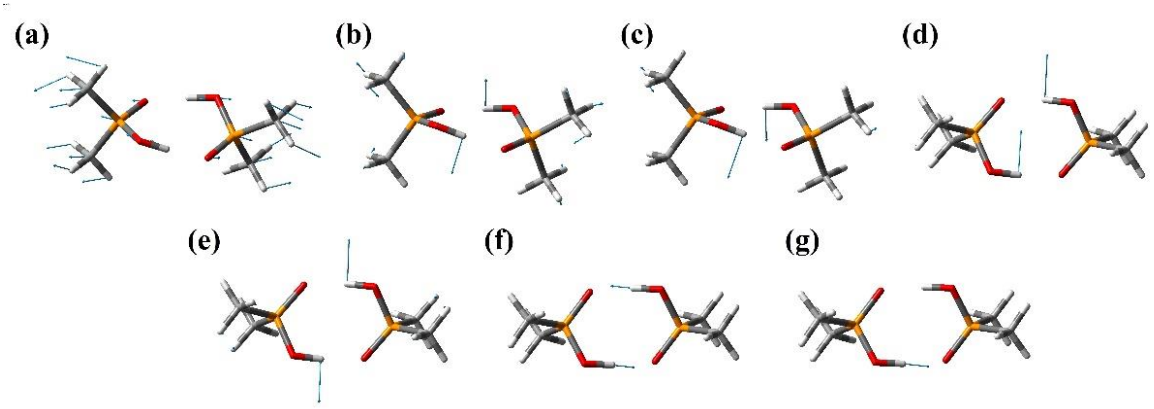

Figure 4.1.Vibrational modes used in calculation of Hadži ABC structure. (a) dimer stretch (b) symmetric OPB (c) asymmetric OPB (d) symmetric IPB (e) asymmetric IPB (f) symmetric OH stretch (g) asymmetric OH stretch. In the harmonic approximation, the fundamental of these vibrational modes occur at 146, 903, 924, 1247, 1295, 2893 and 2980 cm^{-1} respectively.

For a system of this size, computing a seven-dimensional potential energy surface is computationally impractical. Consequently, the number of dimensions was reduced by focusing on only one of the hydrogen bonds. Coupling of the vibrations of neighboring hydrogen bonds (known as Davydov coupling) is eliminated when only one of the hydrogen bonds is considered. Studies disagree on how important this coupling is in terms of describing the vibrational feature.[7,15] Coordinates for vibrations involving just one of the hydrogen bonds were obtained from linear superpositions of the molecular modes shown in Figure 4.1 using equations 4.1 through 4.3. In these equations symmetric, asymmetric and OH stretch are abbreviated as sym., asym. and STR.

$$\boldsymbol{Q_{OPB} = Q_{sym.\ OPB} + Q_{asym.\ OPB}} \quad \textbf{(4.1)}$$

$$\boldsymbol{Q_{IPB} = Q_{sym.\ IPB} - Q_{aysm.\ IPB}} \quad \textbf{(4.2)}$$

$$\boldsymbol{Q_{STR} = Q_{sym.\ STR} + Q_{asym.\ STR}} \quad \textbf{(4.3)}$$

This effectively reduces the number of dimensions to four (the dimer stretch, OPB, IPB, and OH stretch) at the cost of eliminating the Davydov coupling. Transition frequencies were calculated using three-dimensional Hamiltonians (OPB, IPB and OH stretch). Six transitions were found with frequencies in the region associated with the Hadži ABC structure. Assigning each of the final states of these transitions to a specific vibrational state is difficult due to several avoided crossings occurring in this system. From examining the wavefunctions of the final states of these transitions, it is clear that these states correspond to linear superpositions of the |002>, |011>, |020>, |100>, |003> and |012> states (using the ket notation $|\ \nu_{STR}\ \nu_{IPB}\ \nu_{OPB}\ >$). With the three-dimensional Hamiltonian used to calculate these states, the final states of the six transitions correspond the 3rd through 8th excited states. (The first and second excited states are the first

excited states of the two bending modes which are too low in frequency to contribute to the structure).

The spectra of the deuterated isotopologue was calculated using the potential energy surface of the protonated isotopologue. To account for the increase in the mass of the OH hydrogen, the coordinate values of the OH modes were weighted by the square root of two.

4.3 The Protonated Isotopologue

How the frequencies and oscillator strengths of the six transitions that contribute to the Hadži ABC structure depend on the dimer stretch mode for the protonated isotopologue of the dimer is displayed in Figure 4.2. The frequencies of these transitions are displayed in the top panel. Overall the two bending modes give rise to several overtone and combination states. The OH stretch frequency is heavily dependent on the dimer stretch coordinate. As the OH stretch frequency comes close to a combination or overtone of a bending mode(s), an avoided crossing takes place. When the components of the dimer are far apart (1.5 $amu^{1/2}$Å) the OH stretch fundamental is the |0> to |8> transition. This is determined by examining the wavefunction of state |8>. As the components of the dimer come together, a small avoided crossing occurs around 1.3 $amu^{1/2}$Å between the OH stretch and the |012> state. This results in the |0> to |7> transition acquiring oscillator strength at the expense of the |0> to |8> transition.

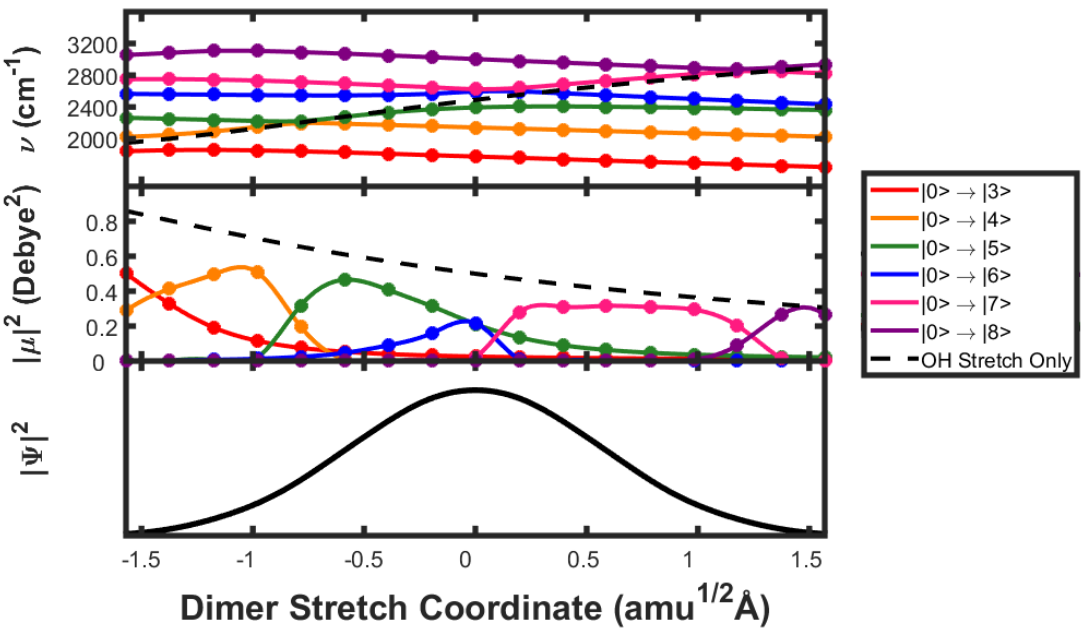

Figure 4.2: Transition frequencies and probabilities versus the dimer stretch coordinate for the protonated dimethylphosphinic acid dimer.

As the components of the dimer come even closer together, a small avoided crossing between the OH stretch and the |003> state and a larger avoided crossing between the OH stretch and the IPB overtone occur near 0.1 amu$^{1/2}$Å. This results in the |0> to |7> transition losing oscillator strength while the |0> to |5> and |0> to |6> transitions gain oscillator strength. As the OH stretch continues to move to lower frequencies, the oscillator strength is shifted almost entirely to the |0> to |5> transition. Near -0.8 amu$^{1/2}$Å an avoided crossing of the OH stretch with the |011> state occurs. At even lower dimer stretch coordinate values, the OH stretch becomes the |0> to |4> transition. Below -1.0 amu$^{1/2}$Å, part of another avoided crossing is observed, this time between the OH stretch and the OPB overtone.

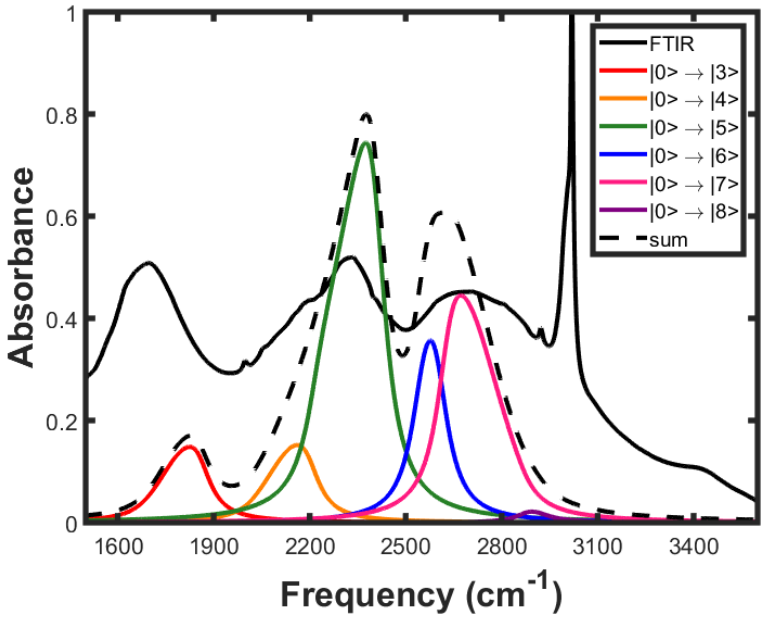

Figure 4.3: Calculated OH vibrational feature of the protonated dimethylphosphinic acid dimer.

The numerous avoided crossings give rise to the unusual lineshape of this feature. The feature calculated from all of these transitions is displayed in Figure 4.3. Like the feature in the experimental spectrum, the sum of all of the calculated features has a very broad three-hump structure. The calculated peak locations of the two higher frequency humps agree quite well with experiment. The peak of the lower frequency hump is calculated to be about 100 cm^{-1} higher in frequency than is observed experimentally. The experimental feature is significantly broader than the calculated feature which could result from the dimer stretch not adequately sampling all possible geometries. This could also be due to underestimating the amount of homogenous broadening in this dimer (which was modeled using 100 cm^{-1} FWHM Lorentzians). The lower frequency hump is also calculated to be much smaller in intensity than the other two humps whereas the experimental spectra show them as being very similar in intensity. This may be due to the functional. Repeating the calculation with a PBE functional results in lower OH stretch

frequencies which produce a higher intensity lowest frequency hump and a lower intensity highest frequency hump. The solvent could also be playing a small role in the discrepancies observed between theory and experiment. The calculations were performed assuming a carbon tetrachloride solvent. However due to the limited solubility of this dimer in carbon tetrachloride, the experimental spectrum of the dimer dissolved in chloroform is plotted. If the calculation were performed with a chloroform solvent, the OH stretch frequencies may be shifted to lower frequencies as was observed for the Py-Ac dimer in section 3.6. However, two-dimensional Hamiltonian calculations (the OH stretch and one of the bends) which were performed with a chloroform solvent, show that this shift is very small and does not have a significant impact on the calculated feature. Overall the results of these calculations provide additional evidence that this unusual feature originates from the OH stretch and bending modes being modulated by lower frequency modes.

4.4 The Deuterated Isotopologue

Oftentimes upon deuteration, the Hadži ABC structure not only changes its frequency range, but also loses its characteristic three-hump structure. The lineshape usually becomes a single hump. In the case of the dimethylphosphinic acid dimer dissolved in chloroform, this hump is centered near 2100 cm^{-1}. To explore if this behavior was captured by the dimer stretch method, the calculation was repeated for the deuterated isotopologue.

How the transition properties of this isotopologue depend on the dimer stretch coordinate is displayed in Figure 4.4. Overall the dependence of the transitions on the dimer stretch coordinate is very similar to the protonated isotopologue. One difference is that the OH stretch is shifted to higher frequencies relative to the bending modes. This is likely due to the potential of the OH

stretch being more anharmonic than that of the bending modes. It also shifts all of the avoided crossings to lower dimer stretch coordinate values. This results in the avoided crossing with the OPB overtone (the lowest frequency avoided crossing) being shifted to a dimer stretch coordinate value that is so sparsely populated that features associated with the |0> to |3> transition will be even smaller than observed for the protonated isotopologue.

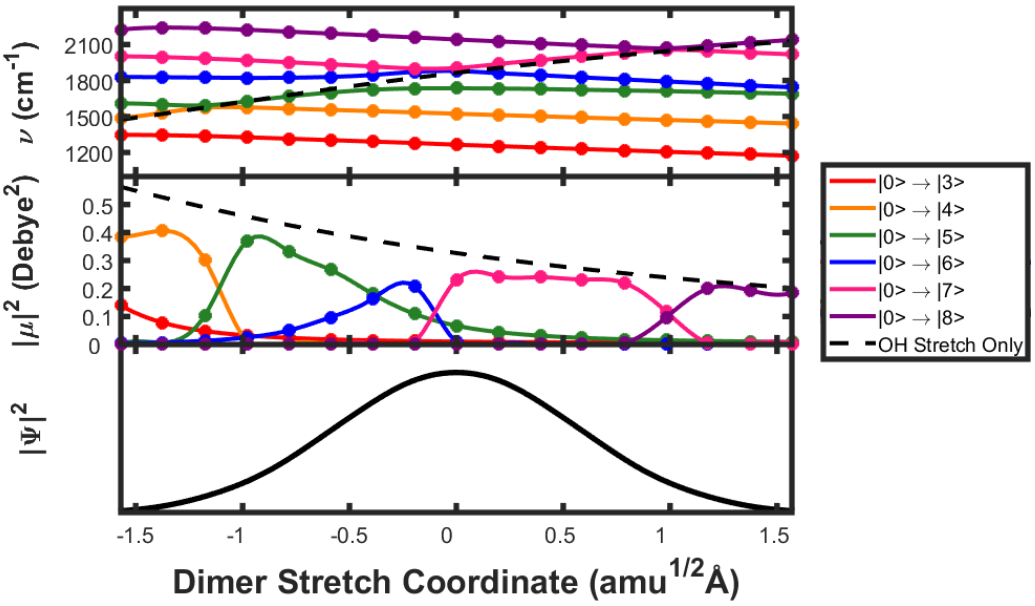

Figure 4.4: Transition frequencies and probabilities versus the dimer stretch coordinate for the deuterated dimethylphosphinic acid dimer.

The calculated vibrational feature of the deuterated isotopologue is displayed in Figure 4.5. The calculated sum of all of the transitions shows one broad hump with a small local minimum of intensity near 1800 cm^{-1}. The calculated results also show that the |0> to |3> feature will be small in intensity and appear near 1300 cm^{-1} with a slight overlap with the rest of the feature. Like in the case of the protonated isotopologue, the experimental feature is significantly broader than the calculated feature. Overall this calculation shows how a three-hump structure

can transform into a single hump. The lowest frequency hump becomes less intense due to the OH/OD stretch frequencies becoming higher relative to the bending overtones and combinations. The remaining transitions become closer in frequency (since deuteration approximately divides the OH/OD frequencies by the square root of two) resulting in a feature that appears as one broad structure.

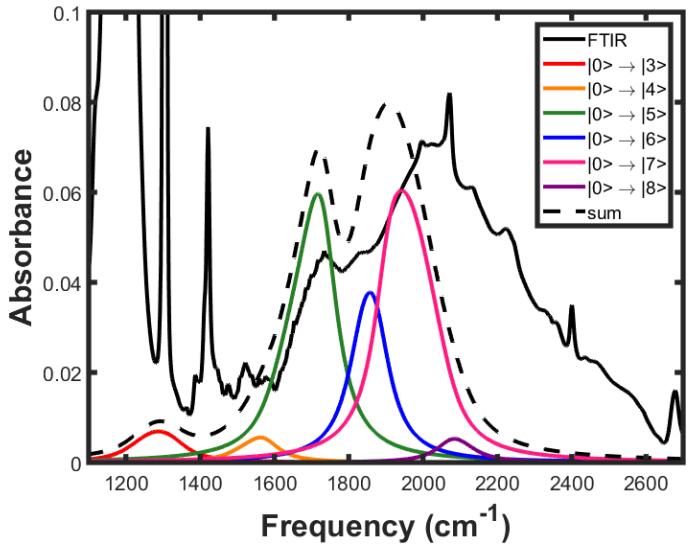

Figure 4.5: Calculated OD vibrational feature of the deuterated dimethylphosphinic acid dimer.

The results of this calculation also indicate that Fermi resonance interactions are a significant part of the origin of this vibrational feature even though it does not have a multi-hump lineshape. This can be observed by examining Figure 4.4. The middle panel shows that at several points along the dimer stretch coordinate, multiple transition have significant oscillator strength. This indicates Fermi resonances (and other forms of coupling) contribute significantly to the vibrational feature, which contrasts with the results of Hanna's calculation of this feature which relied on an empirical model. This demonstrates a potential problem with using empirical models

to understand the origin of these feature. A single-hump lineshape can be reproduced without Fermi resonance interactions. However, as the results of this study show, the presence of a single-hump lineshape does not prove that Fermi resonance interactions do not contribute to the feature. The presence of transitions to combination states (each with varying degrees of coupling with the OH stretch fundamental) also makes developing a purely empirical model based off of the infrared spectrum challenging. Consequently, there are significant advantages to computing these features from first principles in order to better understand their origin.

4.5 Conclusion

Many homodimers of phosphinic, phosphoric and selenic acids have very strong hydrogen bonds. These strong hydrogen bonds produce a three-hump vibrational feature often referred to as the Hadži ABC structure. This structure spans over 1500 cm^{-1} and is among the broadest vibrational features observed in the spectra of hydrogen-bonded dimers. Calculating this feature with the dimer stretch method provided additional insight into its origin. This calculation demonstrated that the broad three-hump structure originates from the OH stretch and various combination and overtone bending states being modulated by dimer stretch modes. The same method was applied to understanding the single-hump vibrational feature found in the deuterated isotopologues of these systems. With these isotopologues application of this method showed how Fermi resonances can be contributing to a feature even if its lineshape resembles a single-hump. Clearly from comparing the results presented in this chapter and the previous one, different strength hydrogen bonds and different dimers can have very different vibrational features. The next chapter will present a systematic investigation of how hydrogen bond strength impacts these types of features by examining how these features change with the acid and base strength of the components of the dimers.

5. The Hydrogen Bond Strength Dependence of the Vibrational Features of Pyridine-Carboxylic Acid Dimers

5.1 Introduction

Not all hydrogen bonds are created equal. The dissociation energy of hydrogen bonds has been documented to vary by over one and a half orders of magnitude (from 1.0 to 40 kcals/mole).[37] A number of properties have been found to correlate with the dissociation energy including the A -- B distance (of a hydrogen bond A-H -- B), the bond angle, the shift in the X-H frequency and the oscillator strength.[2,3,27,37] As an example of these correlations, the OH frequency versus the O -- O distance of several hydrogen-bonded systems is plotted in Figure 5.1

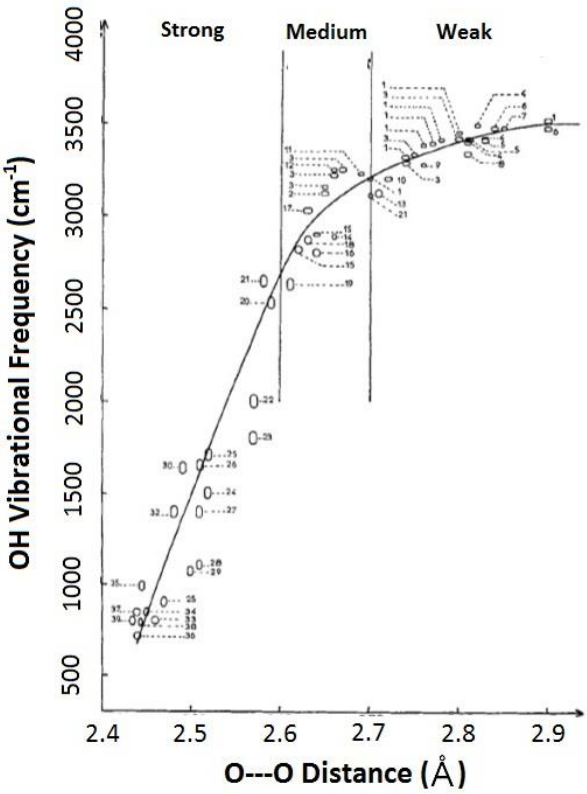

Figure 5.1: Center OH stretch frequency versus O -- O distance for various systems with (O-H – O hydrogen bonds). This is a modified figure from Reference 2.

Figure 5.1 shows how the center OH stretch frequency depends on the O – O distance for various systems with O-H – O hydrogen bonds. The OH stretch frequencies were obtained using infrared spectroscopy and the O – O distances were obtained using x-ray crystallography. From examining the curve, the OH stretch frequency is clearly very dependent upon the O – O distance. Longer O – O distances (which correspond to weak hydrogen bonds) have relatively high OH stretch frequencies, usually above 3200 cm^{-1}. In these systems the hydrogen bond produces a frequency shift of less than 600 cm^{-1}. Medium strength hydrogen bonds have slightly shorter O – O distances and lower OH stretch frequencies. Strong hydrogen bonds can have O – O distances below 2.5 Å and center OH stretch frequencies of less than 1000 cm^{-1}.

One way to systematically tune the strength of a hydrogen bond is to adjust the pK_A of the molecules that form it.[38,39] In the case of acid-base dimers with the proton bound to the acid, the strength of the hydrogen bond can be increased by increasing the strength of the acid or the base. Thus by tuning the acid or base strength, the strength of the hydrogen bond of these systems can be adjusted systematically. In order to explore how the broad vibrational features of hydrogen-bonded dimers depend on the hydrogen bond strength, the dimer stretch method was applied to calculating the OH features of dimers of various carboxylic acids and pyridines of different acid and base strengths.

In addition to providing insight into how these feature change with hydrogen bond strength, calculating the acid and base dependence of these features gives much needed insight into how these types of vibrational features are expected to change during ultrafast pump-probe measurements of photoacids. These experiments electronically excite a photoacid with a visible photon which changes the acid's pK_A. This pK_A change often leads to the proton transferring to the other molecule participating in the hydrogen bond. The dynamics of this process can be

probed with transient UV/visible or infrared spectrscopy.[40–45] Interpreting the results of these experiments is difficult though because it is not clear if the intermediate spectral features that are measured originate from an intermediate geometry created by proton transfer or if they simply are the result of the pK_A change before any proton transfer occurs. This has led to controversies in the literature. By understanding how the features of hydrogen-bonded systems change with pK_A, one can gain better insight into the meaning of the features measured during these experiments.

5.2 Method

The dimer stretch method was used to calculate the vibrational features of the dimers formed by carboxylic acid and pyridines of varying acid and base strength. The series of acids consisted of trifluoroacetic acid (tFAc), chloroacetic acid (ClAc), and acetic acid (Ac). The pyridines base series consisted of 2-chloropyridine (2ClPy), 3-chloropyridine (3ClPy), pyridine (Py), 2,4,6-trimethylpyridine (tMePy) and 4-dimethylaminopyridine (dMeAPy). The structures of each acid and base are displayed in Figure 5.2. The pK_A or conjugate acid pK_A are displayed below each structure. These acids and bases were selected to provide a range of acid and base strengths with minimal changes to the structure of the dimer. All of the combinations of these three acids and five bases resulted in 15 different dimers. The optimized geometries of all of these dimers are planar.

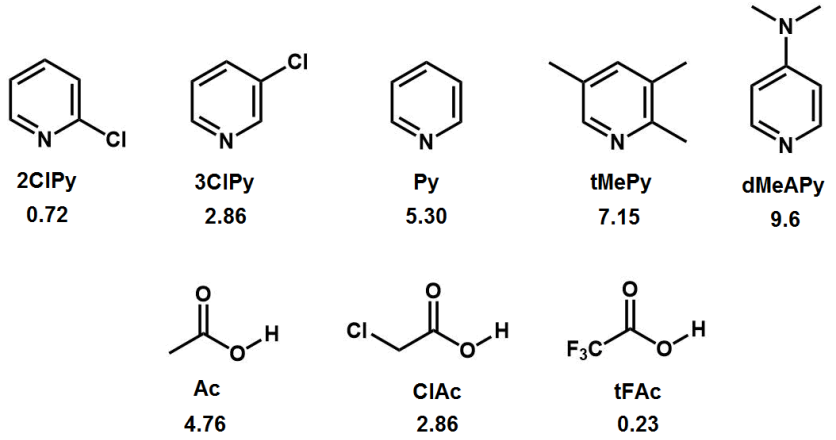

Figure 5.2: Acid and base structures. The top row shows the bases and the bottom row shows the acids that makeup the acid-base dimers examined in this study. The pK_A of each acid and of the conjugate acid of the each base is displayed below each structure.[46–49]

The computational method used to calculate the OH feature of these dimers is almost identical to that presented in Chapter 2. However since the OH features of these dimers extend to much lower frequencies than any presented previously, the coordinates of the high-frequency modes were defined differently. Unlike the previous calculations where the high-frequency modes' coordinates were defined by the normal modes, the OH stretch was defined by moving the hydrogen along the OH bond vector and the OPB was defined by moving the hydrogen perpendicular to the plane defined by the heavy atoms of the dimer. These definitions were used in place of the normal modes to keep the coordinates consistent across the dimer series. The atoms involved in each OH stretch would change if normal mode coordinates were used since some of the dimers have OH stretch normal modes that include carbonyl motion.

Additionally, it is worth clarifying that this study focused on the OH stretch fundamental and the OPB overtone. Other transitions are not included in the computed spectra including the OPB fundamental, the OH stretch overtone and various combination states. These are not

included due to their small spectral contribution relative to the OH stretch and OPB overtone. Additionally, the OPB bend overtone was only allowed oscillator strength if it was within 600 cm^{-1} of the OH stretch fundamental frequency. This was done to avoid coupling between the OH stretch overtone and OPB overtone. This coupling can result in the OPB having a small oscillator strength even when it is not near the OH stretch fundamental. However, since this interaction leads to the OPB overtone having a relatively small oscillator strength (compared with when it couples to the OH stretch fundamental) and is not the focus of this study, this interaction was eliminated by requiring the OPB to be within 600 cm^{-1} of the OH stretch fundamental for it to have oscillator strength.

5.3 Calculated Spectra

Figure 5.3 displays the calculated spectra for all of the dimers investigated in this study. In this figure, the dashed blue lines correspond to spectra calculated using one-dimensional (OH stretch only) Hamiltonians, while the solid blue lines correspond to the spectra calculated using two-dimensional (OH stretch and OPB) Hamiltonians. For most of the dimers, the solid red lines are the experimental FTIR spectra of the dimers dissolved in carbon tetrachloride which are plotted for comparison. Two of the dimers (ClAc-dMeAPy and tFAc-dMeAPy) are not soluble in carbon tetrachloride and consequently the red lines correspond to FTIR spectra of these dimers dissolved in chloroform. They exhibit a large feature centered near 2900 cm^{-1} which corresponds to the C-H stretch of the solvent. Each pink line corresponds to the FTIR spectra of the base only which is plotted to show which features correspond to the base. The acid homodimer spectra of each acid are plotted in cyan at the bottom of each row. Each column corresponds to a different acid and each row corresponds to a different base. Moving from left to right, the acid strength increases. Moving from the top to the bottom, the base strength increases.

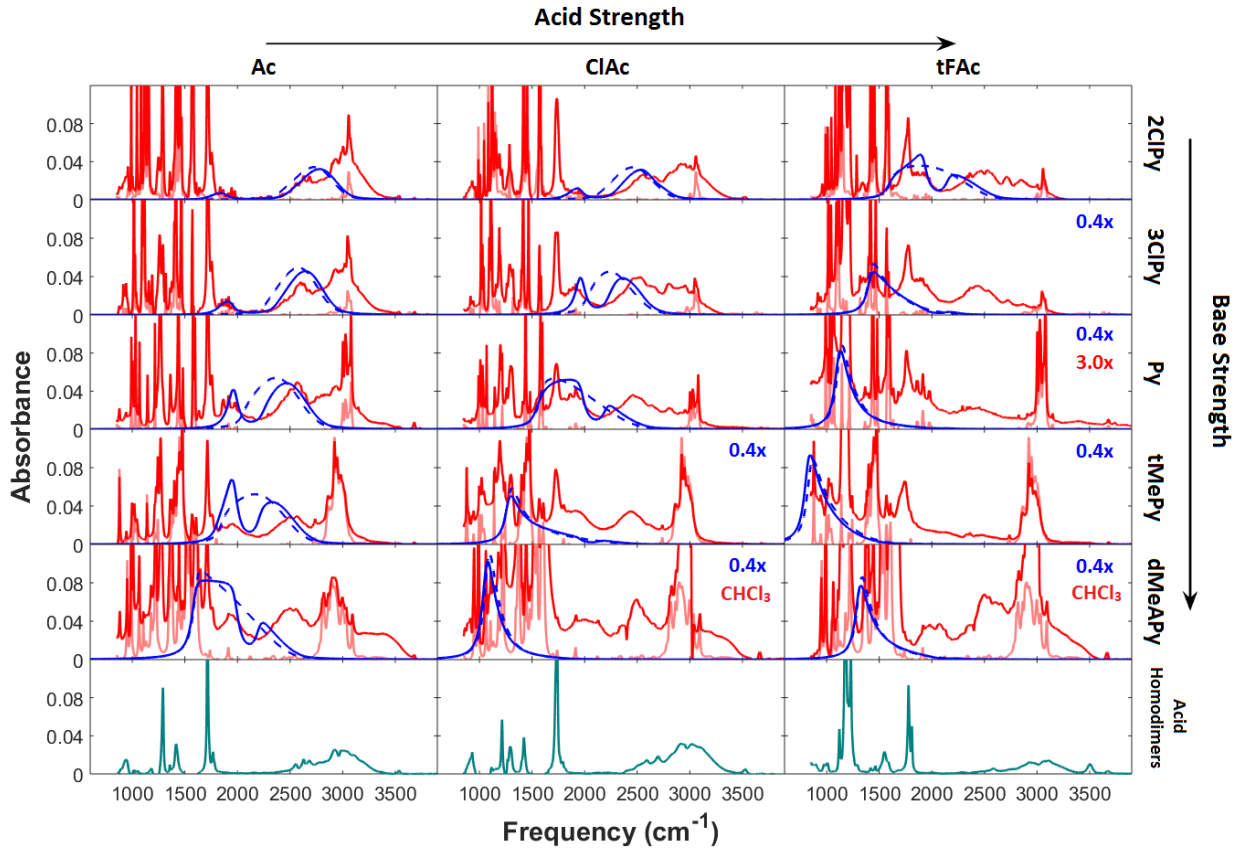

Figure 5.3: Calculated and FTIR spectra of dimers as a function of the acid and base strength of their components. Each column corresponds to a different acid. From left to right they are in order of increasing strength (Ac, ClAc, tFAc). Each row corresponds to a different base. From top to second from the bottom they are in order of increasing strength (2ClPy, 3ClPy, Py, tMePy, dMeAPy). The bottom row shows spectra of the acid homodimers. The solid and dashed blue lines are calculated OH features with and without including the OPB in the Hamiltonian respectively. The solid red lines are experimental FTIR spectra of the dimers plotted for comparison. The solid pink lines are FTIR spectra of the bases only.

The left column of Figure 5.3 shows the spectra of the Ac dimers. In the case of the weakest base bound to the weakest acid (top left: 2ClPy-Ac), the OH stretch frequencies are calculated to be relatively high with a center frequency at about 2800 cm^{-1}. In this dimer, the overtone of the OPB near 1800 cm^{-1} is well separated from the OH stretch frequencies. This

results in a relatively weak Fermi resonance interaction. As the strength of the base bound to Ac increases, the hydrogen bond strength increases giving rise to lower OH stretch frequencies. As the OH stretch frequencies become lower, the intensity of the OPB fermi resonance increases substantially. The Py-Ac, tMePy-Ac and dMeAPy-Ac dimers are calculated to have a continuous double-hump feature which is in agreement with experiment. These continuous double-hump features arise from the avoided crossings that occur at points along the dimer stretch coordinate that are inhabited at room temperature. Unlike 2ClPy-Ac where the humps are well separated, each of the humps in these systems cannot be interpreted as coming from either the OH stretch or the OPB bend overtone. Instead each of the humps in the spectra of these dimers are derived from a combination of the OH stretch fundamental and OPB overtone. As the base strength increases, the avoided crossing is moved to larger dimer stretch coordinate values resulting in more geometries where the OH stretch frequency is well below the OPB overtone. This gives rise to broader lower frequency humps as observed in the spectra of dMeAPy-Ac.

The middle column of Figure 5.3 shows the calculated and experimental spectra for dimers between ClAc and the pyridine base series. The calculated spectra for the weakest base (2ClPy) consists of two features connected by a small plateau of absorbance. The higher frequency hump is centered near 2550 cm^{-1} and corresponds to the fundamental of the OH stretch. The lower frequency features near 1900 cm^{-1} is much smaller and corresponds to the OPB overtone. When compared to the 2ClPy-Ac dimer, however, the feature exhibits a larger OPB overtone peak and lower OH stretch frequencies. This is to be expected since the stronger acid will give rise to a stronger hydrogen bond. Instead the 2ClPy-ClAc dimer appear similar to the 3ClPy-Ac dimer and must thus have a similar hydrogen-bond strength. As the hydrogen bond strength is further increased by moving to stronger bases, these features become continuous two-

hump structures which can be seen in the calculated spectra of 3ClPy-ClAc and Py-ClAc. Py-ClAc has an avoided crossing near the equilibrium geometry giving rise to significant broadness in both humps. In the case of the strongest base (dMeAPy), the OPB plays very little role in the feature. The lack of a strong Fermi resonance interaction is due to most of the OH stretch frequencies being too low to result in an OPB Fermi resonance. The calculated feature arising from the OH stretch extends from 900 to 1500 cm^{-1} with a single peak near 1100 cm^{-1}. ClAc thus forms dimers where the OH stretch frequency is swept from well above to well below the OPB overtone, depending on the base strength, causing the Fermi-resonance to increase then decrease.

The spectra of the tFAc dimers are displayed in the right column of Figure 5.3. In the case of the weakest base (2ClPy), a continuous double-hump feature is calculated spanning from 1500 to 2500 cm^{-1}. This dimer has an avoiding crossing near the equilibrium geometry giving rise to a continuous two-hump feature. Moving to the next strongest base, 3ClPy, the OH stretch frequencies move lower resulting in an avoided crossing that occurs when the components of the dimer are further apart. Since most of the geometries result in an OH stretch frequency that is lower than the overtone of the OPB, the spectra is calculated to have a much larger lower frequency hump and smaller higher frequency hump. The FTIR spectra show the higher frequency hump as being much more substantial for this dimer. As one moves to even stronger bases the OPB overtone continues to have a small role in the computed spectra due to the OH stretch frequencies becoming too low to strongly couple with it. The lowest frequency feature calculated in this study comes from the tMePy-tFAc dimer which extends from 600 to 1400 cm^{-1} and has a maximum near 850 cm^{-1}.

In all of the dimers discussed above, the proton is bound to the acid. Although the exact bond length and distance from the nitrogen depends on the dimer and the dimer stretch

coordinate; the proton is located closer to the oxygen than the nitrogen. A more detailed examination of the location of the proton will be presented in the section 5.5. However, the dimer composed of the strongest acid (tFAc) and strongest base (dMeAPy) examined in this study is calculated to have the proton bound to the base. Therefore, the calculated feature displayed in Figure 5.3 for this dimer corresponds to the NH stretch and OPB NH overtone. In all of the previously computed spectra, stronger bases or acids have led to lower frequency features. However, this feature is calculated to be higher in frequency. Moving to an even stronger base or weaker acid would likely lead to even higher frequencies since this would continue to decrease the proton's affinity for the carboxylate.

The calculated spectra in Figure 5.3 show varying levels of agreement with the experimental spectra. In general, systems with stronger hydrogen bonds and lower frequency calculated features tend to have worse agreement with experiment. In many cases (tMePy-ClAc, dMeAPy-ClAc, 3ClPy-tFAc, Py-tFAc and dMeAPy-tFAc) the calculated spectra show the disappearance of the higher frequency hump when it is clearly still present in the FTIR spectra. The FTIR spectra of these dimers include double-humps and broad absorbance throughout the fingerprint region. Such a broad range of frequencies implies that either the functional is not capturing the full range of hydrogen bond strengths or that a larger range of geometries is needed (beyond scanning one low-frequency mode) to more accurately model the vibrational spectra. Discrepancies in the fingerprint region could also arise from Darling-Dennison (1:1) resonances between the OH stretch and various fingerprint modes since these forms of coupling are not included in the calculation.

Overall we see that changing the strength of the acid or base impacts the range of OH frequencies. The location of the OPB overtone remains rather stable throughout the series,

usually being centered near 1900 cm^{-1}. The strength of the Fermi resonance interaction is determined by how close the OH stretch frequencies are to the OPB overtone. This study shows how the OH stretch frequencies change with hydrogen bond strength. In section 3.4 and 3.6, similar shifts were observed in the OH frequency by changing the functional and the solvent. For example, the PBE functional has been shown to consistently calculate the OH stretch frequencies to be lower than B3LYP across a handful of different systems while the M06-2X functional calculates higher OH stretch frequencies.[5,6] More polar solvents also resulted in lower OH stretch frequencies. Therefore, changing the functional and/or the solvent used in the calculation changes the calculated vibrational features in much the same way that altering the acid or base strength does.

5.4 Spectral Dependence on ΔpK_A and O – N distance

The results of the previous section show a clear correlation between strength of the acid and base and the OH vibrational frequencies. This is perhaps intuitive. Stronger bases and acids are likely to result in a more anharmonic potential and a stronger hydrogen bond.

In order to obtain a better understanding of the results presented in the previous section, we examined how the calculated spectra correlate with parameters like the difference in the aqueous pK_A and the O – N distance. ΔpK_A was defined to be the pK_A of the acid minus the pK_A of the conjugate acid of the base. The mean frequency of the OH or NH stretch was calculated using the feature computed without the OPB. The OPB is neglected in order to avoid Fermi resonance interactions skewing the mean frequency. The results are plotted in Figure 5.4a. Overall this plot shows a correlation between ΔpK_A and mean OH stretch frequency. With the exception of the dimer in which the proton is bonded to the nitrogen (dMeAPy-tFAc), the mean

OH stretch frequency tends to increase with ΔpK_A. This is to be expected since higher ΔpK_A values correspond to weaker acids and bases which in turn should give rise to relatively weak hydrogen bonds. By the same logic, lower ΔpK_A values should give rise to relatively strong hydrogen bonds. At the lowest ΔpK_A value, the proton transfers over to the nitrogen leading to a higher frequency and deviating from the trend set by the other dimers.

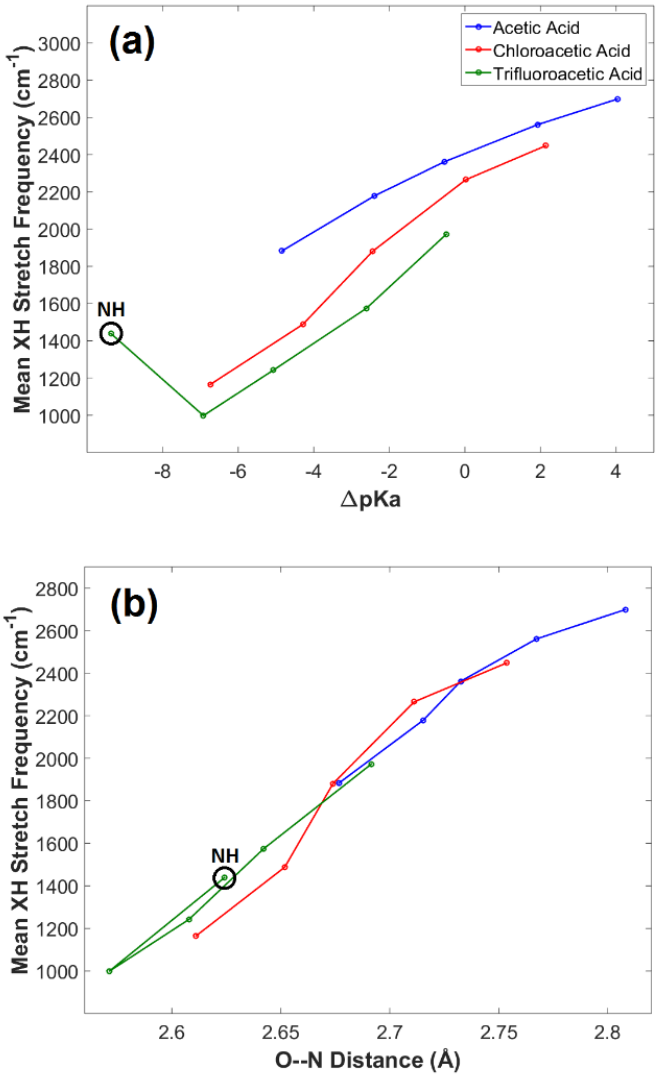

Figure 5.4: Plots comparing ΔpK_A, O – N distance and mean OH or NH stretch frequency. The dMeAPy-tFAc dimer which has the proton bound to the nitrogen is circled and labeled "NH."

Although there is a correlation between mean OH frequency and ΔpK_A, the correlation is not very robust. By examining the trend for different acids in Figure 5.4a, the mean OH stretch frequency can vary a few hundred wavenumbers depending on the acid. This is likely because the acid dissociation constants utilized are calculated using the acid or base dissolved in water while the calculations performed in this study are modeling acid-base dimers dissolved in carbon tetrachloride. Thus although ΔpK_A can be used to obtain a rough estimate of the OH stretch frequencies in these systems, it is not the most robust parameter for determining mean OH stretch frequencies.

A parameter that correlates much better with OH stretch frequency is the O – N distance. Previous studies have shown the distance between the oxygen and/or nitrogen involved in hydrogen bonds correlates well with hydrogen bond strength and OH or NH stretch frequency.[2] The correlation between mean frequency and equilibrium O – N distance is shown in Figure 5.4b. From this plot, one can see that longer O – N distances lead to higher mean frequencies. The correlation of mean frequency with O – N distance is much stronger than with ΔpK_A (Figure 5.4a). Even the dimer in which the proton is located on the nitrogen has an NH stretch frequency that follows the same trend as the OH stretch frequency of the other dimers. The OH stretch frequency likely has a better correlation with the O – N distance because the O – N distance is calculated for each dimer and takes into account the correct solvent. On the other hand, the aqueous pK_A values describe how individual acid and base molecules interact with water.

In order to understand this trend better, we examined how the potential energy curves along the OH stretch changed with the O – N distance. Plots of the OH stretch potential energy curve of dimers of representative O -- N distances are plotted in Figure 5.5. At portions of the potential near the equilibrium geometry there is a clear trend between the anharmonicity of the

surface and the O – N distance. For OH stretch coordinate values between 0 and 0.4 amu$^{1/2}$Å, the potential energy curve increases with O – N distance. This originates from the proton being more attracted to the nitrogen as the hydrogen bond strength increases. The same trend is not observed at higher OH stretch coordinate values. At larger coordinate values the dimers with short O – N distances have higher potential energies. This can be seen by examining the shorter O – N distance dimers in the top right corner of Figure 5.5. This ordering results from shorter O – N distances restricting the location of the proton to a smaller space. In the potentials presented in this figure, this higher OH stretch coordinate effect occurs at energies that are too high to impact the OH stretch fundamental which results in the OH stretch frequency always increasing with O – N distance. However, in principle even shorter O – N distances could lead to potential energy curves where the frequencies decrease with O – N distance due to the small O – N distance confining the proton. This effect can be seen in our dimer series by examining how the OH stretch frequency depends on the dimer stretch modes.

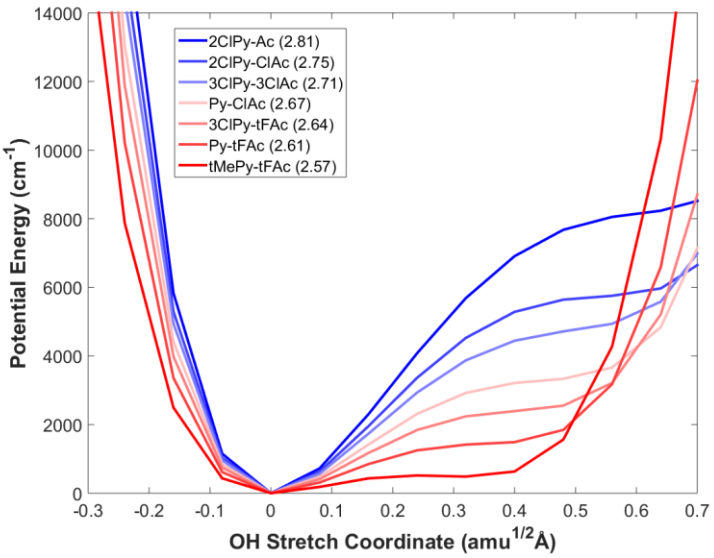

Figure 5.5: Potential energy surfaces along the OH stretch coordinate for dimers of various O – N distances. The O – N distance of each dimer in angstroms is in parenthesis in the legend.

To explore how dimer stretch modes impact the OH stretch potential in cases where equilibrium O – N distance is small, we examined the potential energy surface of tMePy-tFAc. This dimer has the smallest equilibrium O – N distance in the series. Therefore exploring how the dimer stretch impacts its potential provides geometries in which the O – N distance is smaller than any of the equilibrium structures. These potentials are plotted in Figure 5.6. Each line corresponds to a different point along the dimer stretch coordinate. The plotted points along the dimer stretch coordinate correspond to the equilibrium geometry and where the harmonic dimer stretch potential reaches 175 and 700 cm^{-1}. These values were selected to observe the full range of potential surfaces inhabited at room temperature. The geometries where the O – N distance is larger than that of the equilibrium structure have higher energy shoulders. The geometries with smaller O – N distances have a single well which increases in width with the O – N distance. To examine if these geometries with very short O – N distances have OH stretch frequencies that decrease with O – N distance, the relationship between the OH stretch frequency and the O – N distance for all of the computed points along the dimer stretch coordinate was examined. These data (for several of the dimers) are plotted in Figure 5.7. Each of the lines traces out how the OH stretch frequency and O – N distance changes with the dimer stretch coordinate for the bottom 700 cm^{-1} of the harmonic potential of the dimer stretch mode. This plot shows that at short O -- N distances, the OH stretch frequency decreases with O – N distance. The minimum OH stretch frequency corresponds to O – N distances between 2.5 and 2.6 angstroms in all of the dimers examined in this study. At shorter O – N distances, the proton is in a single well potential. Changing the O – N distance changes the width of this well resulting in an OH stretch frequency that decreases with O – N distance. At larger O – N distances, the potential consists of a single well with a larger shoulder (sometimes containing a shallow second minimum). The height of

this shoulder depends on the O – N distance. Larger O – N distances result in shoulders that are higher in the potential giving rise to higher OH stretch frequencies. This picture shows that the commonly used trends between O – O, O – N, and N –N distances and frequencies do not provide the whole story. Although at larger distances, frequency increases with distance. At smaller distances the potential becomes a single well resulting in the frequency decreasing with distance. Accounting for dimer stretch modes is important because theses modes modulate these distances.

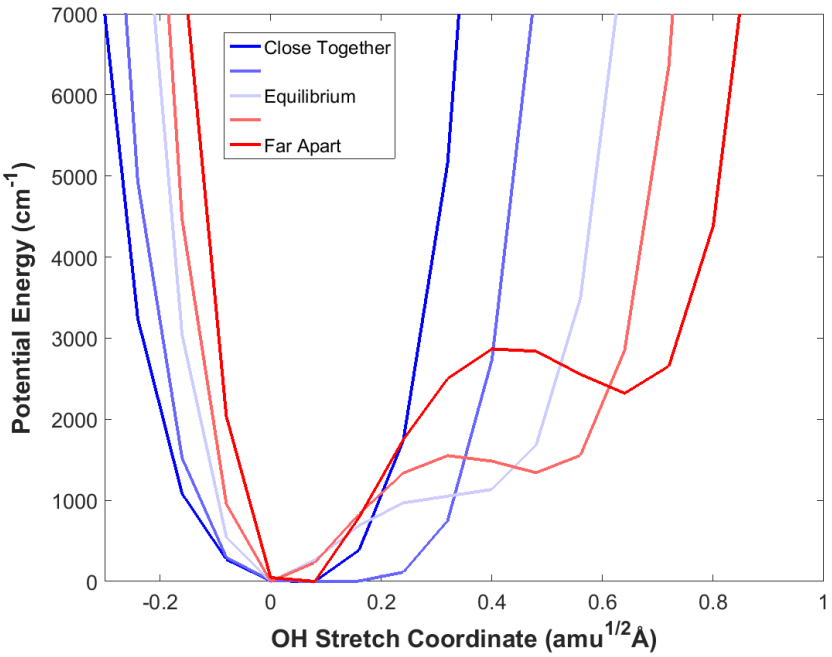

Figure 5.6: Potential energy curves of the OH stretch coordinate at various points along the dimer stretch coordinate for the tFAc-tMEPy dimer. When the dimers are closer together the potential resembles a single well. When the dimers are further apart a shoulder or shallow second minimum develops in the potential. The points along the dimer stretch coordinate sampled correspond to the equilibrium structure and where the harmonic potential reaches 175 and 700 cm^{-1} higher than the equilibrium structure.

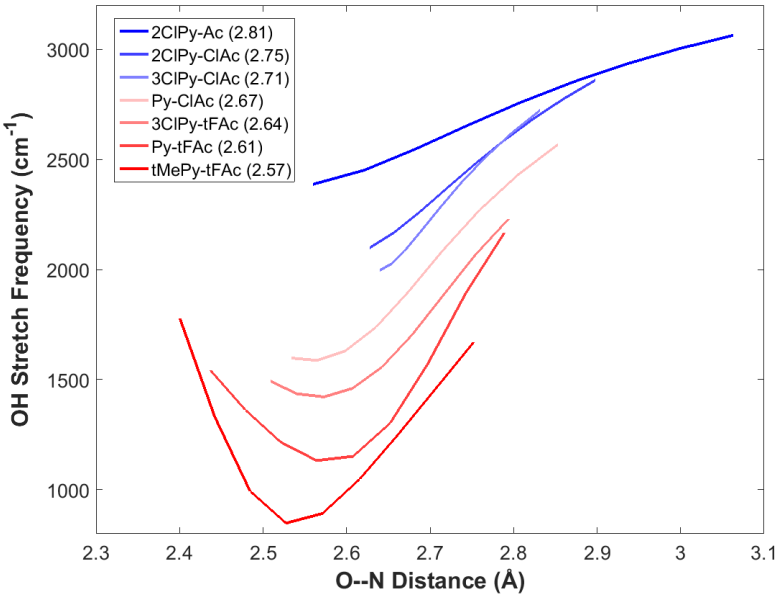

Figure. 5.7: OH stretch frequency versus O-N distances for various dimers. Each line corresponds to the points trace out by the dimer stretch mode. The identity of each dimer is given by the legend which also has the equilibrium O -- N distance (in angstroms) in parenthesis.

This picture also explains why the dimers with low-frequency features plotted in Figure 5.3, have relatively narrow and intense features. In these dimers, the point of minimum OH stretch frequency is near the equilibrium geometry. Since the derivative of the OH stretch frequency with respect to the dimer stretch coordinate is zero at this point, many geometries along the OH stretch coordinate have similar OH stretch frequencies.

5.5 Location of the Proton

In the previous section it was mentioned that all but one of the dimers in our study had the proton bound to the acid. Although there is a large change in geometry when the proton is transferred over to the base, where the proton is located between the acid and the base changes gradually even before the proton is transferred. Stronger hydrogen bonds lead to geometries with

slightly longer OH bond lengths and shorter O – N distances. The optimized geometries where the proton is bound to the acid have OH bond lengths that vary from 0.997 to 1.075 angstroms while the O – N distance varies from 2.57 to 2.81 angstroms. However, only examining the optimized geometry paints a very over-simplified picture. This is because the location of the proton is not a single point in space but instead described by a wavefunction. Additionally, this wavefunction will depend on the dimer stretch coordinate. In order to capture all of this information, contour plots of the square of the ground state wavefunction of the OH stretch versus the dimer stretch coordinate for several of the dimers examined in this study are displayed in Figure 5.8. The dimers in Figure 5.8 sample a range of O – N distances and proton locations. These plots provide a more rigorous picture of the location of the proton relative to the oxygen and the nitrogen. Since the oxygen, hydrogen and nitrogen have bond angles that are within a few degree of linear, 0 on the x-axis of this plot corresponds to the location of the oxygen while 1 corresponds to the location of the nitrogen. The top seven dimers in Figure 5.8 show that most of the proton's probability density is found closer to the oxygen than to the nitrogen. Moving to stronger hydrogen bonds results in the proton density moving closer to the midway point between the oxygen and nitrogen. The bottom panel corresponds to the dMeAPy-tFAc dimer which has most of its proton density closer to the nitrogen. In the case of all of the dimers, the value of the dimer stretch coordinate has some impact on the probability density. Lower values of the dimer stretch coordinate (which correspond to shorter O – N distances) result in the proton density moving closer to the midway point between the oxygen and nitrogen. Overall these data show that location of the proton relative to the oxygen and nitrogen changes very little until the base is strong enough and/or the acid is weak enough for the proton to be transferred over to the base.

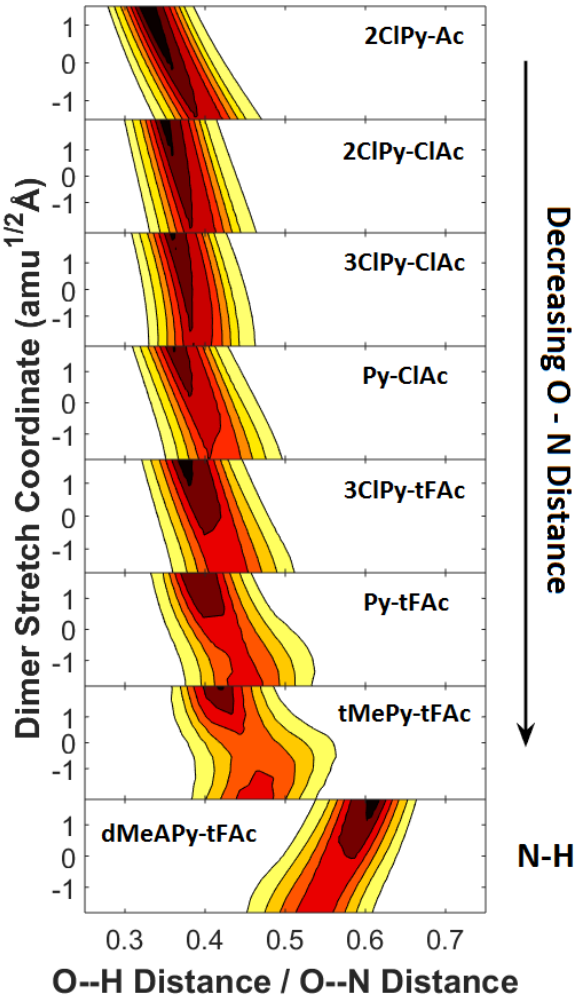

Figure 5.8: Probability distributions of the proton along the OH stretch coordinate for dimers of various O – N distances. The dimers were selected to provide a sampling of different equilibrium O – N distances to demonstrate how the surfaces vary with this distance.

5.6 Conclusion

It has been well documented that there is a strong correlation between the strength of a hydrogen bond and the vibrational frequency of its OH or NH vibration. The strength of a hydrogen bond in an acid-base dimer can be systematically tuned by adjusting the strength of the

acid or base. To examine the hydrogen bond strength dependence of the vibrational features of dimers of carboxylic acids and pyridines, these features were calculated for dimers with components of varying acid and base strengths. Changing the acid and base strengths of the components of these dimer resulted in the OH stretch vibration shifting across a wide range of frequencies ranging from less than 1000 cm^{-1} to nearly 3000 cm^{-1}. This lead to the OH stretch frequencies ranging from well above to well below the OPB overtone (1900 cm^{-1}) which is responsible for the unusual double-hump lineshape found in the vibrational spectra of many of these dimers. The results of this study show that the OH stretch frequencies are well correlated with the O – N distance. At longer O – N distances (> 2.6 angstroms) the OH stretch frequency increases with O – N distance. At these O – N distances, the potential curves have a shoulder from the hydrogen bond and the height of this shoulder is altered by the strength of the hydrogen bond and the dimer stretch coordinate. This results in an OH stretch frequency that increases with O – N distance. The opposite trend is observed at shorter (< 2.5 Angstroms) O – N distances. When the O – N distance is shorter, the potential is a single well the width of which is dictated by the amount of space between the oxygen and nitrogen. Thus in this regime, the OH stretch frequency decreases with O – N distance. These two effects place a lower limit on the OH stretch frequency of roughly 700 cm^{-1} which occurs in geometries where the O – N distances are between 2.5 and 2.6 angstroms. Overall, these calculations provide a more complete understanding as to the origin of these unusual vibrational features. Additionally, understanding how these features change with hydrogen bond strength can also provide insight for interpreting data obtained from ultrafast experiments performed on photoacids.

6. The Temperature Dependence the Vibrational Features of 7-Azaindole-Carboxylic Acid Dimers

6.1 Introduction

It was shown in previous chapters that the broadness of the vibrational features of hydrogen-bonded dimers can be explained by dimer stretch modes modulating the OH stretch frequency and large Fermi resonance interactions. By adiabatically separating these lower frequency modes from the OH stretch and bends, properties of these higher frequency transitions were shown to be very dependent on the lower frequency mode's coordinate. Consequently, the probability distribution along the dimer stretch coordinate has a large impact on the lineshape of the calculated vibrational feature. The dimer stretch method calculates the probability distribution along this coordinate using a Boltzmann-weighted sum of the harmonic dimer stretch eigenstates. Since kT is approximately 200 cm^{-1} at room temperature and the dimer stretch modes typically have frequencies between 80 and 170 cm^{-1}, many of the excited states are heavily populated at room temperature. This can be seen clearly by examining the eigenstates that make up the Boltzmann-weighted sum. Figure 6.1 shows the eigenstates that make up the distribution at room temperature (298 K) and at 10 K for the 7-azaindole-hexanoic acid (7AI-hex) dimer. At 10 K, kT is 7 cm^{-1} resulting in the vast majority of the dimers being in the dimer stretch ground state. However at 298 K, the first five excited states have significant populations. To better appreciate how these changing state populations impact the overall distribution along the dimer stretch coordinate, the overall distributions (the Boltzmann-weighted sums) are displayed in the bottom panel of Figure 6.2. The population of excited states leads to wider distributions which result in a larger range of OH stretch frequencies and consequently broader vibrational features. However, even the ground state spans a large range of geometries which

results in these features having a remarkably small temperature dependence. At lower temperatures, the features are expected to be somewhat narrower with higher peak intensities since all of the dimers are confined to a smaller range of geometries. In order to provide further evidence that the dimer stretch modes are responsible for the broadness of these features, the temperature dependence of these features was investigated theoretically using the dimer stretch method and experimentally by performing FTIR measurements of the dimers suspended in high density polyethylene (HDPE) at cryogenic temperatures.

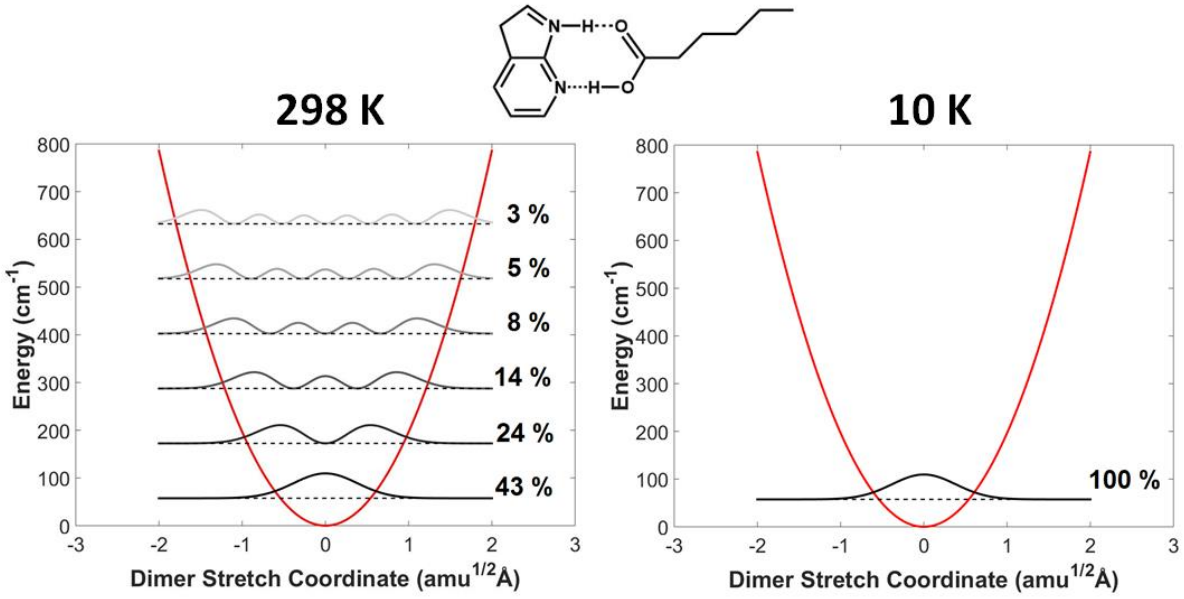

Figure 6.1: Populated dimer stretch states of the 7AI-hex dimer at 298 and 10 K. The squares of the wavefunctions of each of the states are plotted and the probability of each state is displayed to the right of square of its wavefunctions.

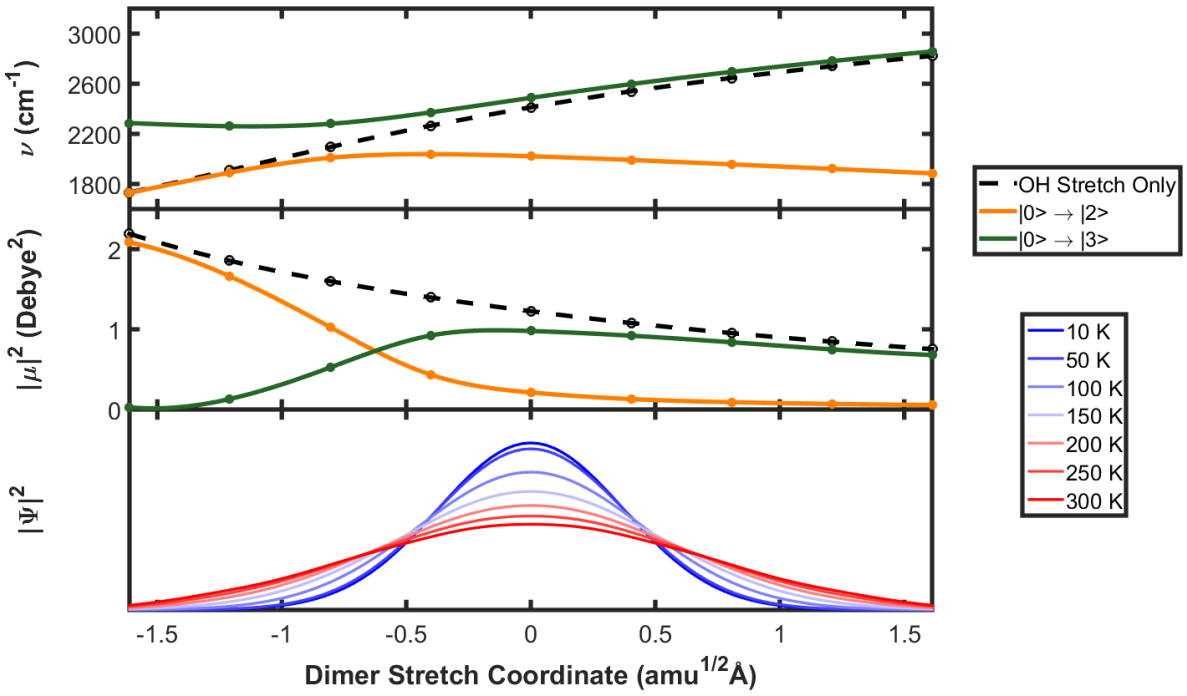

Figure 6.2: Transition properties versus dimer stretch coordinate for the 7AI-hex dimer. The top two panels show the transition frequencies and probabilities. The bottom panel shows how the distribution along the dimer stretch coordinates changes with temperature.

6.2 The 7-Azaindole Hexanoic Acid Dimer

The first cryogenic FTIR measurements were performed on the 7AI-hex dimer. In order to obtain FTIR measurements at such low temperatures, the sample containing the dimers needed to be tolerant of high vacuum and have a homogenous phase across a large temperature range. In order to accomplish this the dimers were suspended in a film of HDPE. A more detailed explanation of how the films were made can be found in Appendix B. However, during the process of making the films, the sample must be raised to the melting point of HDPE (180 ºC). Therefore, the components of the dimer needed to have boiling points above 180 ºC making pyridine and acetic acid unusable. Consequently, the 7AI-hex dimer was utilized since both of the components of this dimer have boiling points significantly above 180 ºC. Furthermore, this

dimer and the 7AI-Ac dimer have almost identical OH and NH features since the length of the carbon chain of the carboxylic acid has very little impact on the pK_A. Spectra were calculated and measured at a variety of temperatures from 10 to 300 K. These spectra are displayed in Figure 6.3.

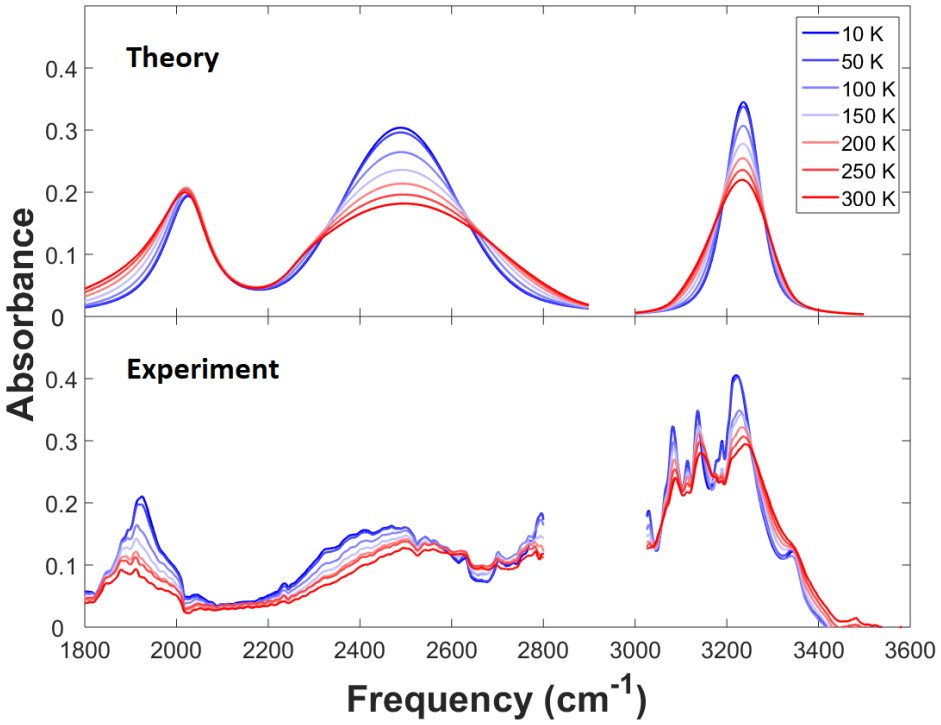

Figure 6.3: Calculated and experimental spectra of 7AI-hex dimer as a function of temperature. The top panel contains the calculated spectra while the bottom panel contains experimental spectra. The theoretical spectra displayed are calculated as two uncoupled features, one being from the coupled OH stretch and OPB and the other from the NH stretch. The OH feature is broadened using 100 cm^{-1} FWHM Lorentzians while the NH feature uses 40 cm^{-1} FWHM Lorentzians.

From the spectra shown in Figure 6.3 it is clear that broad features remain even at temperatures approaching absolute zero. This is in agreement with the calculated spectra which provides further evidence that these broad features originate from the dimer stretch modes. Although the agreement between experiment and theory is not quantitative across the whole

spectrum, the changes predicted with temperature are of the same order of magnitude as one would expect from changes in the populations of dimer stretch states. Some spectral features even have remarkable agreement. For example, the NH stretch does become narrower and with a higher peak intensity as the temperature decreases. The higher frequency hump of the OH stretch does this as well. Some frequencies that are predicted not to change with temperature are also reproduced such at the region near 2625 cm^{-1} and the region between the two humps. The most significant disagreement between theory and experiment is in the region of the lower frequency OH hump. This feature is calculated not to change with temperature, however, the experimental spectra show it increasing with intensity as the temperature decreases. The experimental spectra also show that the higher frequency region of the NH peak (around 3350 cm^{-1}) actually contains another peak which becomes clearly visible at lower temperatures.

The sections of the calculated spectra that are temperature independent correspond to points along the dimer stretch coordinate where the distribution changes very little with temperature. These points correspond to where all of the temperatures nearly cross in the bottom panel of Figure 6.2 (approximately -0.5 and 0.5 $amu^{1/2}$Å). Each of these points correspond to different frequencies for each transition. At these points the NH has frequencies of 3190 and 3275 cm^{-1}. For the higher frequency OH transition these points correspond to frequencies of 2350 and 2625 cm^{-1}. Both points correspond to around 2000 cm^{-1} for the lower frequency OH transition. However, since no transitions occur between 2000 and 2250 cm^{-1} due to the avoided crossing, the absorbance calculated between 2000 and 2125 cm^{-1} comes largely from Lorentzians centered near 2000 cm^{-1}. This results in the region from 2000 to 2125 cm^{-1} having very little temperature dependence.

Overall, these spectra provide further evidence that low-frequency modes are responsible for the broadening of these features. As the dimers are cooled down, their features generally become less broad and have higher peak intensities. However, even at temperatures as low as 10 K, the features retain a remarkable amount of broadness due to the zero-point energy of the low-frequency modes. Although the level of agreement between experiment and theory varies from feature to feature, these types of changes indicate that low-frequency modes are likely the dominant broadening mechanism of these features. Some discrepancy between theory and experiment should be expected considering the functional dependence of the calculation and the limited dimensionality of the model. However, inhomogeneous broadening (due to a range of geometries being present in the film) could be responsible for observing broad vibrational features at low temperatures as well. In order to provide further evidence that the broadness of these features originates from low-frequency modes, the reduced mass dependence of these features as a function of temperature was examined which is presented in the next section.

6.3 The Reduced Mass Dependence of 7-Azaindole - Benzoic Acid Dimers

Although the results displayed in the previous section provide compelling evidence that low-frequency modes are responsible for the broadening of these features, an argument could be made that a variety of geometries (unrelated to low-frequency modes) could give rise to broad features at very low temperatures. Although this seems unlikely to be the dominant broadening mechanism considering the agreement between theory and experiment in the high frequency OH hump and the NH feature shown in the previous section, another way to provide further evidence that low-frequency modes are responsible is to examine the reduced mass dependence of these features.

Like changing the temperature, changing the reduced mass of the dimers will impact the population distribution along the dimer stretch coordinate which will in turn impact the vibrational feature. Since the energy levels of a harmonic oscillator are proportional to the square root of the spring constant divided by the reduced mass, the energy levels and wavefunctions of the dimer stretch state will change with reduced mass. This change has an extremely small impact on the overall distribution at room temperature because as the energy levels of the states change, the distribution of excited states changes as well. However, this change is much more significant at temperatures near absolute zero. Near absolute zero, only the ground state is populated and its zero-point energy dictates the entire distribution. Smaller reduced masses, will have higher zero-point energies and consequently broader features while greater reduced masses will have lower zero-point energies and consequently narrower features. This is demonstrated in Figure 6.4 which shows the temperature and reduced mass dependence of a vibrational feature calculated for a toy model.

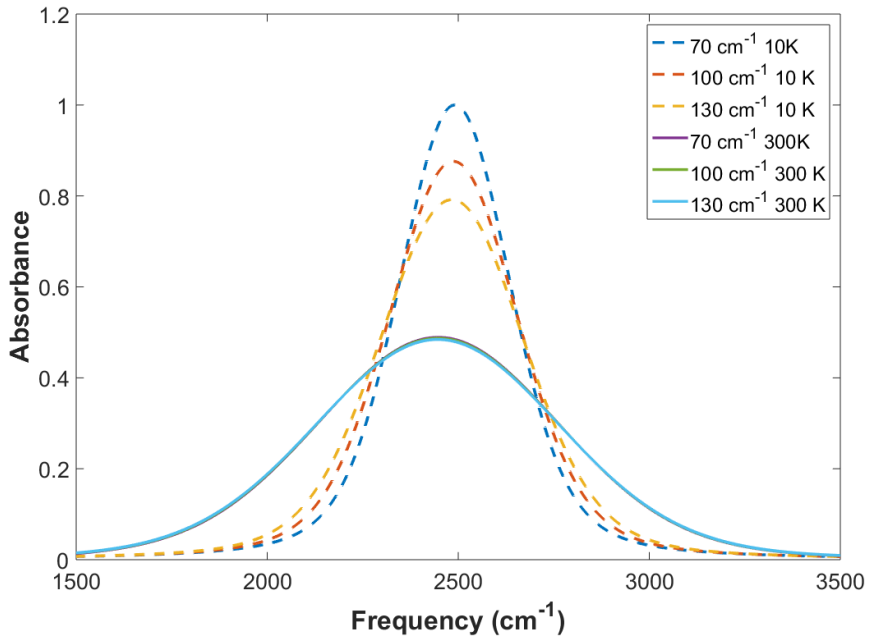

Figure 6.4: Toy model calculation of a broad vibrational feature versus temperature and dimer stretch frequency. The legend gives the dimer stretch frequency (which depends on the reduced mass) and the temperature.

The toy model shown in Figure 6.4 assumes an OH stretch frequency and transition probability that depend linearly on the dimer stretch coordinate. In this model, the relationship between the transition frequency and hydrogen bond length are kept constant. This is equivalent to requiring the spring constant not to change with reduced mass. Each line in this figure corresponds to a different temperature and dimer stretch mode frequency. Since the dimer stretch frequency is proportional to the inverse of the square root of the reduced mass, each of the dimer stretch frequencies correspond to a different reduced mass. Figure 6.3 demonstrates that at 300 K, the vibrational feature will be the same regardless of the reduced mass, but at 10 K these features will all be different. This is because at 10K, all of the dimers are in the ground dimer stretch state and this state's zero-point energy depends on the reduced mass. Heavier dimers have lower dimer stretch frequencies and zero-point energies, and therefore, will have narrower

features. Conversely, lighter dimers have higher dimer stretch frequencies and zero-point energies which results in broader features.

In order to observe this effect, a series of dimers was needed that would have different reduced masses but the same vibrational features at room temperature. In order for these dimers to have similar vibrational features, the components of the dimer needed to have similar acid and base strengths. This was accomplished using benzoic acids substituted with different halogens. Specifically, a series consisting of 4-X-benzoic acid (X = Cl, Br or I) hydrogen bonded to 7-azaindole was chosen. These acids have pK_As of 4.00, 3.96 and 4.00 respectively.[49] The X = F version was not used because it has a pK_A of 4.15. However, since pK_A is not always the best parameter for determining hydrogen bond strength, as was shown in the previous chapter, the O – N distances of these dimers were also calculated using density functional theory. Using the parameters described in chapter 2, the O – N distance (for the hydrogen bond with the OH) were calculated to be 2.702 and 2.701 Angstroms for the X = Cl and Br dimers. The O – N distance of the X = I dimer was not calculated because iodine is not defined for the 6-311++g(d,p) basis set. This indicates they should have nearly the same OH vibrational features at room temperature. This was confirmed experimentally with the spectra displayed in Figure 6.5.

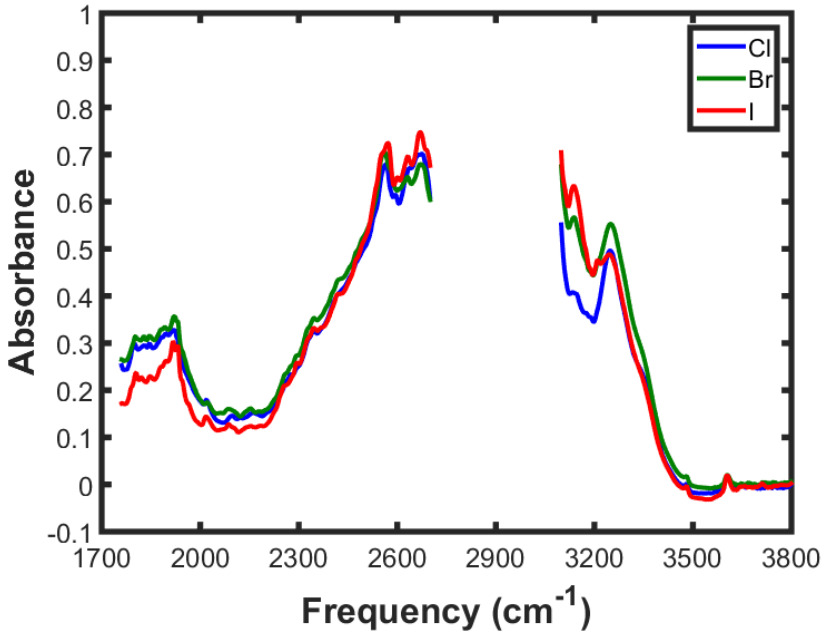

Figure 6.5: Room temperature FTIR spectra of 7-azainodle-4-X-benzoic acid dimers in HDPE (X = Cl, Br or I). HDPE absorbs strongly from 2700 to 3100 cm^{-1} and consequently that region of the spectra has been omitted.

As can be seen in Figure 6.5, this series of dimers have similar OH and NH vibration features at room temperature. The chlorine and bromine substituted dimers have almost identical OH and NH features. The iodine substituted dimer has a slightly less intense NH feature and a slightly smaller absorbance in the region of the lower frequency OH hump. However, overall these dimers have remarkably similar room temperature FTIR spectra.

The calculated spectra for the OH stretch and bend feature are displayed in Figure 6.6. The dashed lines correspond to spectra calculated at 300 K and the solid lines correspond to spectra calculated at 10K. Since the difference between the 10 K spectra is small and slightly different dimer stretch modes can impact the calculation, these spectra were computed using the same potential energy surface with the lower frequency mode's coordinate scaled and the dimer stretch wavefunctions changed to account for the varying reduced mass. Like the toy model

presented earlier, the computed spectra for these dimers at 300 K are almost identical. The differences in the spectra at 10K can be seen most clearly at 2400 cm^{-1} where the iodine substituted dimer is calculated to be the narrowest feature with the highest peak intensity and the chlorine substituted dimer is calculated to be the broadest feature with the lowest peak intensity. The changes in peak intensities in this region correspond to a few percent of the overall intensity. This is much smaller than observed in the toy model presented earlier because the changes in the frequency of the dimer stretch mode are much smaller. The toy model uses frequencies of 70, 100 and 130 cm^{-1} whereas the dimer stretch modes used for the benzoic acid dimers have frequencies of 94.8, 98.3 and 103.4 cm^{-1}. A series that could include a larger range of reduced masses would be ideal; however, since preparing the films requires that the sample be able to withstand temperatures of up to 180 C, lighter acids and bases with lower boiling points could not be used in this experiment.

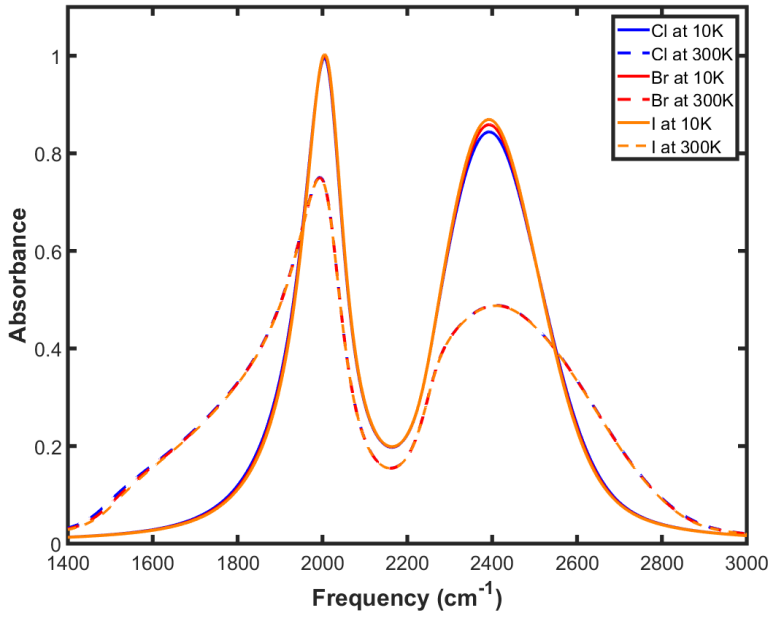

Figure 6.6: Calculated spectra of 7-azainodle-4-X-benzoic acid dimers in HDPE at 10K and 300K (X = Cl, Br or I).

Since the difference in spectra associated with reduced mass is calculated to only be a few percent, and slight variations in the experimental room temperature spectra are of this order of magnitude, having a method for obtaining the reduced mass dependence without having to compare specific spectral features across the dimer series would provide a more robust approach for observing the reduced mass dependence. This can be accomplished by examining how the absorbance changes as a function of temperature and reduced mass. It is expected that in the high temperature regime that the spectra will change with temperature but that these changes will not be impacted by reduced mass since the dimers are still in a Boltzmann-weighted sum of many dimer stretch states. However, in the low temperature limit it is expected that the changes from room temperature will be more substantial for the heavier dimers since they have ground dimer stretch states that are lower in the potential. An example of this is displayed in Figure 6.7.

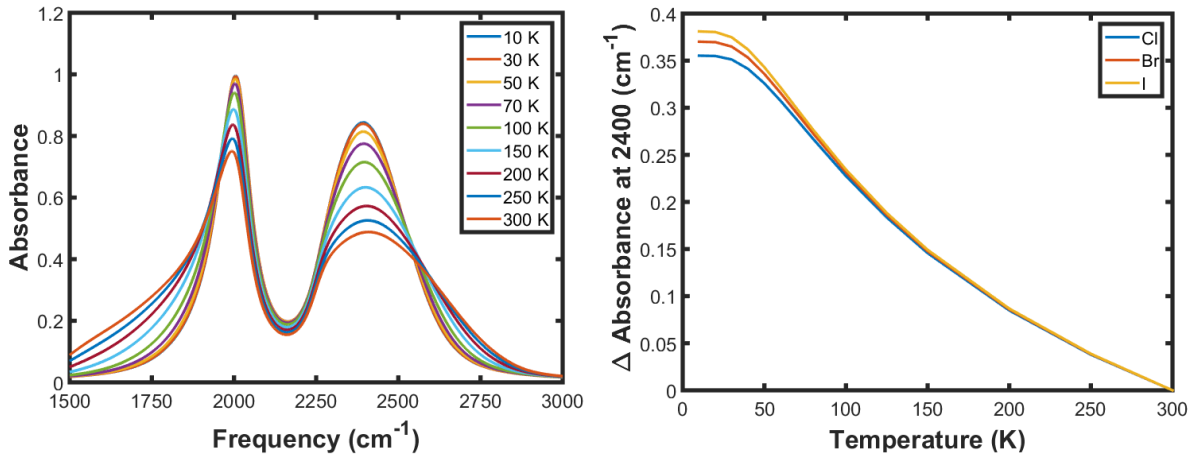

Figure 6.7: Calculated temperature dependence of the OH features of 7-azaindole-4-X-benzoic acid dimers (X = Cl, Br or I). Left: Calculated temperature dependence of the OH feature of the 7-azaindole-4-Cl-benzoic acid dimer. Right: Calculated change in absorbance at 2400 cm^{-1} relative to 300K for 7-azaindole-4-X-benzoic acid dimers.

Figure 6.7 shows how the change in absorbance of the higher frequency hump of the OH stretch can be used to show how the reduced mass impacts the vibrational feature. The left panel shows the calculated temperature dependence of the chloro version of the dimer. This calculation indicates that the frequency at 2400 cm^{-1} will change substantially with temperature. The right panel shows how the absorbance will change relative to 300K at 2400 cm^{-1} for each member of the benzoic acid dimer series. From this plot, it is easy to see that the chloro version of the dimer will change less than the iodo version due to its smaller reduced mass.

This technique will allow for a more robust method for observing the reduced mass than simply comparing spectra of the dimers at various temperatures. Because it relies on a change in absorbance (as opposed to an absolute absorbance), small variations among the room temperature spectra of the dimers should be less problematic. Additionally, this type of analysis could be used for any feature that changes with temperature. This analysis will test if the changes with temperature are due to a redistribution of the populations of the dimer stretch mode eigenstates. Furthermore, it provides an easy way to compare spectra across the whole temperature range, making any trend clearer than if one tried to compare individual temperatures.

Although measurements as a function of temperature have been taken for the benzoic acid dimer series, the data has not yet been fully analyzed. The spectra without the HDPE background removed are displayed in Figure 6.8.

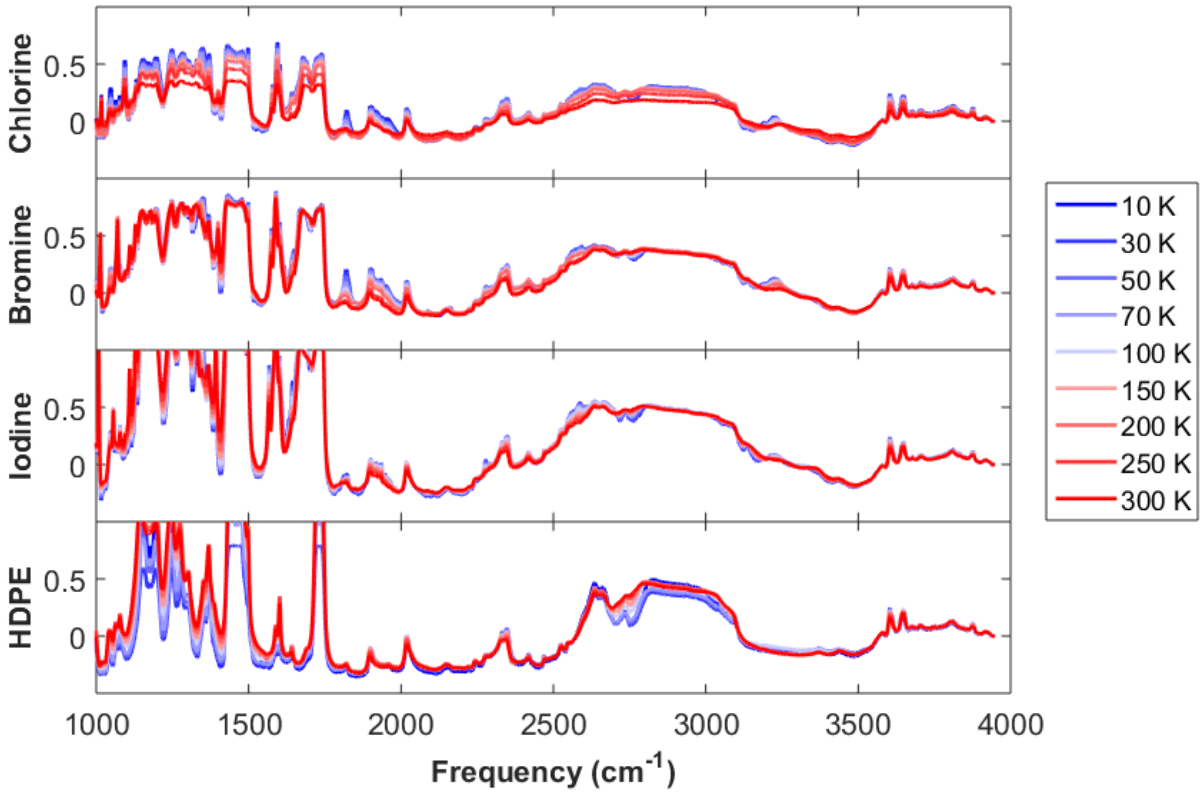

Figure 6.8: Preliminary FTIR spectra of the benzoic acid dimer series. The halogen in the para position of the benzoic acid is indicated on the left. The temperature dependence of HDPE (the background) is displayed at the bottom. The background has not yet been subtracted from the dimer spectra. These data are currently being analyzed.

6.4 Conclusion

The agreement between theory and experiment in the temperature dependent spectra of the 7-azainodle-hexanoic acid dimer has provided additional evidence that low-frequency modes are responsible for the broad vibrational features observed in these types of hydrogen -bonded dimers. Specifically, the temperature dependence of the higher frequency OH hump and the NH feature are well reproduced by the dimer stretch method. These features broaden and decrease in peak intensity as temperature increases. Further evidence that low-frequency modes are

responsible for these features could be provided by examining how the features change as a function of temperature and reduced mass. Spectra of a reduced mass series of dimers have been obtained and are currently being analyzed. The next chapter introduces a different method for calculating the unusual vibrational features. This method relies on a molecular dynamics (MD) simulation to sample a wider range of geometries than can be obtained from one dimer stretch mode.

7. Combined Electronic Structure and Molecular Dynamics Approach to Computing the OH Vibrational Feature of the Pyridine-Acetic Acid Dimer

7.1 Introduction

Although the dimer stretch method was fairly successful at reproducing the double-hump lineshape found in many of the dimers between carboxylic acids and nitrogen-containing aromatic bases, it relies on the approximation that all potential molecular geometries can be adequately sampled by scanning a single low-frequency normal mode. This approximation makes performing these calculations computationally quite feasible. By just performing a handful of potential energy surface scans at different points along a low-frequency mode, one can map out how the transition properties depend on the low-frequency mode's coordinate. This map can be used to build a spectrum that includes many more geometries than those explicitly calculated with electronic structure theory. However, when additional low-frequency modes are added to the calculation, the computation time scales like the number of points sampled along each low-frequency mode raised to the number of low-frequency modes included. This severely limits the number of low-frequency modes that can be included in the calculation, making it very difficult to account for all of the potential molecular geometries. Additionally, even if all of the low-frequency modes could be included in the calculation, scanning them may not provide an adequate sampling all of the potential geometries in the condensed phase.

One potential solution to these problems is to rely on a classical MD simulation to sample molecular geometries rather than scanning all of the low-frequency modes. Because the force fields used to perform molecular dynamics simulations are generally not of spectroscopic accuracy, snapshots of the molecular geometries are often used as an input for electronic

structure calculations. These electronic structure calculations are then used to determine the spectroscopic properties. These methods have been applied to a number of systems including water[3,26,27] and ionic liquids[28] and are often referred to as "combined electronic structure and molecular dynamics methods." Like the dimer stretch method, computing the transition properties associated with every geometry included in the calculation of the spectral feature is computationally impractical so oftentimes a "spectral map" is used to increase the number of geometries that can be included in the calculation of the vibrational feature. These maps are obtained by taking snapshots of the molecular geometry from an MD simulation and calculating the spectroscopic properties of these snapshots using electronic structure methods. These properties are found to correlate with a variable that can be obtained from the MD simulation. This is usually the electric field of some geometric parameter. Once this relationship is established, the spectroscopic properties of additional geometries can be obtained using the map instead of performing additional electronic structure calculations. Like the dimer stretch method, this method maps the transition properties onto a one-dimensional parameter.

7.2 Method

One acetic acid, one pyridine and 64 carbon tetrachloride molecules were simulated using the GROMACS.[50–52] An OPLSaa[53] force field was employed to simulate the system in a cubic cell with 2.2 nm sides. Equilibration was achieved by performing a 1 ns NVT simulation at 298K using a nose-hoover thermostat with a 0.5 fs time steps. Additional details of these simulations can be found in Appendix C. Snapshots were collected every 50 ps from 5 ns NVE production run. Equilibration was verified by the small energy and temperature drifts of 0.02 Hartrees/ns and 0.1 K/ns during the NVE simulation. Density functional theory calculations were then performed on each of the snapshots of the pyridine and acetic acid molecules with a dielectric

continuum model of the carbon tetrachloride solvent in order to obtain the vibrational frequencies and transition dipole moments. Snapshots with an O – N distance of greater than 0.5 nm (dissociated geometries) were excluded which reduced the number of geometries from 100 to 83. This was done because the dielectric continuum cavity is likely not accurate, if solvent molecules are between the pyridine and acetic acid. The location of the OH hydrogen was optimized for each of the snapshots and normal mode analysis was performed using this hydrogen's three degrees of freedom. This resulted in two OH bending modes and one OH stretch mode. These modes defined the coordinates of the potential energy surface scans that were used to compute the spectroscopic properties of each geometry. The transition frequencies and probabilities were calculated from these potential energy and dipole surfaces the same way as they were in the dimer stretch method described in chapter 2.

Once the transition frequencies and probabilities were calculated, a map was created relating the transition properties to the electric field produced by the pyridine molecule projected onto the OH bond vector. The electric field was calculated using the partial atomic charges defined by the OPLSaa force field using equation 7.1.

$$\boldsymbol{E = \hat{u} \cdot \sum_{i=1}^{n} \frac{q_i \hat{r}_{iH}}{r_{iH}^2}} \qquad \textbf{(7.1)}$$

In equation 7.1, $\hat{\mathbf{u}}$ is the OH bond vector, n is the number of atoms in pyridine (11), $\mathbf{q_i}$ are the partial atomic charges of the pyridine atoms, and $\hat{\mathbf{r}}_{\mathbf{iH}}$ is the vector from the pyridine atom $\boldsymbol{i}$ to the hydrogen in the OH of acetic acid. Maps were created relating each of the transition frequencies and probabilities to the electric field. Then the electric fields of snapshots from every 1 ps of the MD simulation were calculated (resulting in over 4000 geometries with O – N distances of less

than 0.5 nm). The electric fields of these geometries were used to compute the transition properties from the spectral maps. Each transition was modeled as contributing a 100 cm^{-1} FWHM Lorentzian profile centered at the calculated frequency with a height of the calculated transition probability. The overall spectral features were calculated by summing the Lorentzians of all of the transitions (either the OH stretch or the OH stretch and one bend overtone) of all of the geometries.

7.3 Normal Modes

Because of the range of geometries given by the MD simulation, the heavy atoms of the pyridine and acetic acid are not always in the same plane. This makes the definitions of the OPB and IPB used in the previous chapters unapplicable to the bending modes in this chapter. However, from examining the computed normal modes of the snapshots, it is clear that the lower frequency bending mode always corresponds to a bending mode that is out of the plane defined by the heavy atoms of the acetic acid, but uncorrelated with the plane defined by the heavy atoms of the pyridine. Similarly, the higher frequency bending mode corresponds to the hydrogen moving within the plane defined by the heavy atoms of the acetic acid. Therefore, in this chapter the bending modes will still be classified as OPB and IPB but the plane being referred to is of the heavy atoms of the acetic acid, not of the heavy atoms of the whole dimer.

It is also worth clarifying that calculating the normal modes using only the three degrees of freedom of the OH hydrogen has a noteworthy impact on the definition of the normal and modes and the spectral features ultimately calculated with them. These changes occur because the full-dimensional normal modes contain signifcant motion of other atoms. For the OH stertch, this is mainly the recoil of the oxygen and for the bending mode it is largely the motion of CH hydrogens. Of the two bending modes, motion of CH hydrogens is more significant for the in-

plane bend. Consequently, the two modes impacted the most by excluding the other degrees of freedom from the normal mode analysis are the IPB and the OH stretch.

Using normal modes that only include OH hydrogen motion with the dimer stretch method leads to vibrational features that are different than those presented in Chapter 3. The computed feature of the uncoupled OH stretch shifts downward in frequency by approximately 150 cm^{-1}. The fundamental of the IPB shifts from 1500 cm^{-1} to 1460 cm^{-1}. This results in the overtone occuring near 2830 cm^{-1}. This overtone participates in an avoided crossing with the OH stretch in which the two transitions come within roughly 250 cm^{-1} of each other, sinilar to the OPB, indicating the OH hydrogen only normal modes calculate stronger coupling between the OH stretch and IPB. The OPB is not as heavily affected since its full-dimensional normal mode does not contain much motion of other atoms. However, the OH stretch moving to lower frequencies does cause the calcuated feature to appear more continuous. In this chapter, the features calculated with the dimer stretch method will be shown for comparison. These features are calculated using the OH hydrogen atom only normal modes to facilitate a more direct comparison of the two methods.

7.4 Spectral Maps

The relationship of transition frequency and probability calculated using only the OH stretch to the projected electric field is shown in Figure 7.1. The transition probability is defined as the norm squared of the transition dipole moment. A linear fit was performed with the frequency data in order to obtain an equation relating the frequency to the electric field which is displayed as equation 7.2. The transition probability was fit using a second order polynomial. The results of this fit are given by equation 7.3. The OH stretch frequency decreases with electric field while the transition probability increases as expected since shorter O – N distances

generally correspond to larger electric fields. The frequencies span from nearly 2000 to 3500 cm^{-1} while the transition probabilities span over an order of magnitude from 0.03 to 0.9 $Debye^2$.

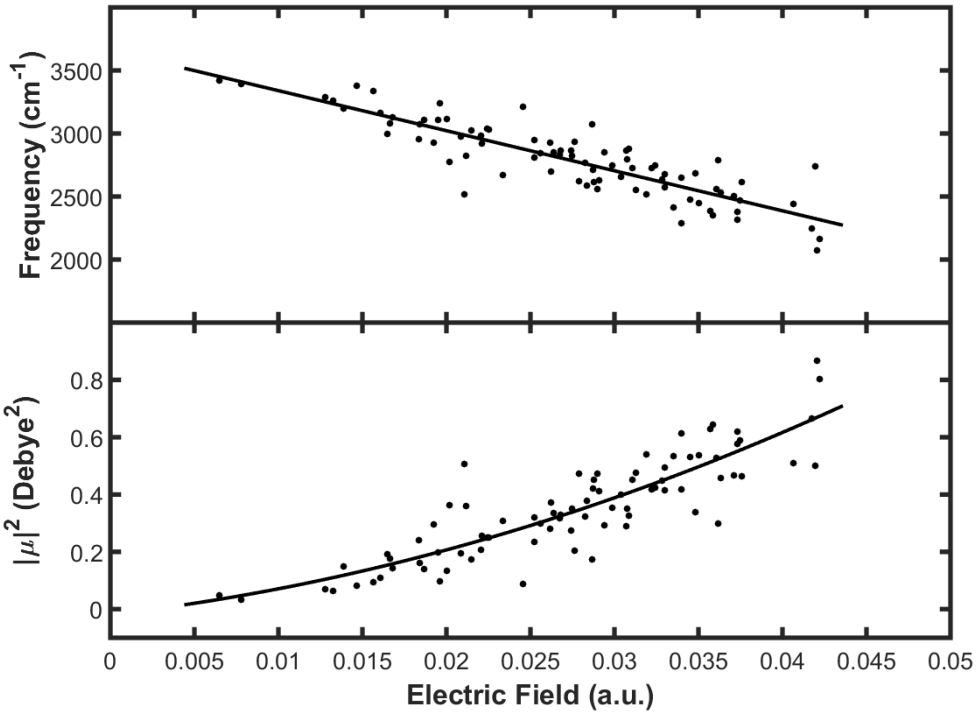

Figure 7.1: Spectral map of transition frequencies and probabilities calculated using only the OH stretch.

$$\boldsymbol{\upsilon(\mathrm{E}) = 3657 - 31770\mathrm{E}} \quad \textbf{(7.2)}$$

$$\boldsymbol{|\overrightarrow{\mu}|^2(\mathrm{E}) = -0.01856 + 6.644\mathrm{E} + 230.9\mathrm{E}^2} \quad \textbf{(7.3)}$$

The spectral maps that do not include any bending modes are relatively simple since there is only one transition. The spectral maps obtained from a calculation that includes the OPB is shown in Figure 7.2. Linear fits were used for mapping the frequecies of the two transitions. These are given by equations 7.4 and 7.5. From the data displayed in the top panel of Figure 7.2, the |0> → |3> transition frequency is decreasing with electric field while the |0> → |2> transition

frequency is increasing with electric field. This trend was also observed with the dimer stretch coordinate in chapter 3. This also indicates that for most of the geometries state |3> resembles the first excited state of the OH stretch while state |2> resembles the overtone of the OPB. At electric field values that are higher than those sampled in the MD simulation, there likely exists an avoided crossing between these two states.

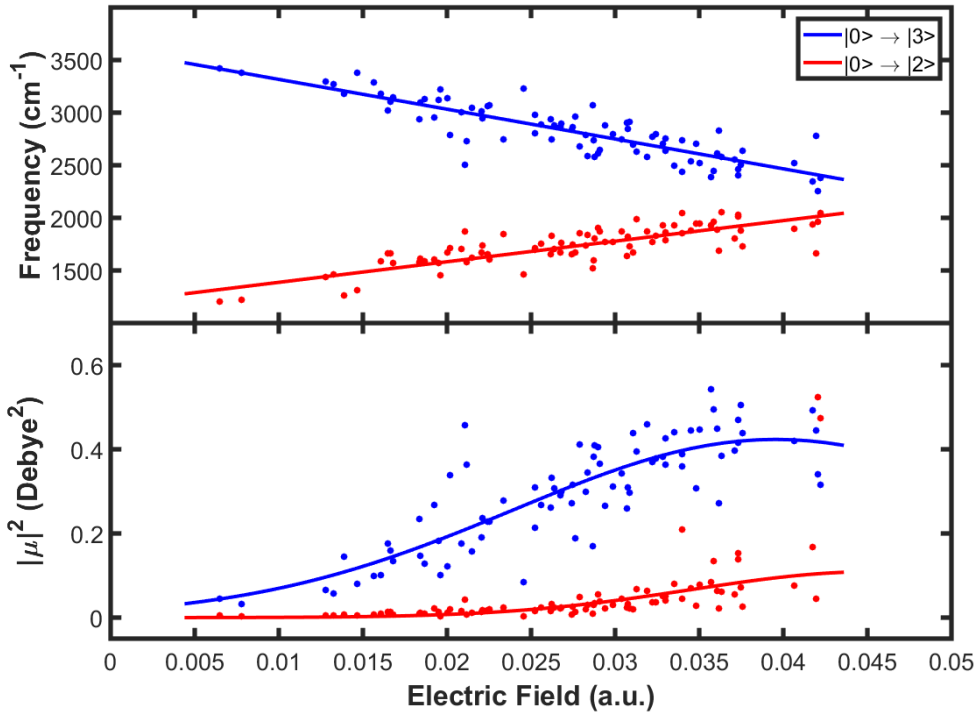

Figure 7.2: Spectral map of transition frequencies and probabilities calculated with the OH stretch and OPB.

$$\upsilon_{|0>\rightarrow|3>}(\mathbf{E}) = \mathbf{3600} - \mathbf{28330E} \quad \textbf{(7.4)}$$

$$\upsilon_{|0>\rightarrow|2>}(\mathbf{E}) = \mathbf{1191} + \mathbf{19560E} \quad \textbf{(7.5)}$$

$$|\vec{\mu}|^2_{|0>\rightarrow|2>}(\mathbf{E}) = \mathbf{0.1094}e^{-\left(\frac{E-0.04546}{0.01552}\right)^2} \quad \textbf{(7.4)}$$

$$|\vec{\mu}|^2_{|0>\rightarrow|3>}(\mathbf{E}) = \mathbf{0.4235}e^{-\left(\frac{E-0.03955}{0.02198}\right)^2} \quad \textbf{(7.5)}$$

The lower panel of Figure 7.2 shows how the transition probabilties change with electric field. These data are fit with Gaussian functions. The $|0> \rightarrow |3>$ transition has a probabilty of 0.03 Debye^2 for small electric fields. As the electric field strength increases so does the transition probability until it reaches a maximum near 0.039 a.u. The $|0> \rightarrow |2>$ transition has almost no oscillator strength at small values of electric field. However, it gains oscillator strength as the strength of the electric field increases. This is because it is approaching the avoided crossing. Overall we see that the OPB calculation shows two transitions that have very different frequencies and transition probabilities for low values of electric field, but begin to exhibit the symptoms of an avoided crossing at the higher electric field values that are populated by this system at room temperature.

Unlike the OPB, the IPB calculation demonstrates its avoided crossing clearly, which is shown in the top panel of Figure 7.3. The crossing occurs near 0.032 a.u., an electric field value that is heavily sampled at room temperature. To account for the avoided crossing in the fit, second order polynomials were used to relate the transition frequencies and the electric field resulting in equations 7.6 and 7.7. As was done with the OPB, the transition probabilites were fit with Gaussian curves, the result of which are given by equations 7.8 and 7.9. Although the correlations with electric field are not perfect for any of the transition properties, the correlations of the transtion probabilites of the IPB calcuation with electric field are the weakest. Especially when the electric field is large, there is a wide spread of transition probabilites. It could be interesting to examine the exact reason for this large spread in future studies.

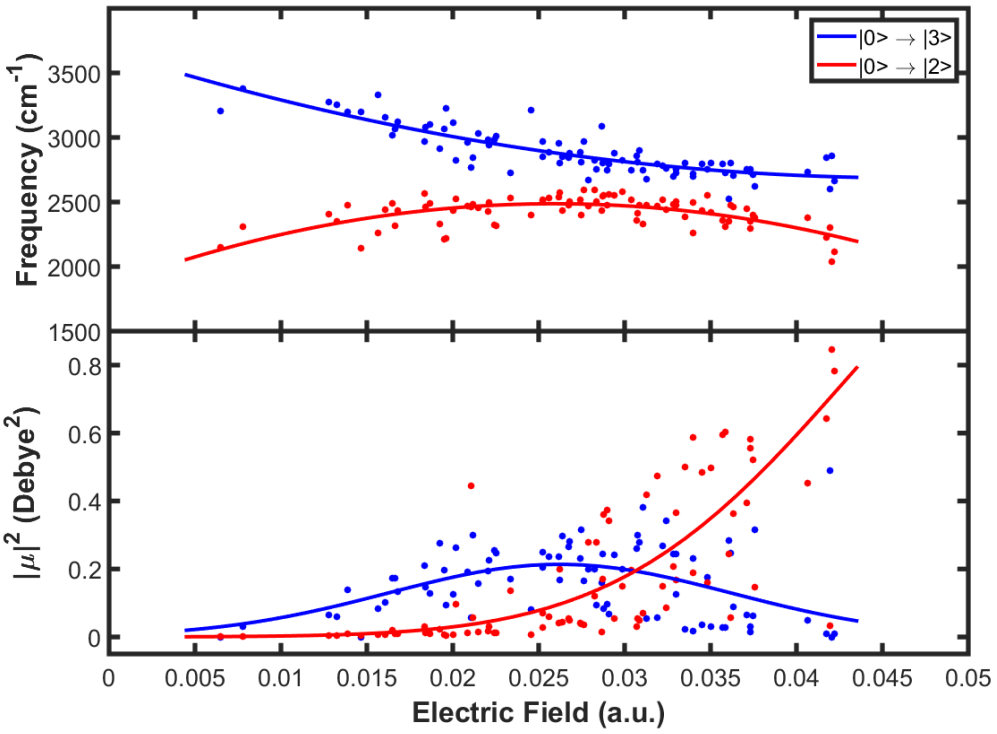

Figure 7.3: Spectral map of transition frequencies and probabilities calculated with the OH stretch and IPB.

$$\upsilon_{|0>\rightarrow|2>}(\mathbf{E}) = \mathbf{1855} + \mathbf{48780E} - \mathbf{940800E^2} \quad \textbf{(7.6)}$$

$$\upsilon_{|0>\rightarrow|3>}(\mathbf{E}) = \mathbf{3663} - \mathbf{41730E} + \mathbf{445700E^2} \quad \textbf{(7.7)}$$

$$|\vec{\boldsymbol{\mu}}|^2{}_{|0>\rightarrow|2>}(\mathbf{E}) = \mathbf{1.243}e^{-\left(\frac{E-0.056}{0.01862}\right)^2} \quad \textbf{(7.8)}$$

$$|\vec{\boldsymbol{\mu}}|^2{}_{|0>\rightarrow|3>}(\mathbf{E}) = \mathbf{0.2138}e^{-\left(\frac{E-0.02622}{0.01408}\right)^2} \quad \textbf{(7.9)}$$

Collectively these spectral maps show that both bending modes participate in significant Fermi resonance interactions. This contrasts with the results presented in Chapter 3 which utilized the dimer stretch method to calculate the vibrational features of the same system and

found the OPB to participate in a much stronger Fermi resonance than the IPB. There are likely a few reasons for this. For one, excluding the motion atoms other than the OH hydrogen from the normal mode analysis results in an IPB which couples more heavily with the OH stretch since the motion of other atoms tends to decrease the coupling. Additionally, using the OH hydrogen only normal modes decreases the fundamental frequency of the IPB from 1500 to 1460 cm^{-1} placing its overtone in a frequency range slightly more susceptible to a Fermi resonance with the OH stretch. The range of geometries sampled could also contribute to the discrepancy. The dimer stretch method only accounts for planar geometries while the MD simulation includes non-planar geometries. The difference in the results of the two methods could be partially explained if non-planar geometries have stronger couplings between the OH stretch and the IPB than planar geometries.

7.5 Calculated Spectral Features

The spectral maps shown in the previous section were used to calculate the transition frequencies and probabilities of over 4000 geometries obtained from snapshots of the MD simulation. The use of these maps allowed for many more geometries to be included than would be possible if electronic structure calculations were required to determine the spectroscopic properties of each geometry.

The calculated feature using the OH stretch only maps is displayed in Figure 7.4. For comparison, the feature calculated using the dimer stretch method with the OH hydrogen only OH stretch is also plotted. Neither of these features overlap directly with the higher frequency OH hump seen in the FTIR. The MD model results in a feature that is higher in frequency, centered near 2800 cm^{-1}, while the dimer stretch method produces a feature lower in frequency,

centered near 2350 cm^{-1}. The higher frequency feature calculated with the MD model also extends to frequencies above 3100 cm^{-1} indicating that the absorbance in this region could originate from high frequencies OH stretches. Part of this shift is likely due to the larger range of geometries present in the MD simulation. Another possible source is that the OPLSaa force field biases the geometries to larger O – N distances.

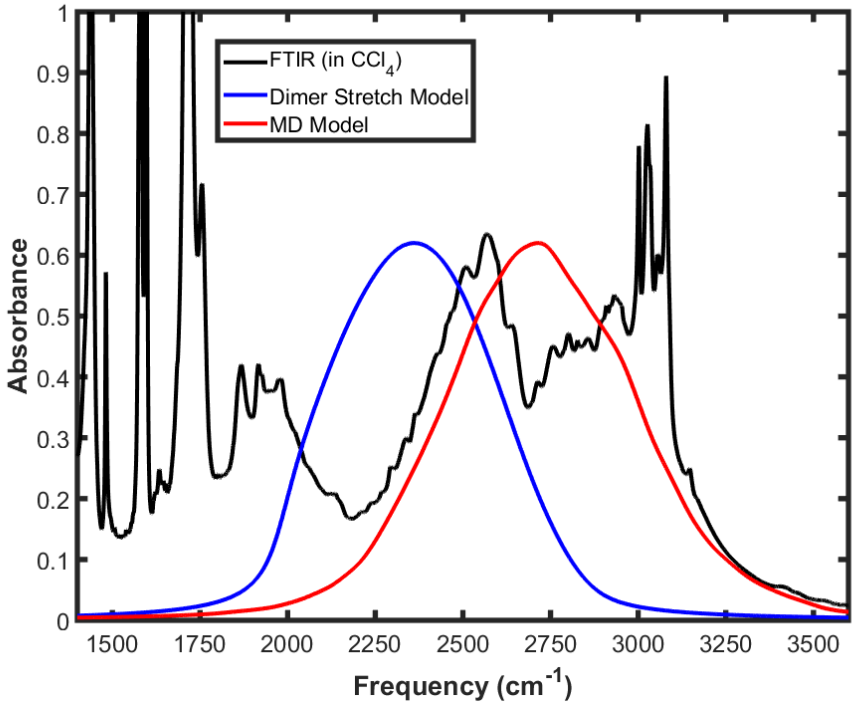

Figure 7.4: Calculated OH feature of the Py-Ac dimer using the OH stretch only maps.

The calculated feature using the OPB and OH stretch maps is displayed in Figure 7.5. This feature has two humps that are connected by a small amount of absorbance. The higher frequency feature is centered near 2800 cm^{-1}, similar to the OH stretch only calculated feature, and corresponds largely to the OH stretch fundamental. The lower frequency hump is centered near 1800 cm^{-1} and corresponds mostly to the OPB overtone. Compared to the dimer stretch feature, the lower frequency hump is broader which is in better agreement with experiment.

However, it is also much lower in intensity which places it further from the experimental spectrum.

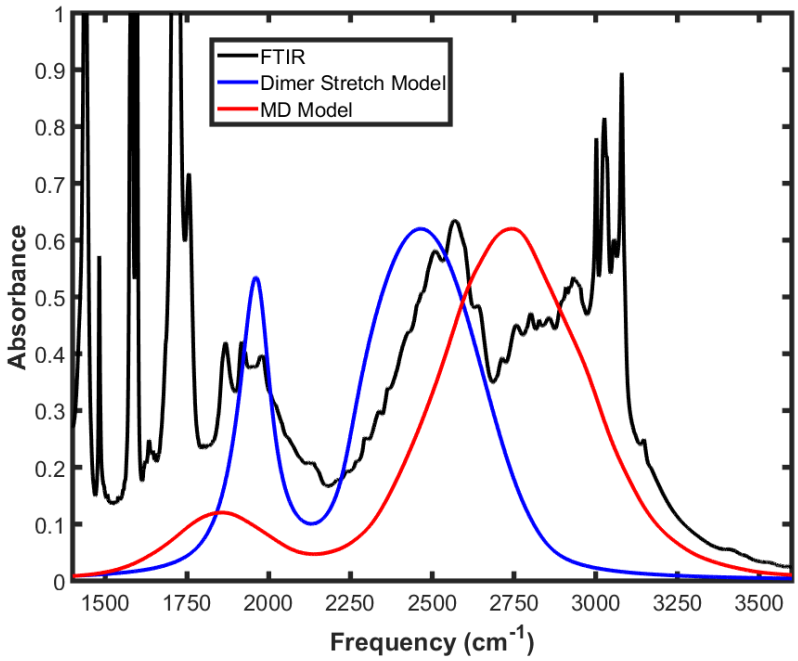

Figure 7.5: Calculated OH feature of the Py-Ac dimer using the OPB and OH stretch maps.

The calculated feature using the IPB and OH stretch maps is displayed in Figure 7.6. The avoided crossing, exhibited in the spectral maps used to calculate this feature, leads to a two-hump structure with the lower frequency hump centered near 2450 cm^{-1} and the higher frequency hump centered near 2850 cm^{-1}. This indicates that some of the absorbance between 2700 and 3000 cm^{-1} could be a third hump originating from a Fermi resonance with the IPB. This interpretation implies that the origin of OH features of dimers between carboxylic acids and nitrogen-containing aromatic bases is very similar to the origin of the Hadži ABC structure.

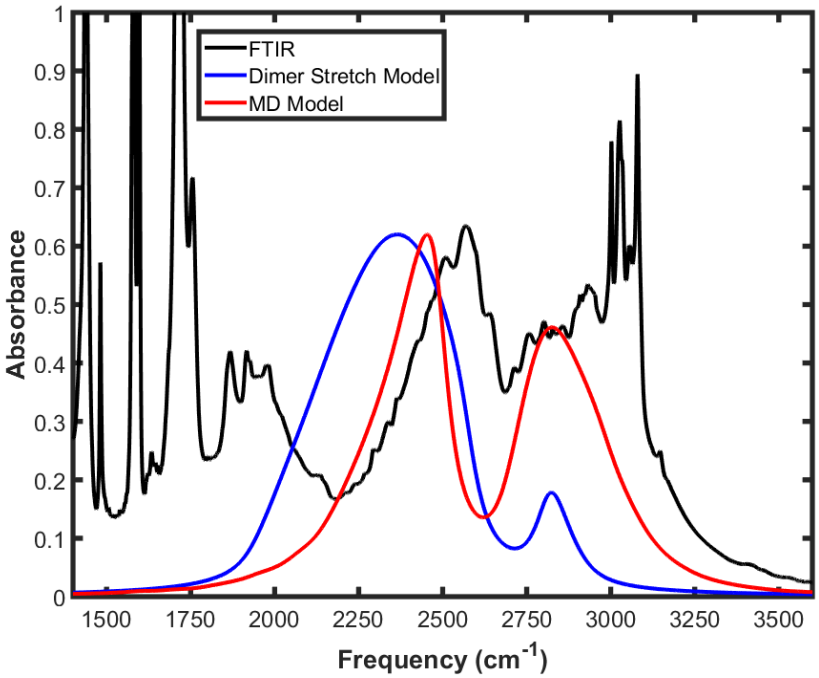

Figure 7.6: Calculated OH feature of the Py-Ac dimer using the IPB and OH stretch maps.

By comparison, the dimer stretch method with the OH hydrogen only normal modes produces a feature with a large hump centered near 2350 cm^{-1} and a smaller hump centered near 2830 cm^{-1}. This structure results from the avoided crossing of the IPB overtone and the OH stretch fundamental. This calculation shows that the two methods produce qualitatively similar features. The MD method calculates that the two humps will be of about equal intensity while the dimer stretch method calculates the lower frequency hump will be significantly larger. This is likely because the OH stretch frequencies sampled by the MD simulation tend to higher than those sampled by the dimer stretch mode resulting in a stronger Fermi resonance with the IPB.

Overall the similarities in the results of the two methods are quite remarkable. Although quantitative aspects of the feature change, the qualitative characteristics remain the same. Furthermore, most of the quantitative differences can be explained by the OH stretch shifting to

higher frequencies when the MD simulation is used to sample geometries instead of the dimer stretch mode. This indicates that the dimer stretch method can provide results that qualitatively similar for a much lower computational cost. The results of these calculations also indicate that both Fermi resonances are important for describing the OH vibrational feature of Py-Ac. Consequently, a three-dimensional Hamiltonian would be ideal for calculating these features. This calculation will be performed in the near future.

7.6 Conclusion

Another method for calculating the vibrational features of hydrogen-bonded systems is a combined molecular dynamics and electronic structure approach. These methods typically take snapshots from an MD simulation and use electronic structure calculations to compute the transition properties of these snapshots. A "spectral map" is then usually developed to relate the transition properties to some parameter that can be obtained exclusively from the MD simulation. These maps allow for the transition properties of many more geometries from the MD simulation to be computed easily. This method was applied to calculating the OH vibrational feature of Py-Ac. This calculation showed that the double-hump structure originates from a Fermi resonance between the OPB and OH stretch being broadened by the distribution of thermally inhabited geometries. The calculation also showed that a Fermi resonance between the IPB and OH stretch is responsible for some of the absorbance between 2700 and 3000 cm^{-1} which could be thought of as a third hump. This method provides a more complete picture of the origin of these features since it is able to include a much larger range of thermally inhabited geometries than the dimer stretch method. However, the features it calculates are qualitatively similar to those computed with the dimer stretch method which indicates that the inclusion of additional geometries has a largely quantitative impact on computed features.

8. Conclusion and Future Prospects

8.1 Conclusion

Hydrogen-bonded systems often have very broad and unusually shaped vibrational features. In many cases the origin of these features is unknown. Consequently, computational methods are often utilized to reproduce these features and thereby obtain insight into their origin. However, calculating these features can be quite challenging. Numerous methods have been developed, each with advantages and disadvantages. This thesis focused on developing methods for calculating the multi-hump features found in many hydrogen-bonded dimers. These methods were applied to several systems. The results of these calculations showed that the broadness of these features largely stems from the range of inhabited geometries produced by low-frequency modes that modulate the hydrogen bond length. These calculations also demonstrated that the multi-hump lineshape results from strong Fermi resonance interactions between the OH stretch and bending modes.

For many systems the dimer stretch method has shown how low-frequency mode are responsible for the broadness of these vibrational features. This method was able to model the double-hump feature found in dimers of carboxylic acids and nitrogen-containing aromatic bases and showed that this unusual lineshape comes from a strong Fermi resonance of the OPB. This method was also able to model the even broader Hadži ABC structure. This study demonstrated that several transitions to overtone and combination bending states contribute to this feature. By changing the acid and base strength of the components of the dimer, the dimer stretch method was able to show how these features change with the strength of the hydrogen bond. This allowed for features originating from dimers where the proton is on the acid or the base to be modeled as well. To further substantiate that dimer stretch modes are largely responsible for the

broadness of these features, the temperature dependence of these features was also examined. As the dimer stretch model predicted, these features remain remarkably broad at temperature as low as 10 K due to the zero-point energy of these modes. Finally, a combined molecular dynamics and electronic structure method was presented and used to calculate the double-hump feature of the Py-Ac dimer. This study showed that even with the larger range of geometries sampled by the MD simulation, the computed features are qualitatively similar to the computationally much less expensive dimer stretch method. Overall, this work shows that low-frequency modes are the primary broadening mechanism for the vibrational features of hydrogen-bonded dimers.

8.2 Future Prospects

A number of extensions of this work could be future projects. In particular, the combined molecular dynamics and electronic structure calculations described in Chapter 7 could be extended in several directions.

One direction the combined molecular dynamics and electronic structure method could be taken is the solvent dependence. The dielectric continuum model used in this work likely does not model more polar solvents well and consequently is unlikely to provide a very accurate description of the solvent dependence of these features. The dielectric continuum model predicts these feature will simply shift to lower frequencies when more polar solvents are used; however, the experimental spectra show the range of frequencies increasing rather than shifting. To account for the effect more polar solvent will have on the transition properties, this study would require developing the method to include clusters of solvent molecules in the electronic structure calculations similar to the approach of Skinner and co-workers.[26,27]

Another investigation using the combined molecular dynamics and electronic structure method could be the acid and base strength dependence. This will be more challenging than the solvent dependence since no OPLSaa force field exists for many of the bases used in Chapter 5. Consequently, this study will likely require developing new force fields or performing *ab initio* molecular dynamics simulations. Performing this study may give additional insight into why the dimer stretch method does not capture the full range of frequencies observed in the experimental spectra of many of the strongly hydrogen-bonded dimers.

Another future topic of investigation using the combined molecular dynamics and electronic structure approach could be to examine how these features change before and after proton transfer. This is difficult to do using standard molecular dynamics simulations because most force fields cannot account for bonds breaking or forming. However, proton transfer could be simulated using reactive force fields or *ab intio* molecular dynamics.

Appendix A: Derivation of the Hamiltonians

In chapter two, the Schrödinger equation is solved variationally to obtain the vibrational states of the system. This is done using a discrete variable representation of the Hamiltonian.[31] This appendix gives the derivation of these Hamiltonians.

The Hamiltonian ($\widehat{\boldsymbol{H}}$) operator is the sum of the kinetic ($\widehat{\boldsymbol{T}}$) and potential energy ($\widehat{\boldsymbol{V}}$) operators.

$$\widehat{\boldsymbol{H}} = \widehat{\boldsymbol{T}} + \widehat{\boldsymbol{V}} \qquad \textbf{(A.1)}$$

The basis functions of the Hamiltonians are delta functions which have the OH stretch and bending normal modes as coordinates. For one dimension, the elements of the kinetic energy operator are given by:

$$\widehat{\boldsymbol{T}}_{\boldsymbol{mn}} = \left\langle \boldsymbol{\phi}_{\boldsymbol{m}} \middle| \frac{-\hbar^2}{2} \frac{\boldsymbol{\partial^2}}{\boldsymbol{\partial Q^2}} \middle| \boldsymbol{\phi}_{\boldsymbol{n}} \right\rangle \qquad \textbf{(A.2)}$$

where $\boldsymbol{\hbar}$ is Planck's constant, **Q** is the normal mode coordinate and $\boldsymbol{\phi_i}$ are the basis set functions. The second derivative, with respect to the normal mode coordinate, is calculated using the finite difference approximation.

$$\frac{\boldsymbol{\partial^2 f}}{\boldsymbol{\partial Q^2}} = \frac{\mathbf{1}}{\boldsymbol{\Delta Q^2}} \sum_{\boldsymbol{i=-N}}^{\boldsymbol{N}} \boldsymbol{A_i f(Q_i)} \qquad \textbf{(A.3)}$$

For a function $\boldsymbol{f}$ of which the values are known for a set of 2N + 1 points that are equally spaced along coordinate $\boldsymbol{Q}$, the second derivative can be approximated as a weighted-sum of these values. This is shown in equation A.3 where $\boldsymbol{\Delta Q}$ is the spacing between these points. The weights ($\boldsymbol{A_i}$) are obtained using Lagrange polynomials. In the limit where N goes to infinity, the matrix elements of the second derivative operator $\widehat{\boldsymbol{O}}$ can be expressed as:

$$\widehat{\boldsymbol{O}}_{\boldsymbol{mn}} = \frac{-(-\mathbf{1})^{\boldsymbol{m-n}}}{\boldsymbol{\Delta Q^2}} \begin{cases} \dfrac{\boldsymbol{\pi^2}}{\mathbf{3}}, & \boldsymbol{m = n} \\ \dfrac{\mathbf{2}}{\boldsymbol{(m-n)^2}}, & \boldsymbol{m \neq n} \end{cases} \tag{A.4}$$

The matrix elements of the kinetic energy operator can then be obtained by adding a constant to the matrix elements of the second derivative operator.

$$\widehat{\boldsymbol{T}}_{\boldsymbol{mn}} = \frac{(-\mathbf{1})^{\boldsymbol{m-n}}\boldsymbol{\hbar^2}}{\mathbf{2}\boldsymbol{\Delta Q^2}} \begin{cases} \dfrac{\boldsymbol{\pi^2}}{\mathbf{3}}, & \boldsymbol{m = n} \\ \dfrac{\mathbf{2}}{\boldsymbol{(m-n)^2}}, & \boldsymbol{m \neq n} \end{cases} \tag{A.5}$$

Although the potential energy is calculated for a finite number of points, assuming N goes to infinity is reasonable if the potential energy of the points that are not included is much higher than the state of interest. Consequently, all of the potential energy surfaces are computed so the minimum potential energy on the edge of the surface was at least 1000 cm^{-1} greater than the final state of the transition. Since the potential energy is known for each point from the potential energy surface scan, the potential energy operator is given by a diagonal matrix:

$$\widehat{V}_{mn} = \delta_{mn} V(Q_n) \quad \textbf{(A.6)}$$

which can be added to the kinetic energy to obtain the Hamiltonian (equation A.1). Equations 2.6 and 2.7 show how the Hamiltonians are constructed for two or three dimensions.

Appendix B: Protocol for Making High-Density Polyethylene Films

1. Suspending Dimers of 7-Azaindole and Hexanoic Acid in High-Density Polyethylene

60 mg of 7-azaindole and 60 µl of hexanoic acid were dissolved in 10 ml of toluene in a 20 ml glass scintillation vial. 500 mg high-density polyethylene (HDPE) was added to the solution and placed on a hot plate set to 135 ºC for 40 minutes. The vial was then transferred to water bath maintained at 80 ºC to evaporate the remaining solvent. The resulting waxy product was then melted and pressed into a film.

2. Suspending Dimers of 7-Azaindole and 4-X-Benzoic Acid in High-Density Polyethylene (X = Cl, Br or I)

20 mg of 7-azaindole and the molar equivalent of the benzoic acid were added to 15 ml of toluene in a 20 ml glass scintillation vial. The vial was then placed on a hot plate set to 135 ºC. After both species dissolved, 500 mg of HDPE was added to the solution. The solution was maintained at 135 ºC for another 40 minutes. The solution was then placed in a petri dish and boiled until all of the toluene evaporated. The resulting waxy product was then melted and pressed into a film.

3. Pressing the Suspensions into Films

Two (2” x 2” x 0.25”) aluminum plates were heated in an oven to 180 ºC. Approximately 100 mg of the waxy dimer suspension was placed on one of the hot plates along with a piece of 0.010” diameter stainless steel wire bent into a square shape slightly smaller than the aluminum plates. The plate was then returned to the oven until the suspension was melted (roughly 20

minutes). The other plate was then used to press the molten sample into a film, the thickness of which was determined by the thickness of the wire. To separate the film from the plates without destroying it, the two plates with the film between them were submerged in room temperature water. Once the plates cooled to room temperate, the film was cleanly separated from the plates.

Since the dimers suspended in HDPE outgas under vacuum, the HDPE films were coated in a layer of Poly(methyl methacrylate) (PMMA). This was done by placing 500 µl of 2% PMMA in anisole on top of the film and allowing the solvent to evaporate for three hours. This was done for both sides of the films.

Appendix C: Molecular Dynamics Simulation Parameters

This appendix gives the parameters for the GROMACS .mdp files used to perform the molecular dynamics simulations described in Chapter 7. The definitions of each of these parameters can be found in the GROMACS user manual. The majority of the parameters were the same for both the NVT simulation (which equilibrated the system) and the NVE simulation (which was used to produce the geometries for calculating the spectral features). If a parameter changed values the NVT parameter value is listed with the NVE value in parenthesis.

integrator	= md
dt	= 0.0005
nsteps	= 2000000 (10000000)
nstxout	= 2000
nstvout	= 2000
nstlog	= 2000
constraints	= none
cutoff-scheme	= Verlet
verlet-buffer-tolerance	= -1
nstlist	= 10
rlist	= 1.09
ns_type	= grid
coulombtype	= pme
vdwtype	= cut-off
dispcorr	= EnerPres
rcoulomb	= 0.9
rvdw	= 0.9
pbc	= xyz
tcoupl	= nose-hoover (no)
tc-grps	= System (undefined)
tau_t	= 0.3 (undefined)
ref_t	= 298 (undefined)
pcoupl	= no
gen_vel	= yes (undefined)
gen_temp	= 298 (undefined)
gen_seed	= 173529 (undefined)

REFERENCES

[1] T. Elsaesser, in *Ultrafast Infrared Vib. Spectrosc.* (CRC Press, 2013), pp. 35–72.

[2] A. Novak, *Hydrogen Bonding in Solids. Correlation of Spectroscopic and Crystallographic Data* (1973).

[3] J.R. Schmidt, S.A. Corcelli, and J.L. Skinner, J. Chem. Phys. **123**, 44513 (2005).

[4] J.J. Loparo, S.T. Roberts, R.A. Nicodemus, and A. Tokmakoff, Chem. Phys. **341**, 218 (2007).

[5] B.L. Van Hoozen and P.B. Petersen, J. Chem. Phys. **142**, 104308 (2015).

[6] B.L. Van Hoozen and P.B. Petersen, J. Chem. Phys. **143**, (2015).

[7] R.E. Asfin, G.S. Denisov, and K.G. Tokhadze, J. Mol. Struct. **790**, 11 (2006).

[8] P.B. Petersen, S.T. Roberts, K. Ramasesha, D.G. Nocera, and A. Tokmakoff, J. Phys. Chem. B **112**, 13167 (2008).

[9] S. Detoni and D. Hadzi, Spectrochim. Acta **20**, 949 (1964).

[10] R. Lindemann and G. Zundel, J. Chem. Soc. Faraday Trans. 2 Mol. Chem. Phys. **68**, 979 (1972).

[11] G. Albrecht and G. Zundel, Zeitschrift Fur Naturforsch. **39a**, 986 (1984).

[12] J.P. Castaneda, G.S. Denisov, S.Y. Kucherov, V.M. Schreiber, and a. V. Shurukhina, J. Mol. Struct. **660**, 25 (2003).

[13] S. Detoni and D. Hadzi, J. Chem. Soc. 3163 (1955).

[14] S. Detoni and D. Hadži, J. Chim. Phys. **53**, 760 (1956).

[15] N. Rekik, H. Ghalla, and G. Hanna, J. Phys. Chem. A **116**, 4495 (2012).

[16] V. Barone, J. Chem. Phys. **122**, (2005).

[17] M.J. Frisch, G.W. Trucks, H.B. Schlegel, G.E. Scuseria, M.A. Robb, J.R. Cheeseman, G. Scalmani, V. Barone, B. Mennucci, G.A. Petersson, H. Nakatsuji, M. Caricato, X. Li, H.P. Hratchian, A.F. Izmaylov, J. Bloino, G. Zheng, J.L. Sonnenberg, M. Hada, M. Ehara, K. Toyota, R. Fukuda, J. Hasegawa, M. Ishida, T. Nakajima, Y. Honda, O. Kitao, H. Nakai, T. Vreven, J. Montgomery, J. A., J.E. Peralta, F. Ogliaro, M. Bearpark, J.J. Heyd, E. Brothers, K.N. Kudin, V.N. Staroverov, R. Kobayashi, J. Normand, K. Raghavachari, A. Rendell, J.C. Burant, S.S. Iyengar, J. Tomasi, M. Cossi, N. Rega, M.J. Millam, M. Klene, J.E. Knox, J.B. Cross, V. Bakken, C. Adamo, J. Jaramillo, R. Gomperts, R.E. Stratmann, O. Yazyev, A.J. Austin, R. Cammi, C. Pomelli, J.W. Ochterski, R.L. Martin, K. Morokuma, V.G. Zakrzewski, G.A. Voth, P. Salvador, J.J. Dannenberg, S. Dapprich, A.D. Daniels, Ö. Farkas, J.B. Foresman, J. V. Ortiz, J. Cioslowski, and D.J. Fox, Gaussian 09, Revis. C.01, Gaussian Inc., Wallingford, CT (2009).

[18] W. Schneider and W. Thiel, Chem. Phys. Lett. **157**, 367 (1989).

[19] J. Dreyer, J. Chem. Phys. **122**, 184306 (2005).

[20] J. Dreyer, J. Chem. Phys. **127**, 54309 (2007).

[21] J. Rheinecker and J.M. Bowman, J. Chem. Phys. **125**, 133206 (2006).

[22] C. Greve, N.K. Preketes, H. Fidder, R. Costard, B. Koeppe, I. a Heisler, S. Mukamel, F. Temps, E.T.J. Nibbering, and T. Elsaesser, J. Phys. Chem. A **117**, 594 (2013).

[23] C.J. Johnson, L.C. Dzugan, A.B. Wolk, C.M. Leavitt, J.A. Fournier, A.B. McCoy, and M.A. Johnson, J. Phys. Chem. A **118**, 7590 (2014).

[24] C.T. Wolke, A.F. Deblase, C.M. Leavitt, A.B. McCoy, and M.A. Johnson, J. Phys. Chem. A **119**, 13018 (2015).

[25] A.B. McCoy, Int. Rev. Phys. Chem. **25**, 77 (2006).

[26] S.A. Corcelli, C.P. Lawrence, and J.L. Skinner, J. Chem. Phys. **120**, 8107 (2004).

[27] S.A. Corcelli and J.L. Skinner, J. Phys. Chem. A **109**, 6154 (2005).

[28] C.A. Daly, E.J. Berquist, T. Brinzer, S. Garrett-Roe, D.S. Lambrecht, and S.A. Corcelli, J. Phys. Chem. B **121**, 208 (2016).

[29] P.J. Stephens, F.J. Devlin, C.F. Chabalowski, and M.J. Frisch, J. Phys. Chem. **98**, 11623 (1994).

[30] P.C. Wilson, E. Bright, Decius, J. C., Cross, *Molecular Vibrations: The Theory of Infrared and Raman Vibrational Spectra* (Dover Publications, New York, 1955).

[31] D.T. Colbert and W.H. Miller, J. Chem. Phys. **96**, 1982 (1992).

[32] K.S. Thanthiriwatte, E.G. Hohenstein, L. a. Burns, and C.D. Sherrill, J. Chem. Theory Comput. **7**, 88 (2011).

[33] P. Hamm and G. Stock, Phys. Rev. Lett. **109**, 1 (2012).

[34] A.M. Stingel, C. Calabrese, and P.B. Petersen, J. Phys. Chem. B **117**, 15714 (2013).

[35] A.M. Stingel and P.B. Petersen, J. Phys. Chem. B **120**, 10768 (2016).

[36] L. González, O. Mó, M. Yáñez, and J. Elguero, J. Chem. Phys. **109**, 2685 (1998).

[37] S.J. Grabowski, *Hydrogen Bonding - New Insights* (Springer, Dordrecht, The Netherlands, 2006).

[38] B. Koeppe, E.T.J. Nibbering, and P.M. Tolstoy, Zeitschrift Für Phys. Chemie **227**, 723 (2013).

[39] B. Koeppe, S. a. Pylaeva, C. Allolio, D. Sebastiani, E.T.J. Nibbering, G.S. Denisov, H.-H. Limbach, and P.M. Tolstoy, Phys. Chem. Chem. Phys. **19**, 1010 (2017).

[40] M.J. Cox and H.J. Bakker, J. Chem. Phys. **128**, 1 (2008).

[41] B.J. Siwick and H.J. Bakker, **3600**, 13412 (2007).

[42] M.J. Cox, R.L.A. Timmer, H.J. Bakker, S. Park, and N. Agmon, **113**, 6599 (2009).

[43] O.F. Mohammed, D. Pines, E. Pines, and E.T.J. Nibbering, Chem. Phys. **341**, 240 (2007).

[44] M. Rini, B.-Z. Magnes, E. Pines, and E.T.J. Nibbering, Science **301**, 349 (2003).

[45] O.F. Mohammed, D. Pines, J. Dreyer, E. Pines, and E.T.J. Nibbering, Science (80-.). **310**, (2005).

[46] H.C. Brown and D.H. McDaniel, J. Am. Chem. Soc. **77**, 3752 (1955).

[47] N. Heine, E.G. Kratz, R. Bergmann, D.P. Schofield, K.R. Asmis, K.D. Jordan, and A.B. McCoy, J. Phys. Chem. A **118**, 8188 (2014).

[48] N. Ikekawa, Y. Sato, and T. Maeda, Pharm. Bull. **2**, 205 (1954).

[49]*CRC Handbook of Chemistry and Physics* (CRC Press, Boca Raton, Fl, 2016).

[50] B. Hess, C. Kutzner, D. Van Der Spoel, and E. Lindahl, J. Chem. Theory Comput. **4**, 435 (2008).

[51] D. Van Der Spoel, E. Lindahl, B. Hess, G. Groenhof, A.E. Mark, and H.J.C. Berendsen, J. Comput. Chem. **26**, 1701 (2005).

[52] H.J.C. Berendsen, D. van der Spoel, and R. van Drunen, Comput. Phys. Commun. **91**, 43 (1995).

[53] W.L. Jorgensen, D.S. Maxwell, and J. Tirado-Rives, J. Am. Chem. Soc. **118**, 11225 (1996).